

1. OVERVIEW OF THE ARIES-I TOKAMAK REACTOR STUDY

Farrokh Najmabadi

Robert W. Conn

Contents

1.1.	DESIGN DESCRIPTION	1-1
1.2.	SYSTEMS STUDIES AND ECONOMICS	1-8
1.3.	REACTOR PLASMA PHYSICS	1-12
1.3.1.	MHD Equilibrium and Stability	1-12
1.3.2.	Transport Analysis	1-21
1.3.3.	Start-Up and Burn Cycle	1-24
1.3.4.	Current Drive	1-25
1.3.5.	Edge Physics	1-30
1.3.6.	Reactor Plasma-Physics R&D Needs	1-33
1.4.	MAGNET ENGINEERING	1-37
1.4.1.	Toroidal-Field System	1-37
1.4.2.	Poloidal-Field System	1-44
1.4.3.	Pulsed Losses	1-46
1.4.4.	Magnet R&D Needs	1-47
1.5.	FUSION-POWER-CORE ENGINEERING	1-49
1.5.1.	Configuration	1-51
1.5.2.	Materials	1-52
1.5.3.	Blanket and Shield Fabrication	1-60
1.5.4.	Neutronics	1-62
1.5.5.	Thermal and Structural Analysis	1-66
1.5.6.	Divertor Engineering	1-67
1.5.7.	Tritium System	1-70
1.5.8.	Power Cycle	1-74
1.5.9.	Maintenance	1-76
1.5.10.	Fusion-Power-Core R&D Needs	1-78
1.6.	ENVIRONMENTAL AND SAFETY FEATURES	1-82
1.6.1.	Material Selection	1-83
1.6.2.	Loss-of-Coolant Accident Analysis	1-84
1.6.3.	Radioactivity Analysis	1-84
1.6.4.	Safety R&D Needs	1-85
	REFERENCES	1-88

1. OVERVIEW OF THE ARIES-I TOKAMAK REACTOR STUDY

1.1. DESIGN DESCRIPTION

The ARIES study was undertaken to determine the economic, safety, and environmental potential of tokamak fusion reactors and to identify physics and technology areas with the highest leverage for achieving attractive fusion power plants [1, 2]. The ARIES program is pursuing several designs, each with a varying degree of extrapolation in physics and technology. This report presents the findings and details of the ARIES-I study.

The ARIES-I design is a conceptual deuterium-tritium (DT) burning, 1000-MWe reactor. The physics basis of ARIES-I is, as much as possible, consistent with existing tokamak experimental data in areas such as magnetohydrodynamic (MHD) equilibrium and stability, plasma transport and confinement scaling, edge-plasma behavior, and current drive (including the bootstrap current). Of course, the dynamics of a burning plasma remain to be explored experimentally. From the technological viewpoint, ARIES-I is based upon extrapolations that in several cases extend beyond present engineering achievements. However, in all cases, the technology and engineering are supported by laboratory data and by trends in industry, often outside the fusion program. In this overview we summarize the technical features of the ARIES-I design.

The cross section of the ARIES-I reactor is shown in Fig. 1.1-1, and the major parameters are given in Table 1.1-I. Parametric systems studies have been used to find cost-optimized designs and to assess the sensitivity of the design point to key physics and engineering assumptions and extrapolations (Sec. 1.2). Studies show that optimum, steady-state first-stability tokamaks [3] have relatively low plasma current and high plasma aspect ratio. The cost-optimized design utilizes moderately high plasma aspect ratio ($A \equiv 1/\epsilon = 4.5$) and low plasma current ($I_p = 10$ MA) at a relatively high poloidal beta ($\epsilon\beta_p \sim 0.6$). The primary reason can be found in the cost and scaling of current-drive efficiency [4] and bootstrap current [5]. Operation at higher aspect ratio maximizes the theoretically predicted self-induced bootstrap current, which in turn minimizes the auxiliary power required to maintain the full plasma current. The lower plasma current also reduces the forces induced by a plasma disruption. Operation at high aspect ratio leads to lower heat fluxes on the divertor target while the trade-off of plasma current

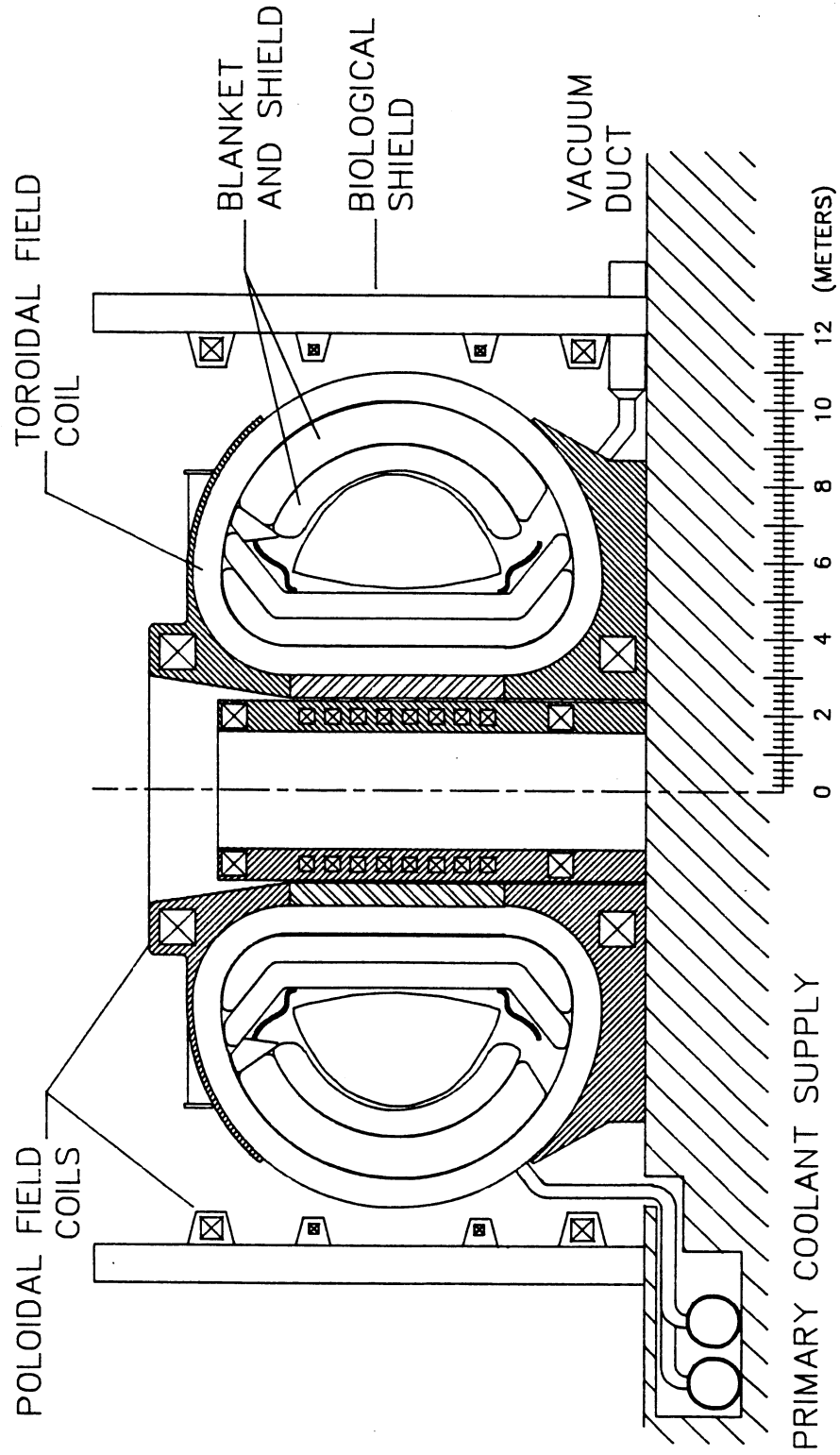


Figure 1.1-1. Elevation view of the ARIES-I fusion power core.

Table 1.1-I.
Operating Parameters of the ARIES-I Tokamak Reactor

Aspect ratio	4.5
Major radius (m)	6.75
Plasma minor radius (m)	1.50
Plasma vertical elongation	1.8
Plasma current (MA)	10.2
Toroidal field on axis (T)	11.3
Toroidal beta	1.9%
Average neutron wall load (MW/m ²)	2.5
Primary coolant	Helium at 10 MPa
Structural material	SiC composite
Breeder material	Sphere-pac Li ₂ ZrO ₃
Neutron multiplier	Sphere-pac beryllium
Coolant inlet temperature (°C)	350
Coolant exit temperature (°C)	650
Fusion power (MW)	1,925
Total thermal power (MW)	2,544
Net electric power (MW)	1,000
Gross efficiency	49%
Net plant efficiency	39%
Recirculating power fraction	20%
Mass power density, MPD (kWe/tonne)	99
Cost of electricity, COE (mill/kWh)	65

and aspect ratio ensures that the plasma has adequate energy-confinement time. Recent studies of confinement scaling with current and aspect ratio [6] are consistent with and support the lower I_p , higher A design choice of ARIES-I.

Equilibrium and stability. The ARIES-I reference MHD equilibrium (Sec. 1.3.1) is computed based on plasma profiles that are consistent with the current-drive (including bootstrap), transport, and impurity-control/particle-exhaust analyses. Plasma vertical elongation of $\kappa_x \simeq 2$ is desirable in order to increase the plasma volume and fusion power. A value of $\kappa_x = 1.8$, however, is chosen based on the vertical stability analysis and the desire to place passive stabilizing elements behind the blanket. The values of on-axis safety factor ($q_o \sim 1.3$) and average plasma-edge safety factor ($q \sim 4.5$) reflect the trade-offs between the equilibrium and stability analyses and the effort to maximize the bootstrap-current fraction. The toroidal beta is 1.9% (corresponding to a Troyon [3] coefficient, C_T , of 3.2% Tm/MA) and is established from high- n ballooning and $n = 1$ kink stability analyses.

Transport. Extensive transport calculations have been performed, using the BALDUR code [7], to gain confidence that the plasma would ignite and achieve the predicated steady-state burn condition (Sec. 1.3.2). These calculations show that the confinement required in the ARIES-I reactor is consistent with the present tokamak energy-confinement data base. An enhancement factor of 2 to 3 over L-mode (depending on the scaling relation used) is needed. A large portion ($\sim 50\%$) of the plasma energy is radiated in the form of synchrotron radiation because of the large on-axis magnetic field, the high electron temperature (~ 20 keV which improves the current-drive efficiency), and the poorly reflecting first wall (SiC composite). The corresponding plasma energy-confinement time (convection and conduction) is 2.4 s. The simulations also indicate that approximately 100 MW of ion-cyclotron range-of-frequency (ICRF) current-drive power is more than adequate to heat the plasma to ignition (Sec. 1.3.3). The transport simulations show that the ARIES-I plasma can be fueled by high speed pellets (~ 5 km/s) and that the resultant density profile would be flat. A more peaked density profile would result in a higher fusion-power density and a larger bootstrap-current fraction, thereby leading to a lower cost of electricity. The more peaked density profile, however, requires a central fueling scheme and/or a large anomalous inward-pinch process, both of which were ruled out for the ARIES-I design.

Current drive. Steady-state operation is to be achieved by using ICRF fast-wave current drive [8] to supplement a significant (68%) bootstrap current predicted by theory for ARIES-I plasma conditions [5]. Neutral-beam current drive has also been studied as an alternative. Fast-wave current drive has been observed in smaller machines [9] and more definitive experiments are planned on DIII-D and JET. Self-consistent current-drive calculations have been performed to ensure that the total driven-current density (including bootstrap) matches the equilibrium current-density profile (Sec. 1.3.4). The current-drive power is estimated to be 92 MW at an ICRF frequency of 141 MHz. The fast-wave launcher is a folded waveguide capable of handling high power (~ 40 MW/m²) [10]. Some 5 MW of lower-hybrid power is also included to drive current at the plasma edge and to aid plasma start-up.

Impurity control. The impurity-control/particle-exhaust system consists of a double-null poloidal divertor with a toroidally continuous target plate (Sec. 1.3.5). Because about 50% of core-plasma energy is radiated and, because there is a high upstream separatrix density (about 10^{20} m⁻³), a high-recycling divertor mode is expected. Two-dimensional edge-plasma computer codes, B2 [11] and EPIC [12], were used to predict the edge-plasma parameters and to ensure self-consistency with core-plasma simulations (upstream densities, temperatures, and fluxes). The results indicate that: (1) The edge-plasma density is high enough that neutrals produced on the first wall and divertor plates will not recycle into the core plasma. (2) With a core particle-to-energy confinement-time ratio, τ_p/τ_E , of 4, adequate α -particle ash exhaust can be achieved. (3) The peak α -particle heat flux on the divertor target is estimated at 4.5 MW/m² for a target inclination angle of 10° at the separatrix strike point. (4) The peak plasma temperature at the divertor target is estimated to be about 25 eV, effectively limiting the production of impurities. The divertor target is coated with tungsten to reduce the sputter erosion to negligible levels. Sputter erosion of the first wall is also found to be small.

Magnet engineering. Operating the reactor in the first stability regime using a high aspect ratio and relatively low plasma current leads naturally to the need for high magnetic field to achieve adequate fusion-power density (which scales as $\beta^2 B^4$). The toroidal field at the plasma center is 11 T and the maximum field at the coil is 21 T. Currently available Nb₃Sn alloys, produced by the powder metallurgy process, can generate fields up to about 21 T [13, 14]. The conductor in each toroidal-field coil is graded, with Nb₃Sn used for the intermediate and high-field regions (≥ 6 T) and NbTi used for low-field zones (≤ 6 T).

Detailed finite-element analyses of the magnet show a maximum von Mises stress of 700 MPa (Sec. 1.4). This level of stress can be handled in a steady-state reactor using industrially available structural alloys. The reference structural material is Incoloy 908 [15-17], one of the materials considered for the ITER magnets [18, 19]. This rather low level of stress for a 21-T magnet is made possible by some unique aspects of the ARIES-I design which include: (1) high aspect ratio, (2) using a bucking cylinder and two structural caps to support the out-of-plane loads, and (3) using copper-niobium (CuNb) high-strength stabilizer [20] which can carry structural load. The design of the poloidal-field magnet system follows the ITER recommendations [19]. The peak field in the poloidal-field system is 12 T and most of the magnets have relatively low field and current density.

Fusion-power-core engineering. The fusion power core (FPC) uses silicon-carbide composite as structural material (Sec. 1.5) which is to be manufactured as a large integrated piece utilizing techniques already in use or under development in the aerospace industry [21-25]. This composite retains many of the desirable features of bulk SiC ceramic but the addition of SiC fibers greatly reduces the brittleness of the material and produces a high fracture toughness. The increase in toughness creates more freedom in engineering design and allows both tensile and compressive stress in the composites. Desirable features of SiC composites include high-temperature capability, high strength, extensive resource availability, and potentially good resistance to radiation damage. In addition, levels of induced activation and afterheat in SiC are quite low, enhancing the safety and environmental features of the reactor. For example, low values of peak temperatures are calculated for the ARIES-I FPC in the case of a loss-of-coolant accident.

The FPC comprises 16 independent toroidal modules. Each module is replaced as a single unit during maintenance operations. The modules consist of one toroidal-field coil, two inboard and two outboard blanket and shield sub-modules, two upper and lower divertor targets, and a section of the vacuum vessel. Each sub-module has 10 nested, U-shaped SiC-composite shells. A sphere-pac lithium-zirconate (Li_2ZrO_3) solid breeder and a beryllium neutron-multiplier mixture are located in the space between the shells (Fig. 1.1-2). Tritium would be recovered by a slow-flowing, low-pressure purge stream of helium between the shells. Sphere-pac pellets of beryllium metal are used as the neutron multiplier in order to obtain an adequate tritium-breeding ratio (1-D TBR of 1.18) and high blanket-energy multiplication ($M = 1.3$).

The FPC is cooled by helium at 10 MPa. The coolant flow is both radial and toroidal, and the inlet temperature is 350 °C. The total blanket-loop pumping power is 19 MW. An

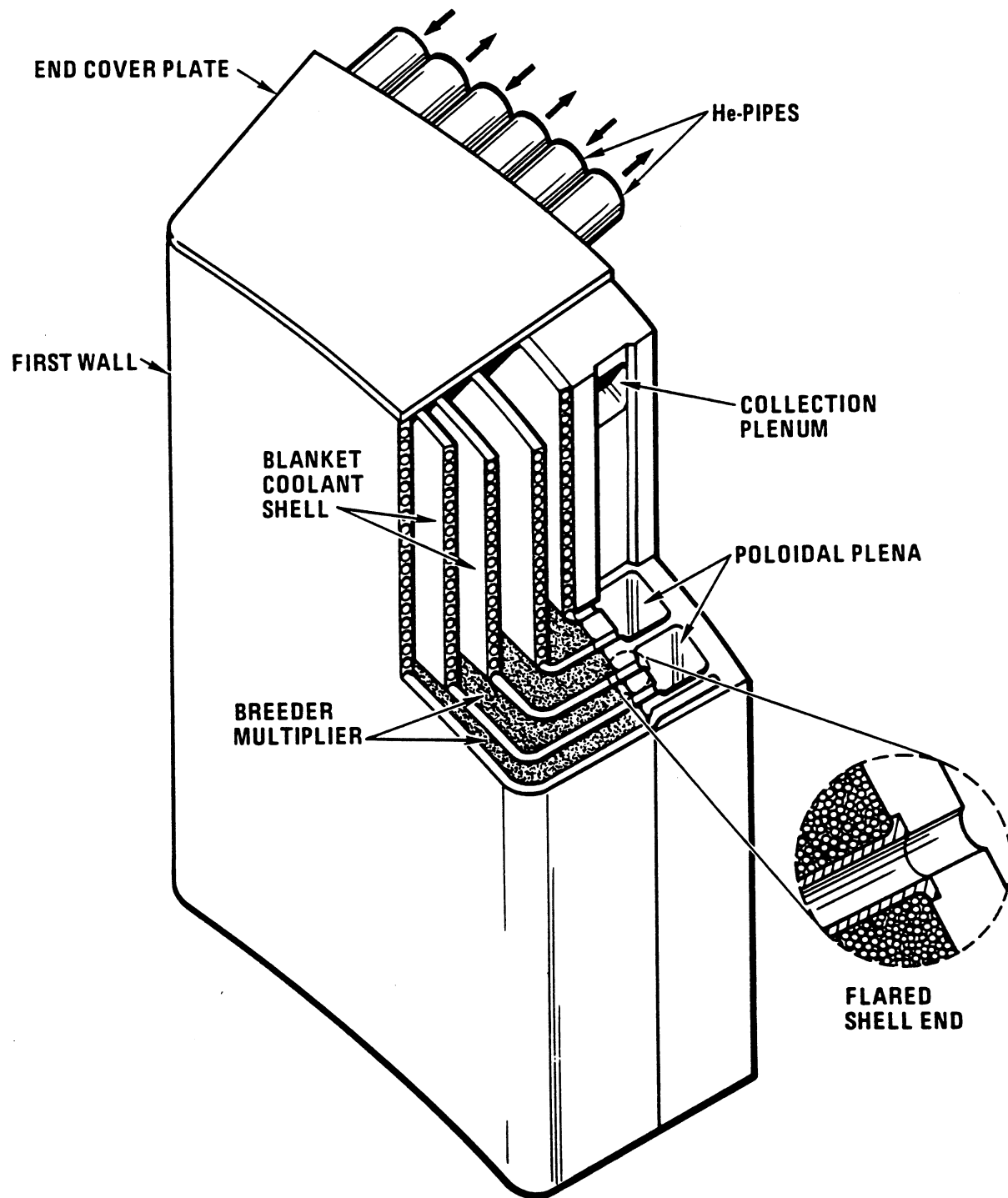


Figure 1.1-2. Schematic of an ARIES-I fusion-power-core module.

advanced Rankine steam power cycle is adopted because the coolant outlet temperature is sufficiently high (650 °C) and because this cycle is planned for near-term, coal-fired power plants [26]. The calculated gross thermal efficiency is 49%.

Economics, safety, and environmental aspects. The ARIES-I reactor is passively safe (Level 2 of safety assurance as defined by ESECOM [27, 28]) and is a low environmental-impact design (Sec. 1.6). The reactor components qualify for Class-C shallow-land burial of waste [29]. The cost of electricity (COE) for an ARIES-I-type tokamak is projected to be about 65 mill/kWh in constant 1988 dollars. This value is comparable to predictions for advanced fission reactors (47 to 78 mill/kWh) and coal-fired plants (50 mill/kWh) developed on the same basis [30, 31]. It is believed that because of excellent safety characteristics, there is the potential for the elimination of the nuclear qualification (N-stamp) requirement for most of the ARIES-I components. (The savings realized by the elimination of the N-stamp requirements, which can be as high as 25%, are not included in the COE value given above.) The COE for ARIES-I is competitive with present-day alternatives if the anticipated cost of future environmental and licensing requirements are included in the price of fossil or nuclear fission power.

1.2. SYSTEMS STUDIES AND ECONOMICS

A parametric systems-analysis computer code was used to identify the cost-optimized reactor operating points and to assess the impact of alternative design choices. The projected cost of electricity (COE) is the object function to be minimized. Results from both detailed plasma modeling and engineering design were fed back and integrated into the model. As such, the systems code was used as a tool in the iterative conceptual engineering-design and system-optimization process. Parametric sensitivity studies of key variables have also been performed to characterize an operating space in terms of a "design window" for attractive tokamak reactors.

The systems code incorporates a plasma model, engineering models (for the coils, power cycle, and other key systems), and an economics package. The toroidal beta is limited by the Troyon relation [3], $\beta = C_T I_\phi / (a B_{\phi 0})$, where $C_T \simeq 0.032$ Tm/MA is a nearly constant coefficient set by kink and ballooning stability considerations. The deuterium-tritium (DT) thermonuclear burn model includes the contribution of the fusion-product pressure to β and assumes $Z_{eff} = 1.65$. The operating temperature is obtained by balancing considerations of fusion power density and current-drive coupling efficiency. Transport

is calibrated against a number of tokamak confinement scaling relations and, in general, requires enhancement factors of ~ 2 to 3 over the L-mode. The efficiency of the current drive is characterized by the coupling efficiency, γ ($\equiv n_e I_\phi R_T / P_{CD} \propto T_e^{0.77}$). A significant fraction ($f_{BS} \simeq 0.68$ for $A = 4.5$ and the assumed temperature and density profiles) of the plasma current is provided by the bootstrap effect, and is calculated self-consistently.

The ARIES-I reactor power-balance equations are solved subject to a specified net output power (*e.g.*, $P_E = 1000$ MWe). The recirculating power includes the current-drive power and an additional 9% of the gross electric power for primary-coolant circulation and other site-power uses. The fusion power core (FPC) is characterized in the systems model in order to estimate the COE figure of merit, which is a strong function of the FPC mass-power density and the recirculating power fraction. The thickness of the inboard blanket and shield is 1.4 m and the outboard (and top and bottom) thickness is 1.8 m. The blanket neutron-energy multiplication is $M_N = 1.3$ and the gross thermal-conversion efficiency is $\eta_{th} = 0.49$.

The toroidal-field (TF) coil model includes 16 D-shaped coils with Nb₃Sn superconductors with a peak field strength on the inboard TF-coil legs of 21 T. The stabilizer current density is set at 200 MA/m², and the coil thickness is determined by a current-density/field-strength scaling [32].

Parametric systems analyses of ARIES-I-type reactors show that the COE is minimum near $A \sim 4.5$. Lower values of the aspect ratio correspond to higher values of plasma current, a lower bootstrap-current fraction, and together result in higher current-drive power and a higher value of recirculating power fraction. Higher values of the aspect ratio are associated with a more massive coil set and lower mass-power-density values. For the range of aspect ratio considered, however, the minimum COE is found near the maximum allowed field on the coil (*i.e.*, 21 T). The variation of COE with maximum field on the TF coil is shown in Fig. 1.2-1. The sensitivity of the COE to the unit cost of the coil is also illustrated.

The cost model assumes future “learning-curve” cost credits: specifically, ARIES-I unit costs for a “tenth-of-a-kind” plant can be $\sim 50\%$ of “first-of-a-kind” ITER-like costs. Indirect costs are estimated at 45% of direct costs. Standard assumptions [30, 33] regarding construction time (6 years), plant availability ($p_f = 0.76$), economies of scale, and operation and maintenance (O&M) charges are used to estimate the constant-dollar (1988) COE. A summary of ARIES-I costs is provided in Table 1.2-I. The projected COE for the ARIES-I reactor is 65 mill/kWh. For comparison, the corresponding values for “median-experience” and “better experience” fission pressurized-water reactors ($P_E = 1100$ MWe)

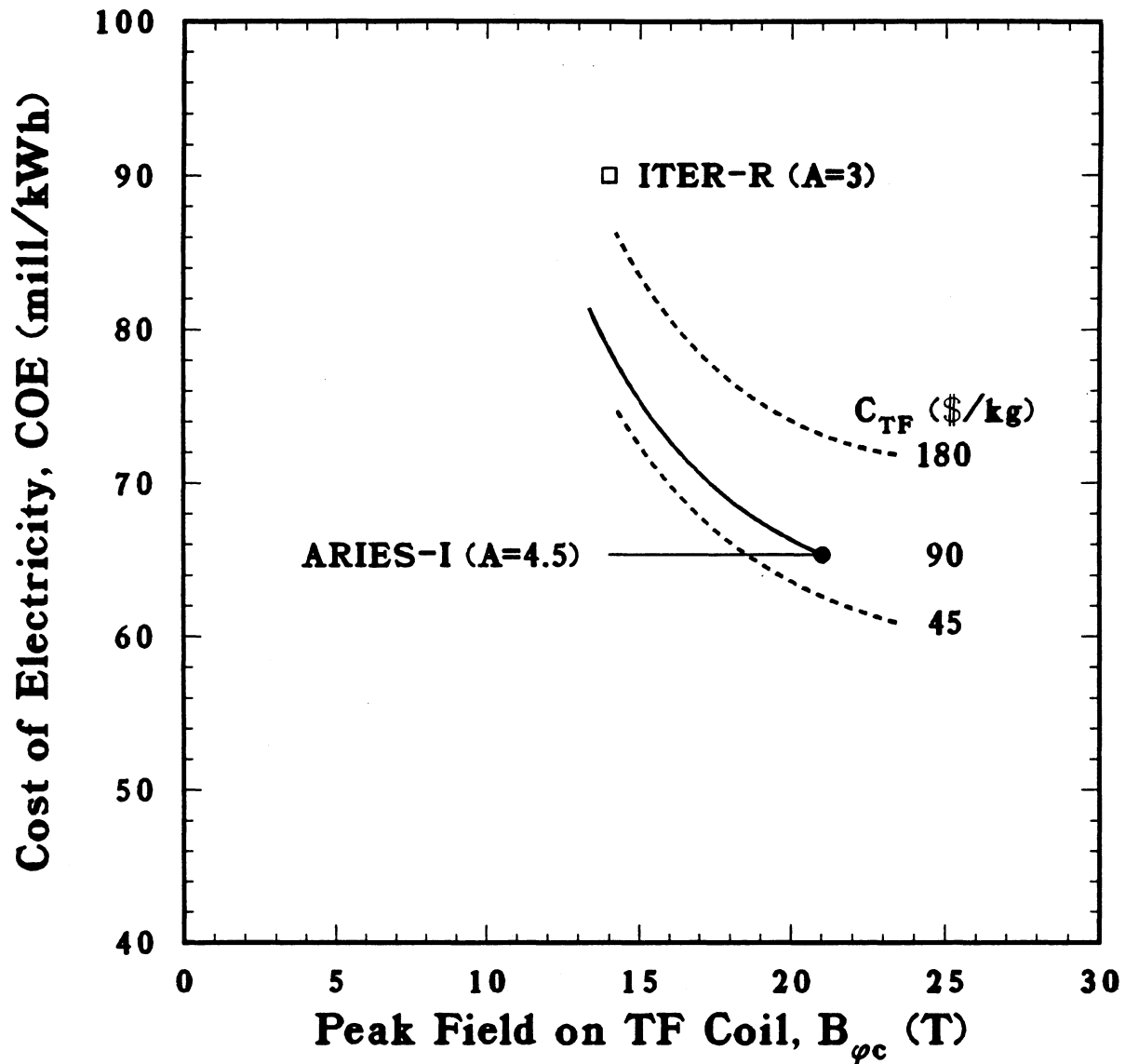


Figure 1.2-1. The variation of COE with maximum field on the TF coil and the sensitivity of the COE to the unit cost of the coil, C_{TF} (\$/kg). A lower limit on the peak magnetic field shifts the minimum COE values to lower values of plasma aspect ratio, but with cost penalties resulting from a higher plasma current and lower bootstrap-current fraction, as is indicated by the 1000-MWe reactor extrapolation of ITER [18].

Table 1.2-I.
Summary Cost Table for the ARIES-I Reactor^(a)

Item	Cost (M\$ 1988)
Land and land rights	5
Structures and site facilities	339
Reactor plant equipment	1,363
Turbine plant equipment	245
Electric plant equipment	137
Miscellaneous plant equipment	50
Special materials	< 1
Total direct cost, TDC	2,141
Construction services & equipment (10% TDC)	214
Home & field office eng. & services (20% TDC)	428
Other cost (5% TDC)	107
Project contingency (10% TDC)	214
Interest during construction	512
Total cost	3,617
<hr/>	
Cost of electricity, COE (mill/kWh)	
Capital return	52.6
O&M (1.43%)	6.7
Blanket replacement	5.6
Decommissioning allowance	0.5
Fuel cost	< 0.1
Total COE	65.3

^(a)In constant 1988 dollars.

are 78 and 46 mill/kWh, respectively, developed on the same cost-accounting basis. Coal-fired plants ($P_E = 2 \times 550$ MWe) costs are projected at 50 mill/kWh [31]. In the above cost estimates for ARIES-I, no safety-assurance cost credits [28] have been taken. The safety credits resulting from the elimination of the N-stamp requirement are estimated to lower the reported COE by 20% to 25%.

1.3. REACTOR PLASMA PHYSICS

The ARIES-I design operates at a relatively high plasma aspect ratio ($A = 4.5$), a low plasma current ($I_p = 10.2$ MA), and a high on-axis magnetic field ($B_o = 11.3$ T). As a result, the poloidal beta is high and a high bootstrap-current fraction of 0.68 is predicted. Because of the low plasma current and high bootstrap-current fraction, only 3.3 MA of current should be driven by external means. Therefore, a steady-state reactor with relatively small current-drive power is possible. Systems-code analysis confirms that an optimum first-stability tokamak reactor operates with high aspect ratio, low current, and high bootstrap-current fraction. The major plasma-engineering parameters are given in Table 1.3-I.

The ARIES-I reactor parameters are found through extensive and self-consistent iterations among magnetohydrodynamic (MHD) equilibrium and stability, transport, current-drive, and edge-physics analyses. Engineering constraints imposed by system integration for a power reactor have also been taken into account.

1.3.1. MHD Equilibrium and Stability

1.3.1.1. Minimizing stored energy of poloidal-field coils

Placing the ARIES-I poloidal-field (PF) coils outside of the toroidal-field (TF) coils permits the use of a multipole expansion technique [34, 35] to describe accurately the PF-coil magnetic fields used in MHD equilibrium computations performed with the Tokamak Simulation Code (TSC) [36] or the HEQ code [37]. Limiting the multipole expansion to hexapole and lower moments minimizes the number of dependent variables required to describe the plasma shape.

Operating at $A \equiv 1/\epsilon = 4.5$ and placing the PF coils outside of the TF coils leads to large stored energy in the PF coils. Using the multipole expansion technique to examine plasma equilibria parametrically for a range of plasma elongation and triangularity

Table 1.3-I.
Plasma Parameters of the ARIES-I Tokamak Reactor

MHD stability regime	First
Current drive	ICRF fast wave
Impurity control and particle exhaust	Double-null divertors
Fueling	Pellet injection
Aspect ratio	4.5
Plasma minor radius (m)	1.5
Plasma vertical elongation, κ_x	1.8
Plasma triangularity, δ_x	0.7
Density-profile exponent factor, α_n	0.3
Temperature-profile exponent factor, α_T	1.1
Average electron density (m^{-3})	1.45×10^{20}
Average ion density (m^{-3})	1.24×10^{20}
α -particle density fraction, n_α/n_i	0.1
Average ^(a) electron temperature (keV)	19.3
Average ^(a) ion temperature (keV)	20.
Plasma radiation fraction	0.5
Energy confinement time (s)	2.5
Bootstrap-current fraction	0.68
Current-drive efficiency ($\text{A}/\text{W}\cdot\text{m}^2$)	0.33×10^{20}
Current-drive power (MW)	97
Peak divertor-plasma temperature (eV)	~ 25
Peak divertor-plate heat load (MW/m^2)	4.5

^(a)Density weighted, volume averaged.

values resulted in a prescription for minimizing the PF-coil stored energy. The results of this analysis are shown in Fig. 1.3-1. Plasmas with shapes corresponding to the region below the δ - κ correlation of Fig. 1.3-1 would not have a separatrix, and those above the correlation would either have a smaller minor radius (larger A) or would require higher multipole moments and larger W_{PF} to maintain the same minor radius.

1.3.1.2. Free-Boundary MHD Equilibria

Given the coil distribution, reference MHD equilibria for ARIES-I are computed using the VEQ code [37], which calculates free-boundary solutions for a given plasma position, shape, and linked poloidal flux while minimizing the stored energy. The plasma shape is chosen to have $\kappa_x = 1.8$ to allow for adequate vertical stabilization and $\delta_x = 0.7$ based on the analysis to minimize the PF-coil stored energy. The plasma pressure profile is consistent with the transport analysis (flat density and narrow temperature profiles), and the current profile is consistent with first-stability operation with high $\epsilon\beta_p$ and with

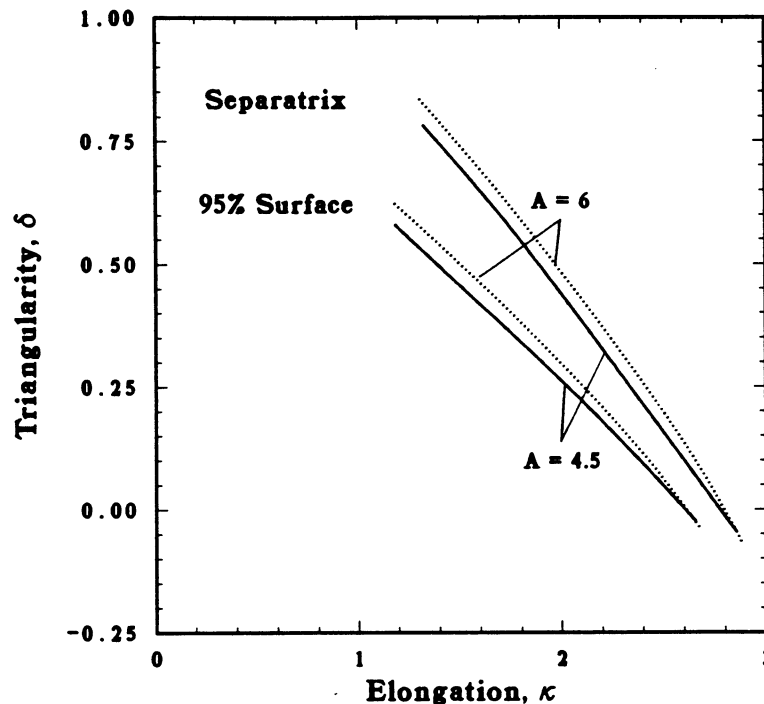


Figure 1.3-1. The correlation between plasma triangularity and elongation, which minimizes the PF-coil stored energy. (Analysis performed for the interim design point I of Table 3.2-I with $A = 4.5$ and $A = 6$.)

current-drive analysis of the driven current-density profile. These constraints led to a choice of profiles that are close to the following pressure, p , and poloidal current-profile, f' , functions:

$$p(x) = p_o \left(\frac{e^{-\alpha x} - e^{-\alpha}}{e^{-\alpha} - 1} \right), \quad (1.3-1)$$

$$ff'(x) = \mu_o R_o^2 p_o \left(\frac{1}{\beta_J - 1} \right) \left(\frac{e^{-\gamma x} - e^{-\gamma}}{e^{-\gamma} - 1} \right), \quad (1.3-2)$$

where x is the poloidal flux normalized to 1 within the plasma. Values of $\alpha = -1.35$, $\gamma = -1.35$, and $\beta_J = 2.29$ were chosen for the equilibrium analysis. The toroidal plasma current density is

$$J_t = R p' + \frac{ff'}{\mu_o R}, \quad (1.3-3)$$

where R is in the direction of the major radius.

The poloidal-flux distribution of the intermediate ARIES-I equilibrium is given in Fig. 1.3-2. Profiles of the plasma pressure, toroidal current density, and safety factor are shown in Fig. 1.3-3. The reference ARIES-I equilibrium, given in Table 1.3-II, is essentially similar to this equilibrium (scaled to $R_o = 6.75$ m).

Analysis leading to the interim MHD equilibria provided an adjustment to the conditions that relate I_p to q , a , B_t , and the plasma shape parameters. This adjusted relationship, used in systems studies, is

$$I_p \bar{q} = 5 a B_t \left[\frac{\epsilon(1.15 - 0.65\epsilon)}{(1 - \epsilon^2)^2} \right] \left(\frac{1 + \kappa_x^2}{2} \right), \quad (1.3-4)$$

where \bar{q} is the average-field safety factor using the averaged poloidal field at the plasma edge. For this class of equilibria, the edge and 95% flux-surface quantities are related through

$$\frac{\delta_x}{\delta_{95}} = 1.59 \frac{\kappa_x}{\kappa_{95}} = (1.13 - 0.08\epsilon) \frac{q_{95}}{\bar{q}} = 1.09. \quad (1.3-5)$$

Different forms of the profile functions can be used to produce equilibria nearly identical to this case in all its global parameters, as are given in Table 1.3-II. The results of the free boundary equilibrium and the PF-coil currents do not change significantly when these different profile functions are used, as long as the global parameters remain unchanged.

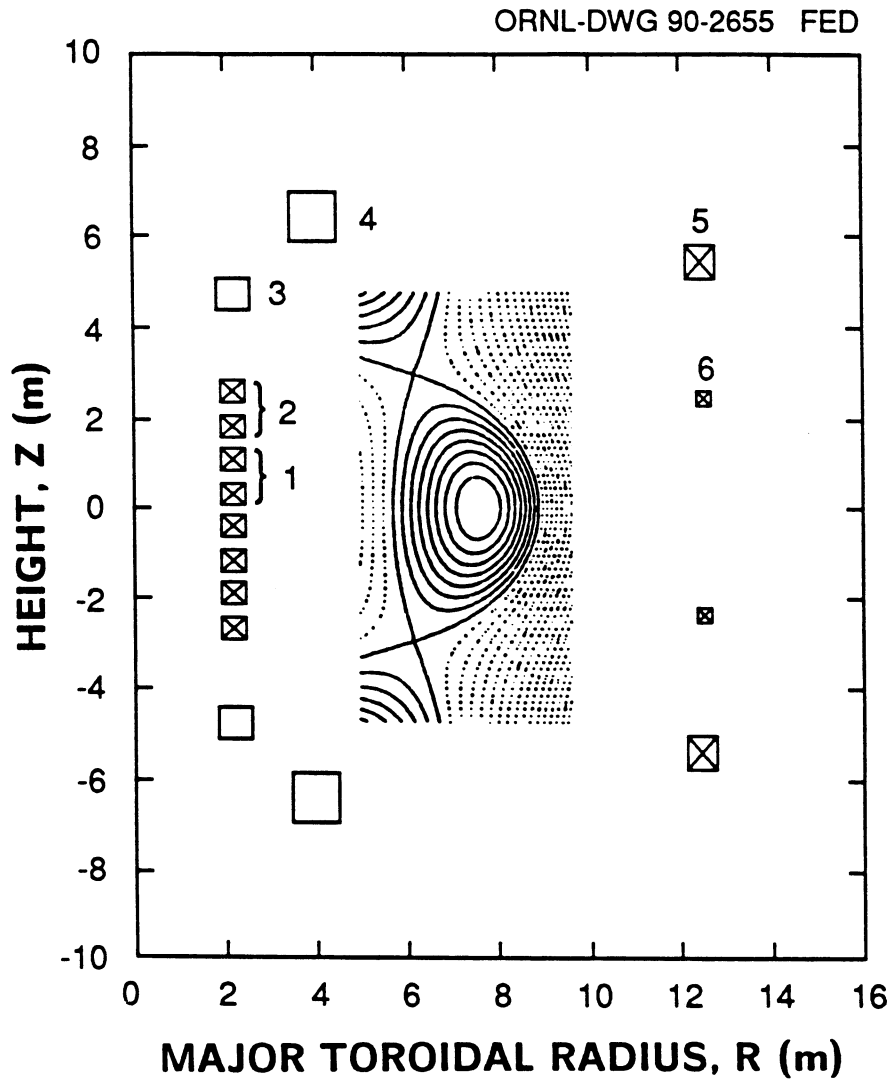


Figure 1.3-2. Plasma equilibrium-flux configuration and PF-coil placement.

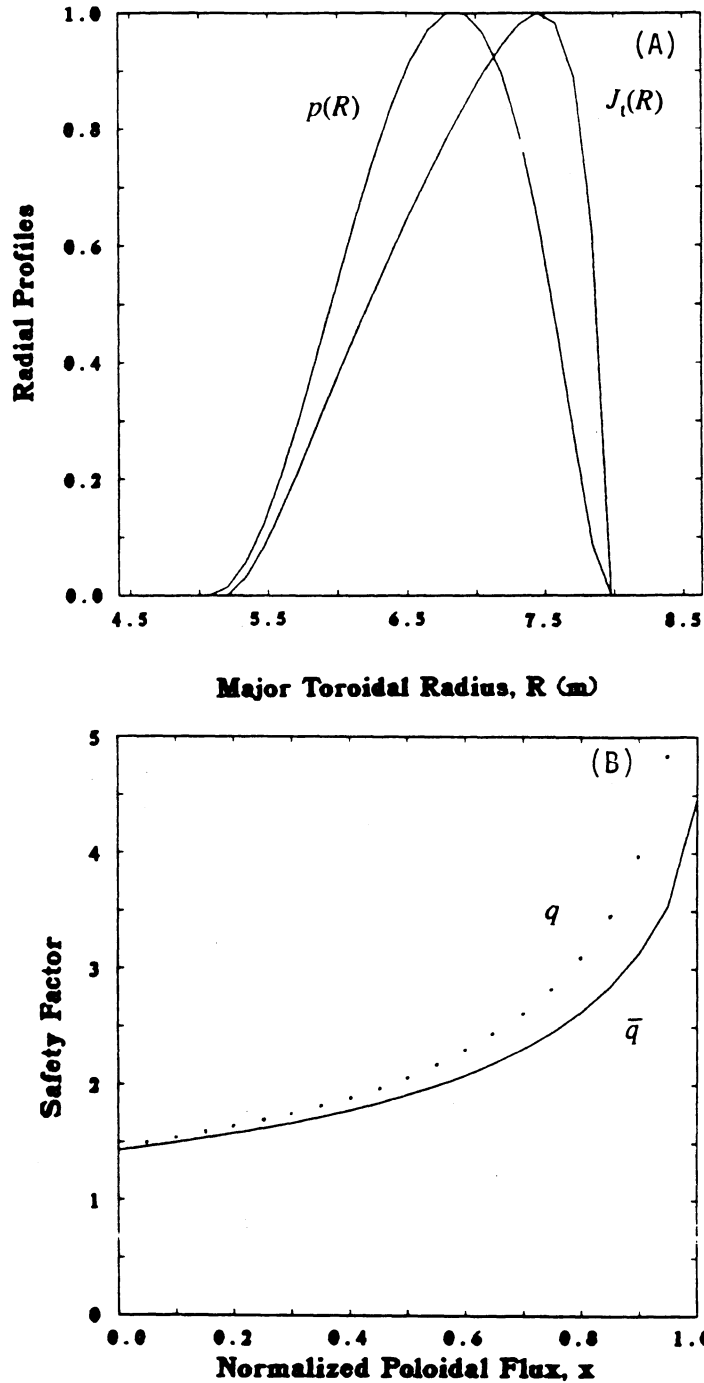


Figure 1.3-3. Profiles of (A) pressure and toroidal current density along the major radius, and (B) q and \bar{q} (the average-field safety factor) along the normalized poloidal flux within the plasma edge. (For plasma equilibrium of Fig. 1.3-2.)

Table 1.3-II.
The ARIES-I Reference Divertor MHD Equilibrium

Major radius, R_o (m)	6.75
Minor radius, a (m)	1.50
External toroidal field at R_o , B_t (T)	11.3
Plasma current, I_p (MA)	10.2
Safety factor on axis, q_o	1.45
Average-field safety factor, \bar{q}	4.40
Safety factor at 95% flux, q_{95}	4.75
Toroidal beta, β (%)	1.92
Poloidal beta, β_p	2.18
Elongation at \times -point, κ_x	1.80
Elongation at 95% flux, κ_{95}	1.60
Triangularity at \times -point, δ_x	0.70
Triangularity at 95% flux, δ_{95}	0.47
\times -point location	
R_x (m)	5.70
Z_x (m)	2.70
Internal inductance, l_i	0.74

Since the ARIES-I reactor uses noninductive methods to assist start-up of the plasma current, the amount of poloidal flux linkage between the plasma and the PF coils can be chosen to reduce the PF-coil stored energy. Some flexibility exists near the condition of minimum stored energy to vary the PF-coil current with a fixed \times -point location: low beta and low linked flux, high beta and low linked flux, and high beta and high linked flux. This data is then used as input to the engineering design of the PF-coil system.

1.3.1.3. MHD Stability Beta Limit

It is usually adequate to examine only the high- n ballooning modes and the low- n ($n = 1$) kink modes to determine the stability beta limit. As an input to design trade-offs involving plasma shaping (profiles, A , and the β limit), our study emphasizes clarifying the dependences of β on A , κ_{95} , q_o , and q_{95} . We use only the traditionally successful profile functions for the analysis. This study, therefore, is limited in its scope, since several other parameters (*e.g.*, δ and the q and pressure profiles) also affect the plasma beta limit. However, this study benefits from an extensive review of the beta limit investigation recently carried out for ITER [38] and from reviews of the large body of information in the literature.

Calculations are carried out for high- A (4.5 and 6.0) ARIES-I plasmas using the PEST equilibrium and stability codes [39] to "fill in" data where needed. The combined data base of the stability analysis covers a range $A = 2.6$ to 6.0, $\kappa_{95} = 1.6$ to 3.2, $q_o = 1.0$ to 2.0, and $q_{95} \leq 5$. The stability data base produced by the PEST code [39] can be represented as the dependence of Troyon factor [3] limit, $C_T = \beta a B_t / I_p$ (in % Tm/MA), on A :

$$C_T \approx 2.8 \left[\frac{1 - 0.4(\kappa_{95} - 1)^2}{(1 - \epsilon)^{1.5}} \right], \quad (1.3-6)$$

which gives $C_T \approx 3.5$ and $\beta \approx 2.06\%$ for the reference plasma parameters in Table 1.3-II.

To ensure complete self-consistency among MHD equilibrium and stability, current drive, and transport analysis, the ARIES-I reference equilibrium is found using a simple pressure function, $p(\psi) = p_o \tilde{\psi}^\alpha$, where $\alpha = 1.4$ and $\tilde{\psi}$ is the normalized poloidal flux. The equilibrium flux contours and profiles of safety factor and toroidal current density of the reference equilibrium are similar to those displayed in Figs. 1.3-2 and 1.3-3. Several sequences of equilibria were tested for stability at different aspect ratios and safety factors. In the range $4.5 \leq A \leq 6.0$, it was always possible to obtain stability at Troyon ratios $C_T \lesssim 3.2$. For the geometry of Table 1.3-II, stable equilibria were found in the range $1.56\% \leq \beta \leq 2.60\%$ as the axis safety factor varied from, respectively, $q_o = 1.50$ to 1.10. All equilibria were stable to $n = \infty$ ballooning modes (tested with the Phillips code [40]) and were stable to $n = 1$ external kinks (tested with PEST II) with the conducting wall at infinity. Generally the edge safety factor, q_a , was roughly four times the axis value, and it was found necessary to avoid integer values of q_a in order to ensure kink stability. Design values of $C_T = 3.2$ (corresponding to $\beta = 1.9\%$) and $l_i = 0.74$ are therefore adopted for ARIES-I reactor. This result is considered conservative relative to the preceding indications of Eq. (1.3-6).

1.3.1.4. Vertical stability

Vertical stability is an important issue for ARIES-I because of the moderate-to-high aspect ratio ($A \geq 4.5$) and the high separatrix elongation ($\kappa_x = 1.8$). A toroidally continuous conducting shell is required to retard the growth of an externally excited vertical instability with a time constant ranging from an Alfvén time ($\tau_A \sim 10 \mu\text{s}$) without a shell to the electrical L/R time constant of the shell, $\tau_{L/R}$. The passive stabilization provided by this shell must be augmented by an active feedback system that provides vertical stability for times $\gtrsim \tau_{L/R}$. A rigid-plasma model (PSTAB) [41] and linear (NOVA-W) [42] and nonlinear [Tokamak Simulation Code (TSC)] [36] deformable-plasma models are used to estimate the conductor location, and size required for passive stabilization. Time-dependent TSC simulations are used to determine the current, voltage, location, and size of the feedback coils.

In a power reactor, placement of passive (metallic) stabilizer elements close to the plasma cause severe engineering difficulties including: (1) neutron damage and activation, (2) nuclear heating which requires active cooling, (3) adverse effects of tritium breeding, and (4) difficulties in assembly/disassembly of components and of maintenance. It is, therefore, desirable to place the passive elements away from the plasma, preferably behind the blanket (at a distance of $\sim 0.6a$ from the plasma surface in ARIES-I). A preliminary analysis of the maximum allowable distance permitted between the plasma and the passive stabilizer elements for vertical stability was performed with the PSTAB [41] code. This analysis led to the choice of $\kappa_{95} = 1.6$ at $A = 4.5$ for ARIES-I. The accuracy of the results of the PSTAB rigid-plasma model was then checked by benchmarking the $\kappa_x = 1.74$ case against the TSC and NOVA-W deformable-plasma models. To calculate τ_v , a radial magnetic field was applied for $1 \mu\text{s}$ to produce an initial ~ 3 -mm vertical displacement of the plasma. The plasma simulation was then continued until the equilibrium effects of the initial perturbation were damped out and the vertical instability asymptotically relaxed to a linear growth rate, as reported by inboard and outboard pickup coils. The results of the benchmark case are given in Table 1.3-III. Agreement between the NOVA-W result and the mean TSC result is good at 4% for τ_v and 2% for f , but agreement between the PSTAB result and the mean TSC result is 20% for τ_v and 19% for f .

The vertical stability of the reference ARIES-I design was studied using the NOVA-W code. This analysis included the stabilization elements behind the blanket, both on the inboard and outboard locations as well as the tungsten divertor plates. The results indicate that the growth time for the axisymmetric mode is 330 ± 5 ms.

Table 1.3-III.
Vertical Stability Benchmark for the ARIES-I Design

Code	Vertical-Stability Time Constant, τ_v (ms)	Stability Parameter, $f = 1 + \tau_v/\tau_{L/R}$
PSTAB [41]	217	1.88
TSC [36]	175 – 186	1.56 – 1.60
NOVA-W [42]	173	1.55

Active feedback. The active-feedback power requirements were determined from TSC simulations. The feedback coils were simulated with a 0.1-m \times 0.1-m cross section of room-temperature copper alloy with a conductor filling fraction of 0.7. The reference design includes a pair of coils outside the TF coils which are easily accessible for maintenance. The reactive power required to drive this coil is ~ 2 MVA, well within the 26 MW of recirculating power set aside for miscellaneous plant needs.

1.3.2. Transport Analysis

The 1-1/2-D, time-dependent BALDUR transport code [7] was used to simulate steady-state core-plasma behavior for the ARIES-I tokamak design and to study the time evolution of plasma density and temperature from a few keV (*i.e.*, typical of ohmic discharges) to a steady-state fusion plasma. In addition to the analyses of the approach to ignition and thermal stability, the BALDUR simulations were used to study fueling of the ARIES-I plasma, the resultant density and temperature profiles, and helium ash buildup and exhaust. The parameters of the steady-state ARIES-I plasma were also used to benchmark the 0-D results of the systems code. Several physics models including an estimate for synchrotron radiation losses and transport models were incorporated in BALDUR for ARIES-I transport analyses.

The transport model that was implemented in the BALDUR transport code was adapted from Houlberg's plasma modeling work on the compact ignition torus [43]. This model is purely empirical and is designed to reproduce the global empirical scalings of

energy and particle confinement time. In addition to global agreement with empirical scalings, this model has been used successfully at the Princeton Plasma Physics Laboratory to predict the density and temperature profiles in certain pellet-fueled TFTR discharges [44]. Houlberg has also been successful in predicting plasma density and temperature behavior on JET discharges using this transport model in the WHIST transport code [43].

The ARIES-I transport model is based on the following assumptions: (1) The ion and electron radial thermal diffusivities are equal. (2) The radial particle-diffusion coefficient, D_{\perp} , is half of the radial thermal diffusivity, χ_{\perp} . (3) The edge thermal diffusivity is five times that at the center. (4) There exists an anomalous inward particle pinch for ions and electrons proportional to the particle diffusion coefficient. The inward pinch is added, following Stotler [44], as a refinement to obtain improved agreement between BALDUR simulations and TFTR discharges in terms of density profiles.

The evolution of the ARIES-I plasma from an ohmic-like plasma with a temperature of 5 keV on axis (typical of plasmas in ohmic equilibrium) to steady-state, fusion-burn conditions was analyzed. The fast-wave current-drive system was used to heat the ARIES-I plasma to ignition. Typically, the ARIES-I plasma achieved ignition in about 5 s and steady state in approximately 20 s of plasma simulation time. The transport simulation of the ARIES-I plasma gives a ^4He particle-confinement time of approximately 7.76 s. The ^4He ash buildup in steady state is 8.6%.

The reference fueling scenario for the ARIES-I plasma includes the injection of 2-mm-radius pellets made of a 50:50 deuterium-tritium (DT) mixture at a frequency of 3 Hz. The pellets are injected at the mid-plane. In general, it was found that for the range of pellet size and speed considered, pellets would ablate in the outer 1/3 to 1/2 of the plasma radius (corresponding to pellet speeds of 5 and 20 km/s, respectively). In the simulations, the pellet fuel ions were transported towards the center by the anomalous inward particle pinch. The density profile was found to be very broad and, without an anomalous pinch term, the density profile would be even flatter.

The plasma pressure and density profiles are found to scale roughly as

$$p(r) = p_o \left[1 - \left(\frac{r}{a} \right)^2 \right]^{\alpha_p}, \quad (1.3-7)$$

$$n(r) = n(a) + p_o \left[1 - \left(\frac{r}{a} \right)^2 \right]^{\alpha_n}, \quad (1.3-8)$$

with $\alpha_p \simeq 1.4$ and $\alpha_n \simeq 0.3$. These profiles were used in other plasma analyses. The electron and ion temperature profiles however are not similar, the electron temperature

being flatter than that of the ions. This difference in the temperature profiles is attributed to the flattening of the electron temperature profile due to a more accurate synchrotron-radiation model in the simulation.

The steady-state plasma-parameter values from the BALDUR simulations are compared to 0-D prediction of the systems code in Table 1.3-IV and good agreement is found. Recall that this plasma transport model predicts the density and temperature profiles of certain TFTR and JET tokamak discharges quite accurately. This empirically benchmarked tokamak transport model predicts ignition and a steady burning plasma for the

Table 1.3-IV.
Comparison of BALDUR Simulation Results with 0-D Predictions
for ARIES-I Plasma Parameters

Plasma Parameters	BALDUR	0-D Simulations
Current-drive power (MW)	96.7	96.7
Alpha power (MW)	375.	385.
Energy confinement time (s)	2.49	2.53
Confinement-enhancement factor, $f_{H,Riedel-Kaye}$	2.80	2.52
Particle confinement time (s)	7.76	9.39
Average electron density (10^{20} m^{-3})	1.39	1.45
Average ion density (10^{20} m^{-3})	1.20	1.24
Average electron temperature ^(a) (keV)	18.3	19.3
Average ion temperature ^(a) (keV)	20.7	20.0
Toroidal beta (%)	2.00	1.90
Effective plasma charge, Z_{eff}	1.73	1.65
Core-plasma radiation fraction, f_{rad}	0.48	0.49
⁴ He ash concentration (%)	8.58	10.0

^(a)Density weighted.

ARIES-I tokamak design as long as the τ_E enhancement factor of 2.5 to 3 over L-mode can be attained. It should be noted that a large portion of the ARIES-I plasma energy is radiated in the form of synchrotron radiation because of the large on-axis magnetic field, the high electron temperature (~ 20 keV) which improves the current-drive efficiency, and the poorly reflecting first wall (SiC composite). At steady-state burn conditions, 52% of the plasma power is radiated (48% by synchrotron, 4% by bremsstrahlung). The corresponding plasma energy-confinement time (convection and conduction) is 2.3 s, corresponding to a confinement enhancement factor of 2 to 3 over the L-mode depending on the empirical scaling law considered.

1.3.3. Start-Up and Burn Cycle

The time required for plasma start-up and shut-down for the steady-state ARIES-I design is short when compared with the burn period, and is considered to be an occasional event in the reactor lifetime. The start-up, therefore, can be performed slowly and under optimal conditions (*e.g.*, minimum power, stress, *etc.*). Furthermore, a rapid current ramp-up is undesirable because of increased power requirements and the demands on the PF-coil system to keep the plasma in equilibrium. For the ARIES-I study, a quantitative modeling and assessment of the plasma start-up scenario was carried out, assuming disruption-free plasma and ensuring compatibility of the auxiliary-power system needed for start-up with the current-drive system required for steady-state operation. While a minimum-power requirement or minimum-energy input has been used frequently as a criterion in designing the start-up phase, it is of secondary importance in the context of a steady-state reactor.

Plasma initiation, current start-up, and current ramp-up have been demonstrated in a notable experiment on PLT [45] using only lower-hybrid waves. A record current-drive efficiency, $\gamma (\equiv n_e I_\phi R_T / P_{CD})$, of 0.34×10^{20} A/W-m² was obtained on JT-60 [46], and a one-hour-long tokamak discharge sustained entirely by lower-hybrid waves has recently been reported in TRIAM-1M [47]. The data base for lower-hybrid start-up and current drive, therefore, is strong and the physics understanding is mature. In ARIES-I, a current ramp-up scenario based on lower-hybrid waves is envisioned, with an input power, P_{LH} , of not more than a few 10s of megawatts. Electronic phasing of the lower-hybrid waveguide grille is a crucial element in this endeavor. At 0° phasing and modest power levels, the plasma is initiated at full radius. The increased power input is balanced against plasma convective losses through toroidal drift which can be adjusted by the vertical field [48]. By introducing a non-zero phase shift between adjacent waveguides in the grille, the current can be initiated and ramped up.

A profile-averaged (0-D), coupled plasma-current model is used for the start-up studies. Analyses indicate that about 20 MW of lower-hybrid power is required to ramp up the plasma current to its full value at low density ($\simeq 1.1 \times 10^{19} \text{ m}^{-3}$) in 2100 s at a characteristic rise-time of 600 s. Since the density is low, the ions remain relatively cold (2 to 3 keV) while T_e increases to values limited by transport and synchrotron radiation losses ($> 10 \text{ keV}$). Penetration of the lower-hybrid waves to the core is still possible at this electron temperature.

After achieving full plasma current, the auxiliary heating and subsequent steady-burn phase is started by increasing the plasma fueling rate and injecting ICRF fast-wave heating and current-drive power. The fast-wave frequency should be set at 172 MHz for second-harmonic deuterium-resonance heating on axis. The density and fusion power are increased to their steady-state levels in $\sim 400 \text{ s}$, using fast-wave power of $\sim 100 \text{ MW}$. As the plasma approaches full-power steady-state operation, the appropriate conditions for efficient fast-wave current drive are set up. The ICRF frequency and power from the launcher modules are adjusted together with the phase shift between adjacent guides to start generating current in the core. Simultaneously, the lower-hybrid power can be decreased to provide the necessary current drive in the plasma periphery.

It should be noted that the simulation results reported in this section represent only a preliminary assessment of a plausible start-up scenario for ARIES-I. Other lower-hybrid-power and fueling strategies should be examined in the course of future work in an effort to reduce the start-up power requirement even further while simultaneously meeting a range of plasma constraints.

1.3.4. Current Drive

Steady-state plasma operation is preferable for a commercial reactor because of the many undesirable features of pulsed operation, such as thermal fatigue of in-vessel components and magnets and the requirement for a thermal-energy storage system. The advantages of steady plasma operation should be balanced against the recirculating electric power needed to maintain the plasma current; for an economical steady-state reactor, the recirculating power fraction should be less than 20%. This can be achieved by reducing the amount of plasma current to be driven by external means (*i.e.*, minimizing the total plasma current and maximizing the bootstrap-current fraction) and by using an efficient, cost-effective current-drive technique.

Three parameters affect the choice of current-drive system: (1) the fraction of the equilibrium current provided by the bootstrap effect, f_{BS} ; (2) the normalized efficiency of

current generation within the plasma, $\gamma \equiv n_e I_p R / P_{CD}$ (where n_e is the average electron density, R is the plasma major radius, and P_{CD} is the absorbed power in the plasma); and (3) the electrical efficiency of the current-drive system, η_{CD} , including the efficiency of the source and transmission, and the fraction of launched power absorbed in the plasma.

One key to increasing the bootstrap-current fraction, f_{BS} , is to operate at high poloidal beta (as in ARIES-I) by raising the on-axis safety factor, q_o , significantly above unity. The bootstrap fraction was estimated for a series of stable plasma equilibria using the best available transport coefficients [5]. Values of $f_{BS} > 0.8$ are achievable with $q_o \simeq 2.1$. The penalty associated with a large safety factor is the reduction of the toroidal beta. Trade-offs between the bootstrap fraction and the toroidal beta have led to the ARIES-I reference design with $f_{BS} = 0.68$, $q_o \simeq 1.3$, and a flat density profile. The bootstrap-current fraction could be increased further (up to 0.9) if a peaked density profile could be provided, which would also increase the fusion power.

Among the current-drive options considered, some had efficiencies that were too low (either low γ or low η_{CD}). Some other options were set aside for other reasons (*e.g.*, lower-hybrid waves are inaccessible to high electron temperatures and many options such as helicity injection involve very speculative physics). The two remaining candidates, the negative-ion neutral beam and ICRF fast waves were studied in detail. Both options are shown to require roughly the same recirculating power. Neutral-beam current drive has a more developed experimental data base. However, the ICRF fast wave is chosen as the reference driver because of its advantages in fusion-power-core engineering and system integration, and because the source technology is more mature than that of multi-MeV negative-ion-beam sources. The ICRF source consists of klystrodes, which are presently used as ultra-high-frequency transmitters in television stations [49]. Folded waveguides are used as the wave launcher [10]. The wall-plug-to-plasma efficiency of the system is estimated at 72% and the unit cost is \$1/W.

Significant improvement in the theory of fast-wave current drive was achieved during this study by including the effects of transit-time magnetic pumping and electron trapping. It was found that these two modifications to the current-drive theory offset each other to some degree. As shown in Fig. 1.3-4, the present, most accurate calculations of γ at various electron temperatures are fortuitously in good agreement with the earlier theory. This figure demonstrates that γ and also the bootstrap-aided efficiency, γ^B , increase with temperature.

For the reference ARIES-I design, the wave frequency is set at 141 MHz to locate the second-harmonic of deuterium resonance on the outboard edge. The wave spectrum and the launcher position and phasing are chosen so that the sum of the driven and bootstrap

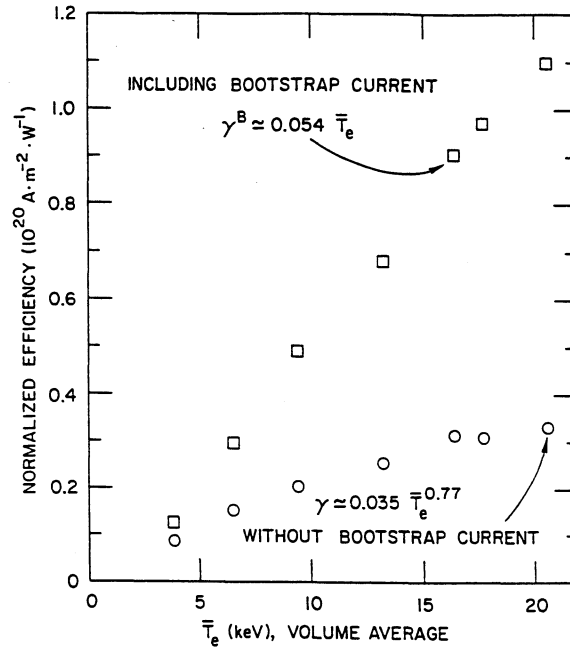


Figure 1.3-4. Fast-wave current-drive efficiency plus bootstrap at finite aspect ratio for stable MHD equilibria: $A = 4.5$, $\alpha_n = 0.3$, $\alpha_T = 1.1$, $Z_{eff} = 1.6$, and single-pass absorption ($\omega \sim 2.5\Omega_{T0}$).

currents matches the equilibrium current-density profile (Fig. 1.3-5). The current-drive power is ~ 97 MW. The normalized efficiency is $\gamma = 0.33 \times 10^{20}$ A/W-m² in the absence of bootstrap current ($\gamma^B = 0.98$ with the benefit of the bootstrap effect). The ICRF power is also used for heating the plasma to ignition. Provision for a small amount of lower-hybrid current-drive power (~ 10 MW) is made to permit current-density profile control and low-density start-up.

The high magnetic field (11.3 T) in ARIES-I provides the unique environment for utilizing the attractive features of the folded waveguide [10] as a wave launcher for current drive. Each waveguide can be considered as a TE₁₀₁ rectangular cavity folded in the long transverse dimension, with the front end covered by a polarizing plate as shown in Fig. 1.3-6. The compact and robust structure, together with its high-power handling capability (~ 40 MW/m² $\sim 4 \times$ loop) [50], makes it superior to loop antennas for reactor application. To couple to a traveling wave spectrum centered at $N_{||} = 1.8$, a 4.0 m \times 0.6 m, 12-waveguide toroidal-array module, phased with $\Delta\phi = 90^\circ$, is used. Two such poloidally stacked modules, shown in Fig. 1.3-6, are located slightly above the equatorial outboard plane to couple 92 MW of power at 141 MHz to drive the required seed current in ARIES-I, while occupying only 0.77% of the first-wall area. The direc-

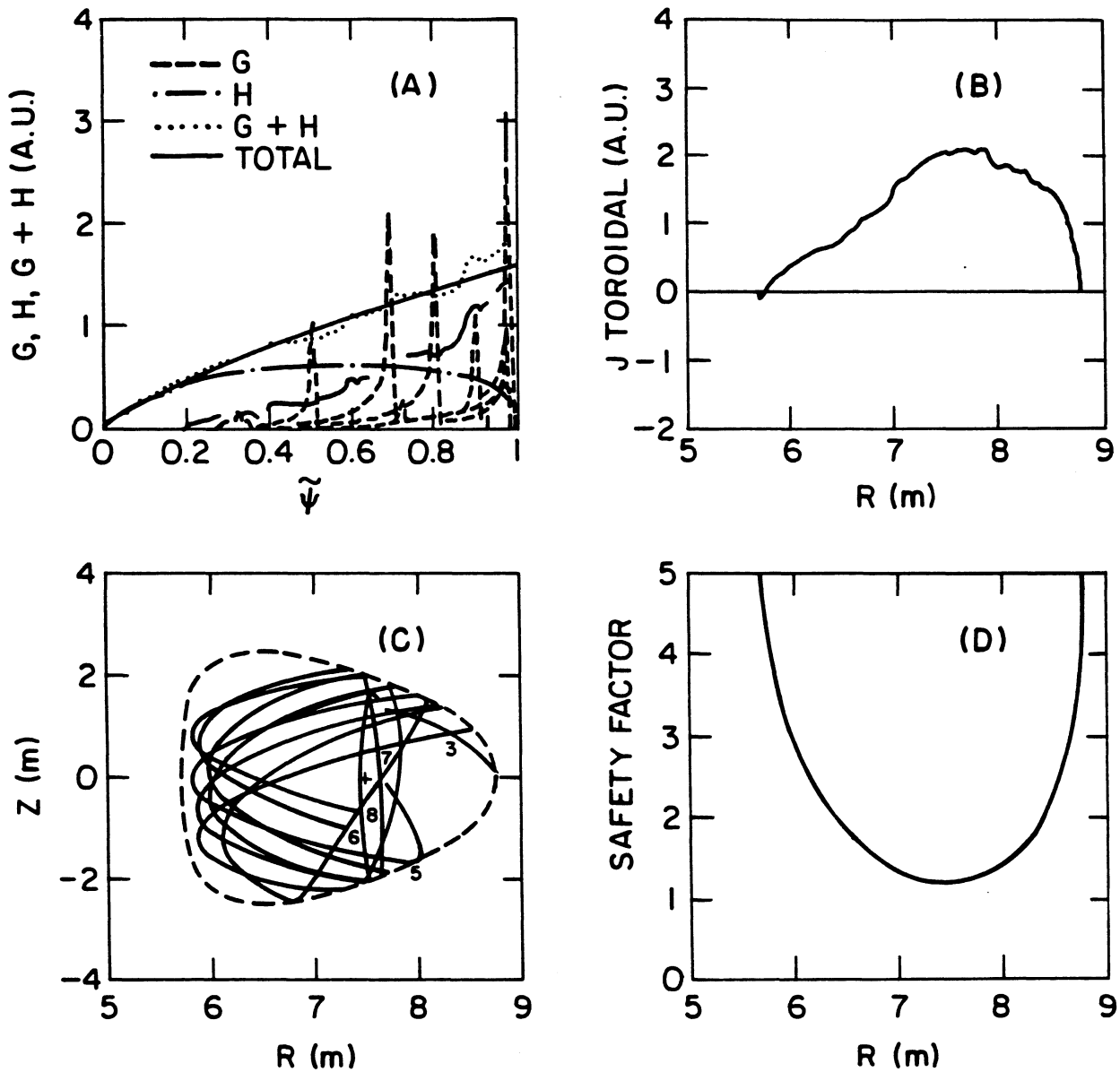


Figure 1.3-5. Converged, stable ARIES-I equilibrium with fast-wave current drive and bootstrap contribution: (A) Current profile contributions from fast wave, G , bootstrap effect, H , and the sum of $G+H$; (B) Toroidal current profile at mid-plane; (C) Projection of five rays (#3: lower-hybrid; #5-8: fast wave) onto minor cross section; and (D) Safety-factor profile at mid-plane.

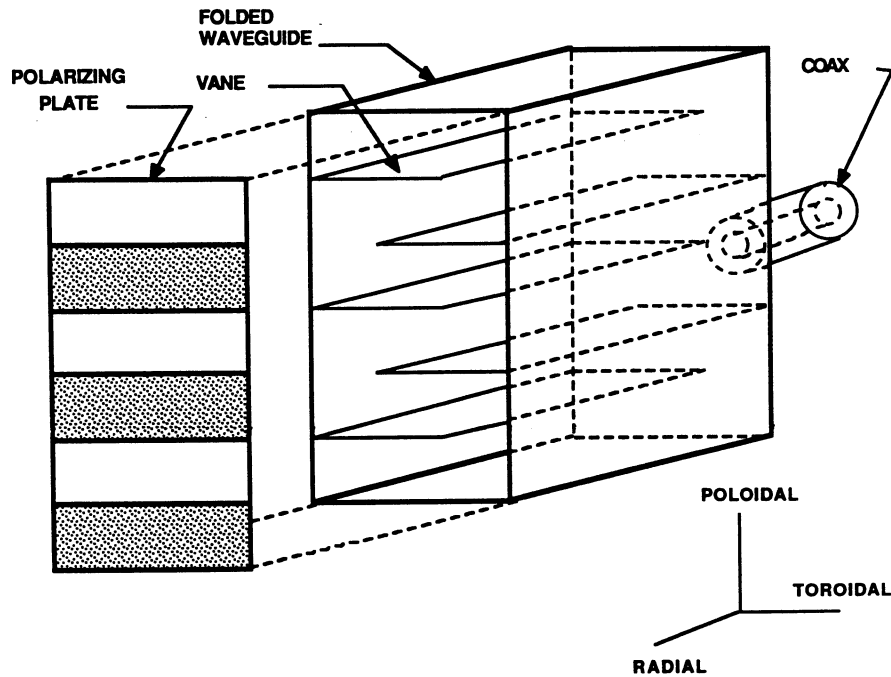


Figure 1.3-6. Isometric view of folded waveguide.

tivity of each module is estimated to be about 95% while the power coupling efficiency is found to be 95.5% for the high scrape-off density profile.

For safety and environmental reasons, the waveguide cavity will be manufactured from SiC-composite structural material. Since the SiC plate is essentially transparent to the radio-frequency (RF) wave, it is possible to envision the cavity as a vacuum-sealed rectangular box coated on the inside with copper. Sustaining a high-quality vacuum inside the cavity will then further enhance the high-voltage capability of the launcher.

The RF system, which includes the coax, vacuum feedthrough, matching and phase-shift circuits, and the RF source, will use off-the-shelf technology primarily, and only a moderate development program is needed to upgrade its key components to the desired operating parameters. Among the variety of tubes considered, the most viable choice appears to be the klystron [49], which is a linear beam device having the desirable features of both a klystron and a tetrode. Present-day klystrons are used as transmitters in UHF-TV stations and are available in sub-MW steady-state units having an efficiency of 70% to 75%. A 90% efficiency for these devices should be within reach with a modest development effort. The wall-plug to first-wall efficiency for the RF system is projected to be 72%, at a unit cost of \$1/W.

1.3.5. Edge Physics

The high power density and plasma temperature in the fusion power-reactor regime must be reduced considerably in the divertor region to reduce the surface heat flux and avoid erosion where the plasma contacts a material target surface. Evidence shows that this can be accomplished with a divertor operating in the high-recycling mode, *i.e.*, exhibiting a high density and low temperature at the divertor target. The high-recycling mode at reactor-relevant parameters has not been demonstrated experimentally. For modeling the ARIES-I edge plasma, two 2-D edge-plasma computer codes, BRAAMS [11] and EPIC [12], were used. These codes were compared previously for the ASDEX divertor tokamak experiment and found to be in reasonably good agreement in that experimental plasma regime [52]. Both codes use a poloidal magnetic-flux geometry. This is represented by analytic transformations in the BRAAMS computational grid while in the EPIC grid this is computed directly from the MHD magnetic-flux equilibria data. The BRAAMS code has an analytic neutral model in which the recycling is dependent upon a recycling parameter, R , while the EPIC code models the neutrals as a diffusing fluid and the plasma-neutral interactions evolve a fully self-consistent recycling regime. Both codes include large, anomalous, inward advective-flux terms (-20 m/s) in order to arrive at realistic radial scale lengths at the mid-plane for the plasma density (≤ 0.1 m).

To ensure consistency with 0- and 1-D BALDUR core-plasma simulations, the edge-plasma analysis uses the particle and heat fluxes at the separatrix as inputs. The computational analyses indicate that the resultant plasma density at the separatrix would be high ($\sim 10^{20}$ m⁻³) and a high-recycling divertor is formed. Furthermore, assuming that the ratio of α -particle to electron density is similar to that of the core plasma, calculations show that effective ash exhaust is achieved. The ARIES-I edge-plasma parameters are given in Table 1.3-V. The EPIC electron temperature distribution is shown in Fig. 1.3-7. The peak plasma temperature at the separatrix strike point is about 20 to 25 eV, while the peak heat flux is in the range of 3 to 4.5 MW/m².

First-wall erosion rates were determined assuming the carbon is sputtered from the SiC. The average sputtering yield is taken to be 0.04. No credit is taken for redeposition since the sputtered material is swept towards the divertor. The sputtering contributions from D, T, and α -particles are comparable and the total first-wall erosion is computed to be 0.3 mm/y. The divertor target plate is designed with a thin tungsten coating on the SiC-composite coolant tubes. The estimated tungsten erosion rate, dominated by α -particles, is 0.5 mm/y (assuming a conservative value of 0.15 for the ratio of net-to-gross erosion). Thermal response of the divertor plate to full-power plasma disruption was analyzed using 2-D thermal and thermo-fluid dynamic codes. It was found that each

disruption results in ablation of 48 μm from the tungsten coating and the divertor target can survive at least 20 full-power disruptions before any need for recoating.

Table 1.3-V.
ARIES-I Edge-Plasma Parameters

	B2 Results ^(a)	EPIC Results
Separatrix		
Plasma density (10^{20} m^{-3})	0.9 – 1.3	1
Ion temperature (eV)	520	300
Electron temperature (eV)	260	220
Mid-plane scrape-off layer		
Density e-folding length (cm)	4	5
Power e-folding length (cm)	2	2
First-wall plasma density (10^{18} m^{-3})	1.2	3
First-wall plasma temperature (eV)	25 – 30	20 – 25
Divertor plasma (peak value)		
Ion temperature (eV)	11	22
Electron temperature (eV)	22	25
Plasma density (10^{20} m^{-3})	9	8
Particle flux ($10^{23}/\text{m}^2\text{-s}$)	2.2	2.6
Heat flux (MW/m^2)	4.5	3.0

^(a) For recycling parameter, $R = 0.98$.

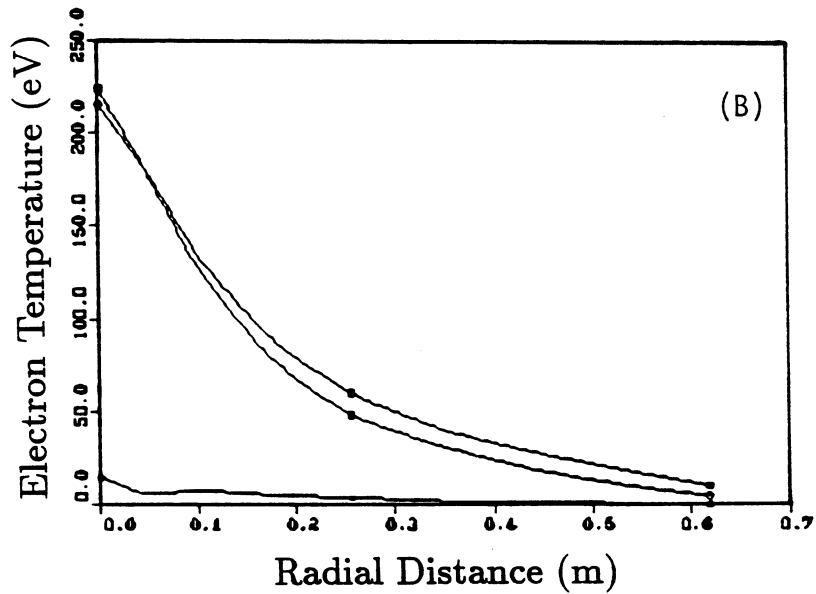
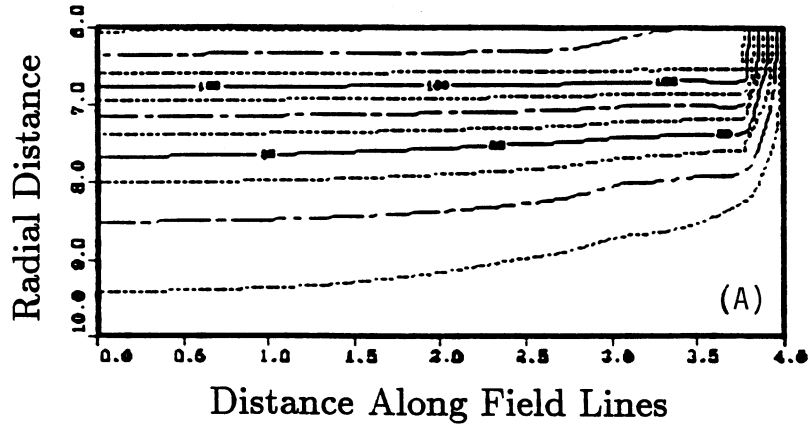


Figure 1.3-7. (A) Plasma electron temperature contour in the scrape-off layer; and (B) Radial electron temperature profile in the scrape-off layer at the outboard plane, at the \times -point, and across the divertor target.

1.3.6. Reactor Plasma-Physics R&D Needs

The ARIES-I reactor parameters are found through extensive and self-consistent iterations among MHD equilibrium and stability, transport, current-drive, and edge-physics analyses. Engineering constraints imposed by system integration for a power reactor have also been taken into account. The regime of operation of the ARIES-I plasma is different from current tokamak experiments in many aspects including:

1. Operating at a relatively high plasma aspect ratio ($A \equiv 1/\epsilon = 4.5$), a low plasma current ($I_p = 10.2$ MA), a high poloidal beta ($\epsilon\beta_p = 0.6$), and plasma current profiles characterized by on-axis safety factor, $q_o \approx 1.3$, and 95% flux safety factor, $q_{95} > 4$.
2. Operating at $A \equiv 1/\epsilon = 4.5$ and placing the PF coils outside the TF coils leads to large stored energy in the PF coils. Minimizing this energy will place constraints on the choice of plasma elongation, κ , and triangularity, δ .
3. Operating at MHD-stability beta limit against high- n ballooning and $n = 1$ kink modes with the conductive wall at infinity, and using plasma profiles consistent with current-drive (driven current density) and transport (flat density and narrow temperature profiles) analyses.
4. Placing the passive conductor for stabilizing the vertical motion of the plasma behind the blanket, which reduces the engineering constraints (cooling, neutron damage, *etc.*), leads to a reduced plasma elongation, $\kappa_x = 1.8$.
5. Operating an ignited plasma with high synchrotron radiation caused by high on-axis magnetic field, high electron temperature, and a poorly reflective first wall. Absence of deep fueling techniques leads to a flat density profile.
6. Operating at steady state utilizing ICRF fast-wave current drive to supplement a significant bootstrap current.
7. Operating with poloidal divertors in a double-null configuration and in high-recycling mode with high separatrix density.

The specific R&D needs for each plasma physics area are described below.

Equilibrium, stability, and transport R&D needs. The ARIES-I plasma operates in the first stability regime and the plasma beta is consistent with the predictions of the MHD stability theory, which has proven to be in remarkable agreement with experimental findings. ARIES-I operates at a relatively high plasma aspect ratio and a low plasma current to achieve a high poloidal beta ($\epsilon\beta_p = 0.6$) and a high bootstrap-current fraction of 68%. It is further argued that the trade-off of plasma aspect ratio with current ensures that the device has adequate confinement time. The experimental data base for high $\epsilon\beta_p$ plasmas is growing rapidly and large bootstrap-current fraction has been observed in many experiments. Separately, recent results from TFTR confirm the ARIES-I tradeoff of plasma aspect ratio with current.

Even though experimental trends are encouraging, further experiments with large plasma aspect ratio and high $\epsilon\beta_p$ are needed, preferably in a large tokamak, to provide an adequate data base and to confirm the ARIES-I regime of operation. These experiments should demonstrate that ARIES-I-type plasma profiles can be maintained at steady state (longer than plasma skin time) with current-drive power levels estimated for ARIES-I. Furthermore, the scaling of plasma energy confinement at high aspect ratio should be established.

Of course, the data base for burning-plasma dynamics in systems dominated by α -particle heating is non-existent. Issues such as α -particle-driven instabilities, α -particle transport and removal characteristics, and thermal stability of fusion burn can only be addressed in the next generation of tokamak experiments with a burning-plasma core. The value of the α -particle confinement time has a strong impact on the performance of the reactor.

Although the ARIES-I plasma profiles (density and temperature) are consistent with present tokamak experience, it is not clear that a burning plasma will have similar profiles. The ARIES-I density profile is quite flat. Utilizing deep-fueling techniques and/or anomalous inward-pinch processes to produce a more peaked density profile can result in improved reactor performance and should be pursued. Experiments should be undertaken to resolve the degree to which fueling and heating by the current-drive system can affect and control the plasma profiles; the results could lead to achieving a higher Troyon coefficient and plasma beta.

The ARIES-I reactor is designed to absorb the losses, forces, and voltage transients resulting from a full-power disruption. However, it is argued that because of steady-state operation and large on-axis safety factor, the probability of disruption is very small (*i.e.*, disruptions are caused by system faults). Understanding causes of disruption and means to avoid and/or control disruptions are critical issues that should be resolved.

Start-up R&D. There appear to be no major R&D issues related to lower-hybrid current ramp-up and current drive specific to ARIES-I since the relevant data base is already well developed. Acquiring ample operational experience in plasma initiation, current start-up, and current ramp-up on a large tokamak reactor, such as ITER, is most important. Similar experience with the auxiliary-heating and density-rise phase, smooth transition from lower-hybrid to fast-wave current drive, and the approach to steady-state burn will be valuable. The start-up transient codes should be improved by incorporating more precise physics models, particularly in the areas of current drive and transport. This may entail the inclusion of self-consistent plasma-profile evolution in the modeling analysis. It is noted that the start-up simulation results represent only a preliminary assessment of a plausible start-up scenario for ARIES-I. Other important features of the start-up scenario also remain to be examined. In particular, scenarios involving slower fusion-power ramp-up may be desirable from the viewpoint of safe operation of the steam generator and turbine systems, while divertor protection may require a more rapid density buildup.

Fast-wave current-drive R&D. The experimental data base for fast-wave current drive is very small. Fast-wave current-drive experiments in large tokamaks (*e.g.*, on DIII-D or JET) at $T_{eo} \geq 5$ keV are needed to verify current-drive efficiencies estimated for the ARIES-I design. Experimental study of controlling the pressure profile, in conjunction with current profile tailoring, is also of interest since profile control may allow access to higher stable Troyon ratios. For fusion devices, experimental studies of α -particle damping of the fast-wave current drive are also crucial.

To date, all of the experimental data on the folded-waveguide coupler have been collected from a test stand. The high-power properties of the waveguide should be verified in the presence of a plasma in a tokamak device. In this regard, a series of tests could be carried out, progressing from a low-power, single-waveguide coupling demonstration to high-power, current-drive experiments with a phased-array launcher. There is a need to develop an advanced modeling tool for the waveguide coupler, which could be used to analyze experimental data and project performance in a reactor plasma.

The following are critical engineering issues specific to the ARIES-I (or other power reactors) folded waveguide that need special attention: (1) fabricating the waveguide structure with SiC composite, (2) cooling the waveguide structure, (3) reducing the radial thickness (or length) by using diaphragms, (4) contouring the vane tips and diaphragms to reduce local peak fields, and (5) optimizing the coax-feed location and detailed geometry. To design for the high-performance launcher, electrical properties of SiC composites in

the ion-cyclotron-to-infrared range of frequencies and under a neutron fluence, including data on radio-frequency (RF) surface breakdown, should be studied and documented. With regard to the RF support system, demand for technological extrapolation appears to be moderate. Upgrading the efficiency (to 90%) and power output (to 5 MW) of tubes such as klystrodes, Resnatrons, and tetrodes is a crucial development issue that needs to be addressed. Likewise, to accommodate a varying plasma load, the appropriate matching and phase-shift circuits for high-power applications need to be developed.

Neutral-beam current-drive R&D. The alternative current-drive option for ARIES-I is high-energy, negative-ion neutral beams (NBCD). There is a growing experimental data base for NBCD and relatively good agreement between theory and experimental results exists. The technological requirements for an NBCD system for ARIES-I, however, is quite challenging when compared to the fast-wave current-drive system. Although rapid progress has been made in RF quadrupole technology, two critical goals remain to be accomplished: scaling up the pulse length from milliseconds to continuous operation, and upgrading the current capability from 10s to 100s of mAs [53]. Similarly, while present-day negative-ion sources already have the current density and gas efficiency required for ARIES-I application, their pulse lengths need to be extended to steady-state operation [53]. Substantial development will also be required to produce efficient steady-state laser systems for use in photodetachment neutralizers [54].

Edge-physics R&D. The impurity-control/particle-exhaust system is probably the most challenging subsystem in a fusion device. The ARIES-I reactor utilizes poloidal divertors in a double-null configuration. The divertors operate in the high-recycling mode, *i.e.*, exhibiting a high density and low temperature at the divertor target. The high-recycling mode at reactor-relevant parameters has not been demonstrated experimentally. The ARIES-I divertor performance is based on extrapolation of analytical and computational models that are calibrated to present-day experimental data.

Large uncertainties exist in the models and assumptions used in edge-physics codes and experimental edge-physics data, especially from large tokamaks, are needed to further refine these codes. Also needed is extensive theoretical and computational effort to improve the physics models and reduce the uncertainty. Innovative approaches to the impurity control system, such as gas and/or impurity injection in normal divertors and gaseous (or slot) divertors, should also be pursued. Finally, experiments to demonstrate plasma power and particle control (both fueling and pumping) at steady state (or for a time scale longer than wall absorption or degassing) are crucial to a power reactor.

1.4. MAGNET ENGINEERING

The engineering design and critical issues of the toroidal-field (TF) and poloidal-field (PF) magnet systems for ARIES-I are summarized here. The design of the TF magnet is driven by the high field (21 T) and by the decision to limit the use of advanced magnet materials (both for the conductor and the structure) to those that already exist in the laboratory (although extrapolations to the sizes and lengths required for use in a tokamak fusion-power reactor may be required). The reference TF magnet uses plates of Incoloy 908 and internally cooled, cabled, Nb₃Sn ternary superconductor. The stabilizer is CuNb which carries structural loads.

The design of the PF-magnet system follows the ITER recommendations [19] and has few, if any, developmental issues. The PF coils in ARIES-I are external to the toroidal-field system. They are superconducting, using internally cooled, cable-in-conduit conductor. The peak field in the poloidal-field system is only 12.8 T. Normal and off-normal pulse losses in the PF- and TF-coil systems are sufficiently low so that they do not impact overall refrigeration requirements. The magnets have built-in margins that are sufficient to survive disruptions without quenching.

1.4.1. Toroidal-Field System

Conductor. Currently available Nb₃Sn alloys [13, 14] are capable of producing fields up to about 21 T. Other superconductors exist in the laboratory for use at even higher magnetic-field levels [*e.g.*, Nb₃Al and Nb₃(Al,Ge)] but no full-scale manufacturing experience exists. It is concluded that fields higher than 21 T, although feasible, would require tape conductors. The sensitivity of the tapes to pulse losses, both normal and during disruptions, would lead to unacceptably long down times.

The conductor in the highest field region of the ARIES-I magnet is multifilamentary Nb₃Sn. Numerous techniques exist for producing binary and ternary Nb₃Sn. In general, each technique attempts to provide good mixing between the Nb and the Sn, and high-temperature ($\sim 700^\circ\text{C}$) heat treatment for growth of the superconducting phase. Critical field, temperature, and current density vary with ternary additions and processing. The most widely used method for producing Nb₃Sn is the bronze process, which combines Nb and bronze in a geometry that provides a large surface-contact area. The composite is then heat treated ($\sim 700^\circ\text{C}$ for ~ 72 h), causing the Sn to diffuse out of the bronze and react with the Nb. At the end of the heat treatment cycle, Nb₃Sn surrounded by impure Cu remains. The best high-field Nb₃Sn-based superconductor, however, has

been produced by powder metallurgy processing. In this process, Nb or Nb-1.2 wt % Ti powder is poured into a Cu can containing a central Cu rod. The can is swaged and extruded, and a hole is drilled in the Cu rod. Rods of Sn or Sn-3 wt % Ti are inserted into the drilled hole. The wire is drawn further and heat treated. The critical current density of such powder-metallurgy-produced Nb_3Sn is shown in Fig. 1.4-1 [14].

Magnet design. The ARIES-I design minimizes the size of the TF-magnet system subject to the following restrictions: (1) superconductor critical current, (2) superconductor stability, (3) quench protection, (4) superconductor strain, (5) stress and strain in structural materials, (6) heat removal, (7) pumping power, (8) conductor fabrication, and (9) magnet construction.

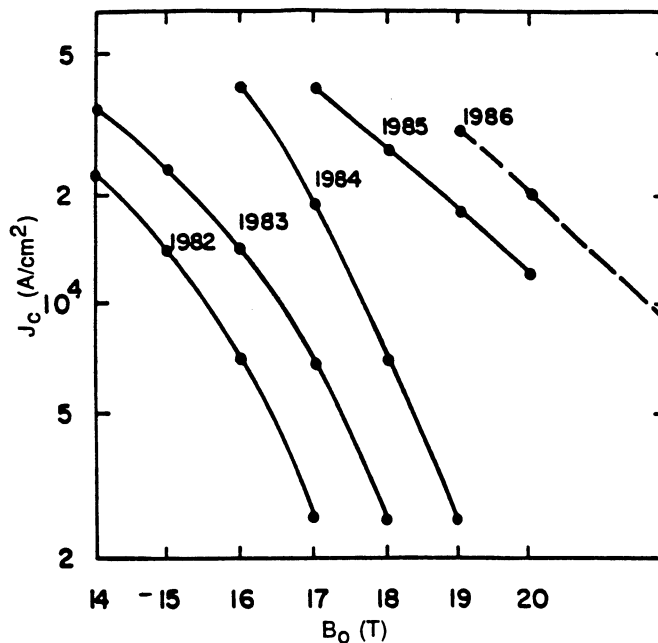


Figure 1.4-1. The critical current density, $J_c(B)$, of powder-metallurgy-produced Nb_3Sn at 4.2 K [14].

The reference TF-coil design uses structural plates manufactured with grooves into which the conductor is wound, in a manner similar to the Westinghouse coil of the Large Coil Project (LCP) [55]. Thus, rather than winding all of the materials in the magnet, only the conductor requires winding. This facilitates fabrication by removing the stiffest material from the winding process. A group of 22 such plates are placed together inside a case to make a coil. The cross section of the ARIES-I TF coil is shown in Fig. 1.4-2(A) illustrating the plate design. A schematic diagram of a typical turn showing the main parameters is illustrated in Fig. 1.4-2(B).

Although optimizing every turn of the conductor separately results in the absolute minimum in magnet size, it also leads to an excessive number of joints (= no. of coils \times no. of rows). Using the same conductor everywhere, however, is very inefficient. As a compromise, the ARIES-I coil uses five conductor grades, Nb₃Sn for the intermediate and high-field (≥ 6 T) regions and NbTi for low-field (< 6 T) zones. Because the depths of the grooves in the plates are determined by the design of the conductor, a different depth is required for each grade. Coolant requirements are based upon 2-kW/m³ uniform heat loading throughout the coil, which is a conservative assumption since only the highest field turn would experience this level of heating. There are 32 dump circuits (two per coil). The main properties of the 21-T TF coils are listed in Table 1.4-I.

In order to accommodate the large stresses, the conductor/stabilizer carries a substantial load ($\sim 20\%$). Copper-niobium (CuNb) high-strength stabilizer [20] is used in the ARIES-I design (with an allowable stress of 800 MPa and Young's modulus of 185 GPa). In a high-field magnet, the stored energy is sufficiently large that stabilizer requirements are dictated by quench protection and not by stability. In the ARIES-I magnet, the allowed stabilizer current density is increased by two mechanisms: (1) increased winding-pack current which becomes feasible in the plate geometry and (2) halving the effective stored-energy per coil by adding an extra layer of electrical insulation between the center plates in each coil. Each half coil is then driven by a separate power supply and current lead. Thus, although there are 16 coils mechanically, there are 32 coils electromagnetically.

Because of its superior mechanical properties and low coefficient of thermal expansion, Incoloy 908 [15-17] has been selected as the base material for the plates. For the coil cases, Fe-Cr-Ni is preferred so that the differential thermal contraction will induce a compressive pre-strain in the conductor and the plates. An equivalent tensile stress of 1000 MPa has been allowed for the isotropic design. Based upon the proposed design criterion for cryogenic systems [56], steel is required to have $\sigma_y \geq 1500$ MPa and $S_{m,T} \geq 2000$ MPa at 4 K. The ARIES team also considered the possibility of utilizing

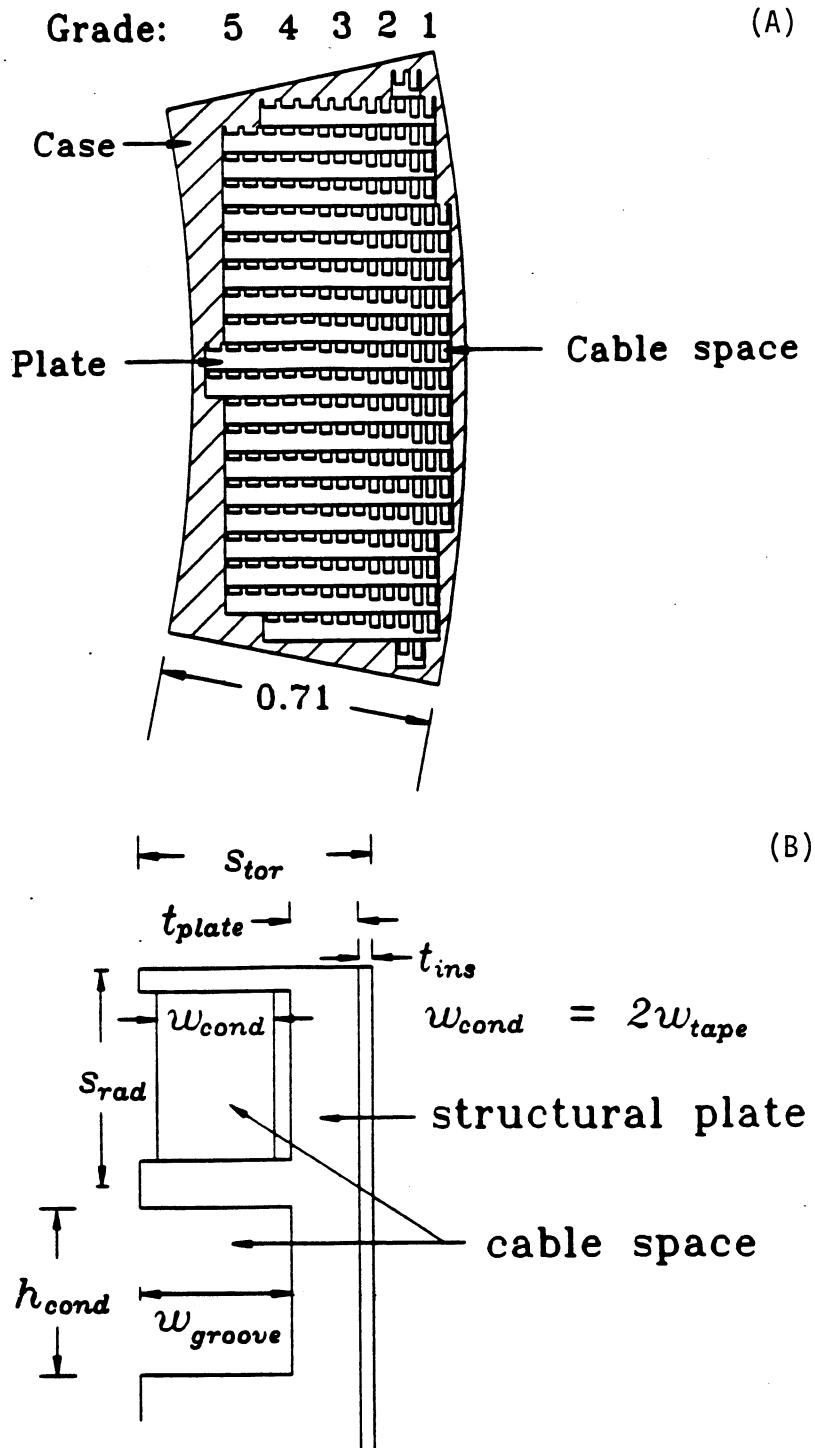


Figure 1.4-2. (A) The cross section of the inner leg of the reference ARIES-I TF-coil design, illustrating the structural plate concept; and (B) Schematic diagram of a typical turn, indicating the main design parameters.

Table 1.4-I.
The ARIES-I TF-Coil Parameters

Magnetic field (T)	21.04				
Pack current (kA)	100				
Maximum voltage (kV)	20				
Number of coils	16				
Ripple on axis (%)	0.15				
Ripple on edge (%)	1.49				
Radial build (m)	0.71				
Average current density (MA/m ²)	25.7				
Stabilizer current density (MA/m ²)	156				
Total stored energy (GJ)	132				
Circuit stored energy (GJ)	4.1				
Vertical stress, stabilizer ^(a) (MPa)	774				
Vertical stress, case ^(a) (MPa)	888				
Conductor Detail					
Grade	1	2	3	4	5
Maximum field (T)	21	18	14	9	4
Critical current density (10 ⁸ A/m ²)	2.40	4.98	12.5	35.5	46.5
Critical temperature (K)	4.6	6.5	9.1	12.4	6.6
Radial build (cm)	3.8	4.0	4.4	5.0	5.1
Plate thickness (cm)	1.85	3.28	4.30	4.84	4.96
Conductor height (cm)	2.10	2.30	2.70	3.30	3.41
Superconductor fraction	0.433	0.269	0.128	0.032	0.038
Stabilizer fraction	0.567	0.731	0.872	0.968	0.962

^(a)Design code results; finite-element analyses indicate slightly lower stresses.

metal-matrix composites for the magnet structure. In addition to higher strength, composites have larger Young's modulus which minimizes the strain in the superconductor (important for Nb_3Sn). Development of these materials may lower the overall costs of the coils but they are not adopted for the reference design.

Structural analysis. Support of the electromagnetic forces acting on the TF coils is provided by three structural members: two torque shells and a bucking cylinder (Fig. 1.1-1). The torque shells are axisymmetric toroidal caps that counteract the overturning forces in the upper and lower hemispheres. The arrangement of loads is such that comparatively small forces have to cross the machine at mid-plane, most being balanced in their own hemisphere. The small overturning forces at the outboard mid-plane are constrained by the stiffness of the leg of the TF coil. The bucking cylinder restrains the inward radial forces of the TF coil, as well as a small overturning force on the inner leg of the coil. There is zero torque on the components where the top and bottom of the bucking cylinder meet the torque shells. There is little or no force transmitted between the cylinder and the shells and, therefore, very little interconnecting structure is required. Also, TF coils are bucked against the bucking cylinder (gaps between the TF coils ensure that the coils do not wedge against each other). The cross section of each TF coil is kept constant.

The ANSYS computer code has been used to analyze a model of the ARIES-I reactor for in-plane and out-of-plane loads. The finite-element analyses indicate that the average vertical stresses in the throat of the TF coil on the mid-plane are ~ 700 MPa, the radial stresses are ~ 140 MPa, and the equivalent average stress on the mid-plane, with all the loads added, is ~ 770 MPa. Accounting for space for gaps, cooling, and insulation, the average equivalent stress (von Mises) in the TF coil is ~ 840 MPa. In the support structure (bucking cylinder and toroidal shells), the toroidal stress is ~ 850 MPa, and there is little net vertical load (because of the uncoupling) and small radial loads. The equivalent stress is ~ 900 MPa, lower than that chosen as allowable.

Cryostats. Another important component from the point of view of maintenance is the cryostat for the TF coils. Instead of a large cryostat for the entire device, each coil has its own cryostat with two kinds of exterior surfaces. The first, occurring over the entire bore surface and some of the sides and outer surface, is the conventional type and the vacuum vessel is the visible component. The inward progression is: the super-insulation and heat-shield layers within the vacuum, followed by a structural helium vessel and

conductor matrix (or a matrix containing small-scale helium confinements such as tubes with the case being only structural).

The second type of exterior surface is visible and exposes the face, completely uninsulated, of the helium vessel or other major structural case. At the periphery of this face, a G10 plate connects the edges of the conventional exterior surface and the visible cryogenic components, forming a continuous flat face. Although this face is vacuum sealed, the magnet is not operable in this face-exposed condition because the matrix is not coolable with one face of its casing exposed to air. For magnet operation, each of these exposed faces must butt against an identical face in an adjacent fusion-power-core module, the bucking cylinder, or the torque shells. After the faces are aligned, the cryostat is evacuated and cool-down can begin. A typical TF coil with the interface surface is shown in Fig. 1.4-3.

Application of this new, cold-face concept eliminates the need to carry very large loads from cold to warm structural elements. When the heat leakage resulting from out-of-plane forces is calculated on the basis of cold-to-warm structure requirements, it is 10 times higher for a conventional design than for the proposed ARIES-I cold-face cryostat system.

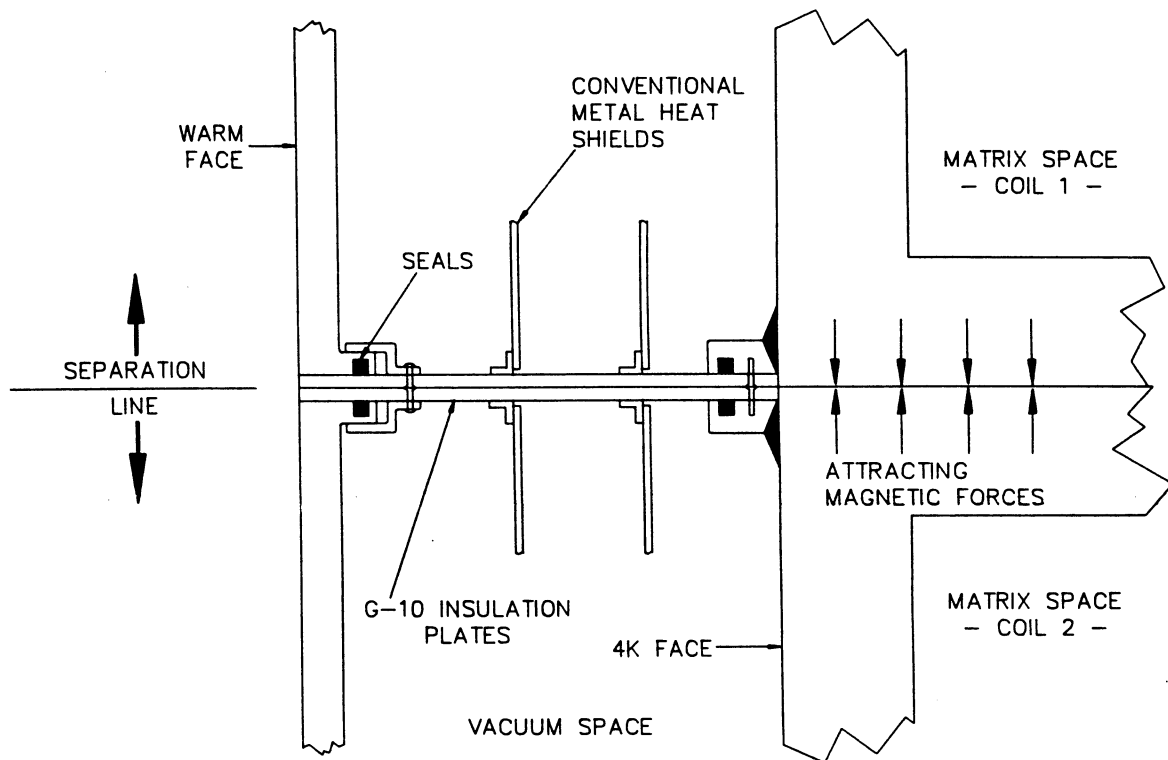


Figure 1.4-3. Cold-face cryostat showing cold-to-cold surface interface.

Moreover, because the cryostat system also deals with the center-post butting forces, the total benefit would be several times larger (*i.e.*, a factor of 50 over conventional design). Additionally, at least 0.15 m of space on each of the coil cross-section dimensions is saved. The use of the cold-face cryostat gives a new capability of avoiding heat leak and allows for TF-coil removal. This cold-face interface concept, however, requires the machining of large components with more precision than is necessary for a conventional design.

1.4.2. Poloidal-Field System

The poloidal-field (PF) magnets are responsible for forming and shaping the elongated plasma during the start-up and steady-state burn. In ARIES-I, all of the PF coils are external to the TF magnets and are superconducting, using internally-cooled, cable-in-conduit, ternary Nb₃Sn, as in ITER [18], and have few, if any, developmental issues. Most of the PF magnets have relatively low fields and current densities. However, analysis of conductors for ITER has shown that the use of niobium-titanium (NbTi) does not yield any cost savings when the conductors are designed to reasonable standards of energy and temperature margins, recovery from disturbance, and the universal design criterion of meeting a minimum fraction of conductor critical current.

The poloidal-field system is designed to control the plasma over a range of beta and internal inductivity. It is not designed to provide full ohmic initiation and start-up, but is capable of providing a substantial fraction of the ohmic requirement with assistance from the RF current-drive system. A trade-off study of the poloidal-field system led to the selection of a 22-V-s flat-top capability. Since there is no quantitative flat-top requirement, the design criterion was to stay within the flux swing regime in which cost increases very slowly with capability. The PF-coil set is described in Table 1.4-II.

The ARIES-I PF-coil design follows the ITER recommendations [18, 19], with the exception that the Tresca membrane allowable stress is 800 MPa for ITER and 1000 MPa for ARIES-I. The tensile stress limit in ITER of 450 MPa is based on fatigue crack-growth limits in the pulsed tokamak experiment. Since ARIES-I is limited to under 1000 cycles, fatigue is less limiting than the Tresca membrane and bending stress in the conductor conduits. The ARIES-I coils are more conservative than those of ITER in that they are also designed for energy margins greater than 0.5 J/cm³ and for fractions of critical current in the well-cooled recovery regime.

Trade-off studies of the PF coils show that the design for ARIES-I is qualitatively different from that of pulsed tokamak systems (*e.g.*, ITER and CIT). Since there is no

Table 1.4-II.
ARIES-I PF-Coils Winding-Pack Dimensions

Coil	R (m)	dR (m)	Z (m)	dZ (m)	Turns	Current (MA)	
						High- β	Low- β
PF1	2.2	0.75	± 0.75	1.5	400	-5.1	-16.3
PF2	2.2	0.75	± 2.25	1.5	400	-3.6	0.98
PF3	2.2	1.0	± 4.75	1.0	400	14.6	19.9
PF4	4.0	1.2	± 6.4	1.2	500	24.5	23.9
PF5	12.5	0.75	± 5.4	0.75	300	-8.1	-12.4
PF6	12.5	0.75	± 2.4	0.75	100	-1.8	2.2

ohmic start-up, the design does not require maximization of volt-second capability. However, a design philosophy used in some previous steady-state designs that all volt-second capability should be eliminated in order to minimize cost is unnecessarily aggressive. Conventional methods for minimizing stored energy lead to designs with unrealistically small fractions of metal in the coil winding packs. Furthermore, because of the flatness of the cost and energy minima, a significant amount of flat-top and start-up volt-second capability can be included for a small additional increase in coil costs. Given the probable need to handle off-normal conditions, a modest flat-top capacity of 22 V-s is selected and includes the flat-top capability needed at full current for either high- or low-beta plasmas. Additional constraints on overall metal fraction and copper-to-noncopper ratio were added to ensure coil fabricability.

In order to evaluate the capabilities of the poloidal-field system, MHD equilibria were generated over a range of flux linkages at high and low beta. The design process has led to a reference PF-coil design with a capability of 144 V-s, which can provide 60% of the volt-seconds needed for start-up without RF assist and 22 V-s for full-current flat-top at high and low beta. The peak field in the PF coils is only 12.8 T and the pulsed losses in the PF coils are modest in comparison with those of the TF coils because the volume of superconductor is much smaller.

The peak poloidal-field energy, which is dominated by the low-beta plasma requirements, is 17.8 GJ for ARIES-I and is comparable to that of ITER. Because of the slow charging of the coils, the peak-power and power-supply requirements are modest, comparable to those of JET and less expensive because of the absence of on-site pulsed-power facilities. A SAVAR power-factor correction-control circuit [57] is used to prevent large circulating reactive power in the utility line feeding the poloidal-field circuits.

1.4.3. Pulsed Losses

A poloidal-field pseudo-scenario has been developed for ARIES-I because occasionally the reactor will be shut down and subsequently restarted (scheduled and unscheduled shutdowns). At each start-up, it is necessary to initiate the plasma, ramp up the plasma current, and heat the plasma to ignition and burn. The poloidal-field system must be designed for a finite probability of disruption, although that probability will be considerably smaller than it is in present-day experiments. The ARIES-I reactor is designed to absorb the losses, forces, and voltage transients resulting from start-ups, shutdowns, and disruptions at any time.

Losses in the PF- and TF-magnet systems were calculated for an entire scenario. It is assumed that a disruption could be either current-conserving (all PF coils retain their pre-disruption currents) or flux-conserving (all PF coils retain their pre-disruption flux), and the effects of the two types of disruption models were calculated at each point in time. The total losses were integrated and local heating of conductor and conduit helium was modeled in order to evaluate the energy and temperature margins of each magnet at every time point during normal and disruption scenarios. The goal was to find a design whose margins would be everywhere greater than the allowable 0.5-K temperature margin and 0.5-J/cm³ energy margin.

Losses in both the PF and TF coils are dominated by hysteretic mechanisms. The total pulse-loss energy in the TF coils during a full scenario (start-up, burn, and shutdown) is 1.06 MJ. This energy can be absorbed adiabatically and is easily removed during the burn or shutdown periods. The heat flux for transition to the ill-cooled regime is 3.3 W/cm² at the worst location on the high field side. The Joule heat flux is only 0.91 W/cm², so the cable conductor is in the well-cooled regime. In order to have an adequate energy margin against disruptions, the fraction of the conductor enveloping the helium in the high-field grade was increased to 7% by reducing the cross section of the structure in the first grade. Also, while the bulk of the magnet is at a bath temperature

of 4.2 K, the inlet helium temperature of the first row is subcooled to 3.8 K. The lowest energy margin is 140 kJ/m^3 , a value that, while not conservative, is sufficient for stability.

Since the burn is steady, the PF magnets are only required to absorb pulsed field energy during start-up, shutdown, and off-normal conditions. Unlike ITER, there is no problem of temperature ratcheting between pulses. The hysteresis losses in the PF coils during ramp-down are larger than those from disruption losses, so that neither a current-nor flux-conserving disruption can increase the pulsed losses in the system. The total pulsed-energy loss in the PF coils during a full scenario (start-up, burn, and shutdown) is 1.6 MJ, while that in the TF coils is 1.06 MJ. This energy level can be absorbed adiabatically and removed during the long pulse or shutdown periods.

1.4.4. Magnet R&D Needs

The design of the PF-magnet system follows the ITER recommendations [19] and has few, if any, developmental issues. The successful operation of a superconducting toroidal-field system with $B > 20 \text{ T}$ and $E_{stored} > 100 \text{ GJ}$, however, will require a significant development program. Presently, many of the materials used in this design are only available in small laboratory samples and are not optimized for the desired properties of strength, current density, *etc.* A magnet-technology development program leading to the availability of the 21-T ARIES-I TF-magnet system in 20 to 25 years is outlined in Fig. 1.4-4.

Superconductor material R&D. During the past few years, the progress in improving the performance (critical field and current density) of the powder-metallurgy-produced Nb_3Sn superconductors has been steady. It is expected that this type of superconductor will be available soon in long lengths. An R&D program is required to produce the necessary property data base leading to conductor development for high-field coils. Superconductors capable of producing higher fields, such as Nb_3Al and $\text{Nb}_3(\text{Al},\text{Ge})$, exist only in the laboratory-size scale. Development of these superconductors should start with optimization of the manufacturing process and, therefore, will require a longer R&D time.

Stabilizer material R&D. Stabilizer materials that can carry substantial loads are necessary in order to accommodate the large stresses in a high-field coil. Copper-niobium and Al-SiC are two examples of high-strength stabilizers. Since fabrication of high-strength stabilizers may require special processes, a conductor development program is

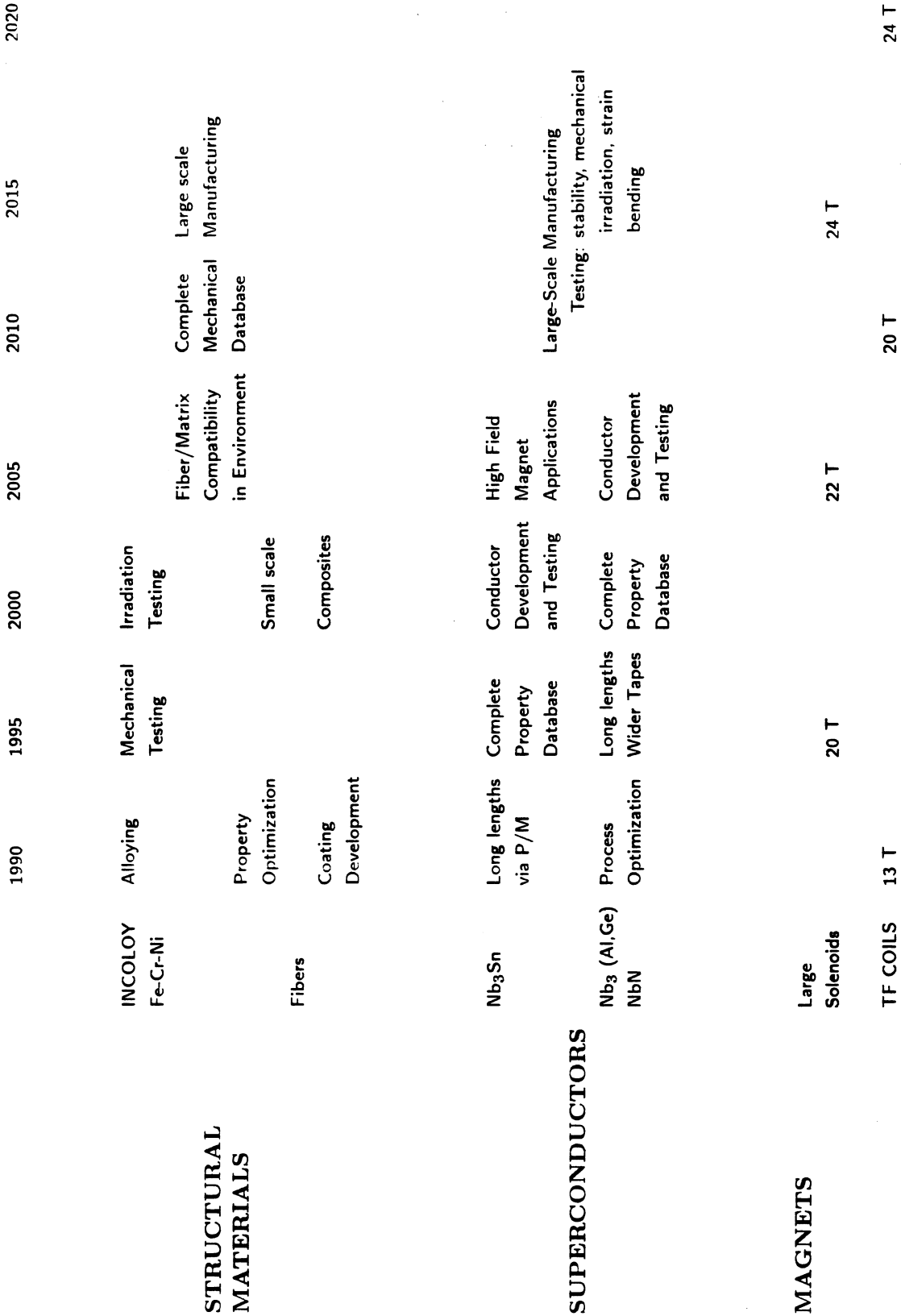


Figure 1.4-4. Magnet-technology development path.

needed to demonstrate that the conductor can be fabricated such that the stabilizer and the superconductor are in intimate contact.

Structural materials R&D. Isotropic steels such as Fe-Cr-Ni and Fe-Mn-Cr alloys and cold-worked-then-aged Incoloy 908 are commercially available in large samples. Further alloying to improve properties together with mechanical and irradiation testing of these materials are key R&D issues.

Composite materials may be capable of simultaneously obtaining higher strength, stiffness, and fracture toughness than metals. To obtain high strength in all directions, metal-matrix composites are the leading candidates. In these composites, the high-strength metal matrix (*i.e.* Incoloy 908 and Fe-Cr-NI alloy) is further reinforced by high-strength fibers (*i.e.*, C, SiC, B, *etc.*). For these composites, the interaction of alloying elements with the fiber material is a serious concern. The R&D program should first be aimed at producing small-scale composites to demonstrate fiber/matrix compatibility during the manufacturing process.

Magnet design R&D. The magnet design effort, of course, builds upon success and progress in superconductor, stabilizer, and structural material development. The aim is to develop large-scale TF coils for a commercial fusion facility. Therefore, in addition to optimization of the design, key items are the operational issues such as reliability, availability, maintainability, and safe operation of both the magnet system and the reactor.

1.5. FUSION-POWER-CORE ENGINEERING

To arrive at the reference ARIES-I design, several different combinations of first-wall, blanket, and shield options were evaluated, including designs presented in the "Blanket Comparison and Selection Study" [58] and in the TITAN studies [59]. Various combinations of coolant, structural material, breeder material, and blanket configuration were evaluated. The chosen design uses an integral first wall and blanket and a separate helium-cooled shield. The reference ARIES-I blanket is low activation with high neutronic and thermal-hydraulic performance. A summary description is given in Table 1.5-I. The elevation view of the ARIES-I fusion power core (FPC) is shown in Fig. 1.1-1 and the schematic of an FPC module is given in Fig. 1.1-2.

Table 1.5-I.
Summary of the ARIES-I Blanket Design

Material	
Structure material	Silicon-carbide composite
Coolant	Helium at 10 MPa
Breeder/multiplier	Li ₂ ZrO ₃ and Be sphere-pac mixture of 1.0- & 0.1-mm pellets
Configuration	
Structure	17 nested, U-shaped shells forming the poloidal modules
Coolant	Poloidal flow in the plena, distributed radially, and cooling the first wall and the blanket toroidally
Breeder/multiplier	Layers of solid-breeder and Be sphere-pac mixture located between the breeder-zone coolant shells
Fabrication	Preformed U-shaped shells to be fitted, one layer after another including internal supports as needed, into the grooves of the reflector/plenum assembly to form the poloidal module; the outer shell is the first wall
Structural analysis	Peak total stress is 77 MPa, well below the 140-MPa design limit
Purge flow design	Area between coolant shells forms the purge channels; helium-purge gas pressure is ~0.4 MPa
Neutronics	Tritium breeding ratio = 1.23 Blanket energy multiplication = 1.30
Thermal hydraulics	Coolant channels embedded in the U-shaped shells; pressures drops and peak material temperatures are acceptable; total first-wall and blanket-loop pumping power is 19 MW; inlet and outlet temperatures are, respectively, 350 and 650 °C
Blanket T inventory	Low, 1 g in the solid breeder, but potentially higher (kg level) in the Be and SiC materials if tritium recoil implantation and retention prove to be a problem

1.5.1. Configuration

The ARIES-I blanket design uses SiC composites as the structural material, 10-MPa helium as the coolant, Li_2ZrO_3 with isotopically tailored zirconium as the tritium breeder, and beryllium metal as the neutron multiplier. Both Li_2ZrO_3 and Be are used in the form of sphere-pac pellets. The FPC is segmented into 16 self-contained modules. Each module consists of one toroidal-field (TF) coil, two inboard and two outboard first-wall, blanket, and shield sub-modules, two upper and lower divertor targets with support structure, and a section of the vacuum vessel. Each poloidal sub-module comprises 17 nested, U-shaped, SiC-composite shells, as is shown in Fig. 1.1-2. The sphere-pac solid-breeder and Be-metal neutron-multiplier mixture is located between the shells. Tritium is recovered by a slow, low-pressure purge flow of helium between the shells.

The cylindrical helium-coolant channels are embedded in each of the 17 SiC-composite shells. The helium coolant enters the blanket from the inlet plena which are located in the shield behind the blanket and reflector. It then flows radially inward through the shells. It cools the shells while flowing in the toroidal direction before it turns and flows radially back into the coolant outlet plena. This routing configuration was selected to provide adequate cooling of the blanket materials and to minimize the blanket pressure drop. The maximum blanket pressure drop of 22 kPa is at the first wall. The corresponding total blanket internal- and external-loop pumping power is 19 MW. The high coolant-outlet temperature of 650 °C leads to a thermal conversion efficiency of 49%.

The shield incorporates multiple layers of aluminum sheets sandwiched between He-cooled, SiC shells to provide passive stabilization against vertical motion of the plasma. There are 40 layers of 1-mm-thick aluminum sheets and 40 layers of 19-mm-thick SiC shells for an overall shield thickness of 0.8 m. The SiC shells, with internal passages for helium flow, are manufactured by using the same method as is used for the blanket shells. All of the aluminum sheets within a module are electrically connected together at the back of the shield. Neighboring shield modules are also electrically connected together with a detachable jumper to provide a complete toroidal circuit. The vacuum vessel is outside of the shield and is made of a low-activation steel.

An important design criteria for any tokamak reactor is that the FPC should survive plasma disruptions. Since the ARIES-I FPC is made of SiC composite, the only electrically conducting materials are the passive-stabilization aluminum sheets and the vacuum vessel. Analysis shows that most of the electromagnetic force generated by a plasma disruption appears on the aluminum sheets and, in effect, the aluminum shells shield the vacuum vessel from disruption forces. The disruption-induced electromagnetic

forces generated in each of the aluminum sheets are restrained by the neighboring SiC shells. The ARIES-I FPC design provides an ideal solution for supporting disruption forces: no forces appear on the delicate first-wall and blanket components, and the forces are distributed more or less uniformly in the shield where they are absorbed and reacted by a massive structure.

1.5.2. Materials

1.5.2.1. Structural material

Silicon-carbide (SiC) ceramics have been considered previously as candidate structural materials for fusion reactors [60]. Silicon carbide has excellent high-temperature capabilities, good thermal-shock resistance, chemical stability, and good environmental resistance. These characteristics, coupled with low induced activation and low afterheat, make SiC a very promising material for future fusion-reactor applications. However, monolithic ceramics display two major problems: (1) a high sensitivity to flaws, either internal (generated during processing) or external (occurring during component use), and (2) brittle catastrophic failure. Thus, monolithic ceramics have low toughness and a statistical spread in strength that result in low reliability and, therefore, have limited applications. Nevertheless, favorable physical and chemical properties of SiC have led to large-scale R&D efforts in the U.S. [61] and Japan [62, 63] for aircraft parts (especially the leading edge of wings) and for advanced heat engines, which will require structural reliability at temperatures as high as possible (up to 1500 °C). The large-scale industrial effort [21–25] to develop SiC materials is motivated by the two important characteristics of SiC: high resistance to oxidation and excellent thermal-shock resistance.

Reinforcing the ceramic matrix with a second phase material is an approach used to enhance performance characteristics of ceramics. Silicon-carbide fibers are generally used to reinforce SiC matrix ceramics. Strength of ceramic materials is increased by transferring the load from the matrix to the fibers, which takes advantage of their superior tensile strength. Fracture-toughness values for ceramic matrix composites (CMCs) are very high because energy is absorbed as fibers are pulled out of the matrix causing crack deflection, arrest, or blunting. Figure 1.5-1 compares the typical stress-strain curves for monolithic SiC and unidirectionally reinforced SiC-composite materials. The fracture toughness of a material is directly proportional to the area under the stress-strain curve and it represents the energy required to fracture a material. The figure clearly shows the large improvement in fracture toughness of composites over monolithic SiC. The strain

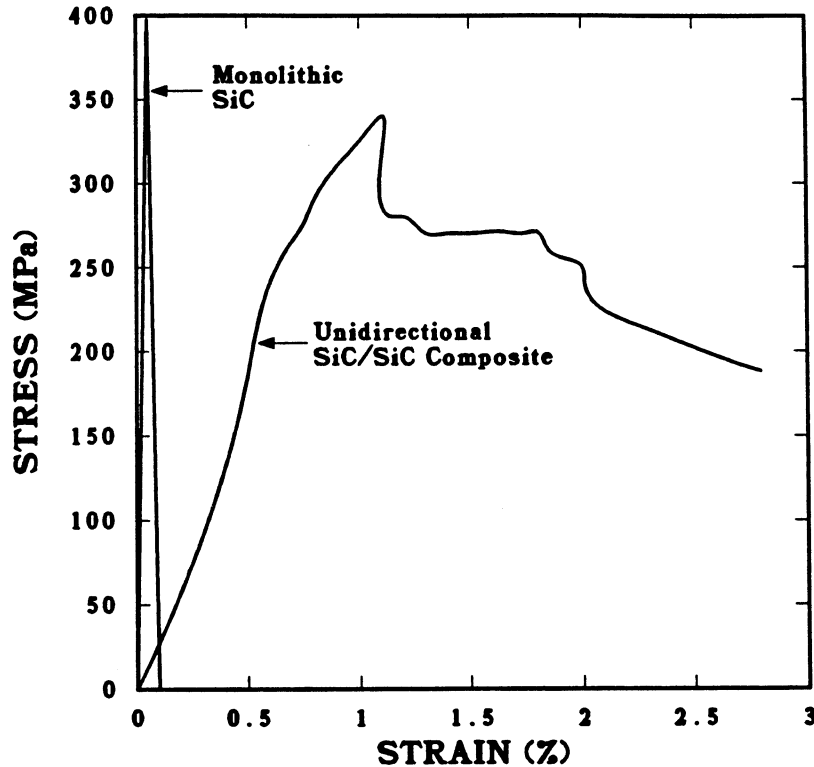


Figure 1.5-1. Stress-strain curve of a 2-D, flat (unidirectional), SiC-fiber-reinforced SiC-matrix composite [64].

tolerances of SiC composites greatly exceed those of monolithic ceramics. Strain values above 2.5% are routinely measured for such composites [64], whereas monolithic SiC exhibits strain values of less than 0.1% at initiation of fracture (Fig. 1.5-1).

Ceramic composite materials are still in their developmental infancy (5 to 10 years), and, consequently, thermomechanical data are limited. Typical thermomechanical properties of 2-D, flat, SiC composite are given in Table 1.5-II. Silicon-carbide-composite materials exhibit good mechanical strength at high temperatures ($>1000^{\circ}\text{C}$) associated with a high strain-to-failure value. These composites are resistant to high-temperature thermal shock and thermal cycling. They need very high energies for crack propagation, with increasing values when damaged regions extend. Thus, SiC composites are potentially damage-tolerant ceramics that do not suffer from catastrophic failure behavior.

Most 3-D, reinforced SiC composites are either products of classified development or are proprietary of an industry. Therefore, because of the lack of public data, thermomechanical properties of these composites have to be estimated using micromechanical design equations. The composites industry has developed numerical codes to estimate

Table 1.5-II.
Two-Dimensional, Flat, SiC-Composite Properties [65]

Density (kg/m ³)	2,400
Tensile strength (MPa)	250
Strain at failure (%)	8
Bending strength (MPa)	
27 °C	320
500 °C	350
1000 °C	380
Thermal conductivity (W/K-m)	
27 °C	25
500 °C	19
1000 °C	18
Fracture toughness (MPa-m ^{1/2})	
27 °C	26
500 °C	27
1000 °C	27
Thermal shock resistance ^(a) (MPa)	
27 °C	320
500 °C	300
1000 °C	280

^(a)Sample is heated to indicated temperature then dropped into cold water; the remaining bending strength is measured at room temperature.

thermomechanical properties of composites as functions of composite characteristics (*i.e.*, fiber volume fraction, matrix void fraction, and fiber orientation). The code, CLASS, used for ARIES-I was developed by Materials Sciences Corp. [66]. To avoid an overestimation of SiC composite properties, the constituent (*i.e.*, fiber and matrix) properties were chosen very conservatively. Furthermore, no allowance was made for likely future improvements in matrix densities above 90%. Also, to reflect the effects of neutron irradiation, fiber and matrix neutron-irradiation data were reviewed and used. Properties of the SiC composites used in the ARIES-I design are given in Table 1.5-III.

It is important to note that because of inherent microstructural characteristics, composite materials behave in unexpected and surprising ways (different from metals) when placed in a neutron and ionizing radiation environment. The primary reason is that metals and ceramics are of different bonding types (metals: communal ownership of valence electrons; ceramics: ionic or covalent bonds). As a result, in metallic alloys, the stability and properties depend in large measure on the average, rather than local, distribution and position of dissimilar atoms. In ceramics, it is the local distribution of dissimilar atoms that determines its properties. Thus, ceramics may have a higher tolerance to displacive radiation than metals. In addition, metals have the ability to plastically deform before failure (ductile failure), whereas ceramics do not show plasticity (brittle failure).

Because composites are a relatively new material, no data on neutron irradiation effects have been reported. Based on a limited number of neutron-irradiated experiments on bulk SiC and on SiC fibers, the following observations can be made:

- The presence of a second lattice, and the additional stoichiometric point-defect constraints, distinguish the radiation-damage response of ceramics from that of metals. Both the lattice and stoichiometry effects are likely to mitigate radiation damage in ceramics.
- Dimensional changes in SiC saturate around 3×10^{24} n/m² for irradiation temperatures below 1200 °C.
- Voids and helium bubbles have not been reported in neutron-irradiated SiC for temperatures below 1200 °C.
- Irradiation-produced dislocations inside the SiC matrix seem to be the primary trap sites for other irradiation-produced defects (including helium atoms), thus formation of voids or bubbles is impeded.

Table 1.5-III.
Properties of the SiC Composites Used in the ARIES-I Design

Property	Composite ^(a)	CVD Layer
Density (kg/m ³)	2,500	3,100
Young's modulus, E (GPa)		
E_x	364	320
E_y	360	320
Poisson's ratio, ν	0.16	0.17
Thermal-expansion coefficient, α (10 ⁻⁶ /K)		
α_x	4.4	4.5
α_y	4.3	4.5
Thermal conductivity, k (W/K-m)		
k_x	15	15
k_y	12	15
Allowable stress (MPa)		
Primary	140	140
Secondary	190	140

^(a) Properties were calculated using the CLASS code [66] with a ply orientation pattern of -45°/0°/45°/90°, a fiber volume fraction of 60%, and a void fraction of 10%.

- Silicon carbide will probably withstand a much higher burnup than metallic alloys because of the polycrystalline nature of ceramics.
- In the event that large helium-generation rates lead to the formation of helium-filled bubbles, these bubbles will have a pronounced effect on crack behavior. Crack/pore interactions in glasses and other ceramics have been shown to increase the fracture toughness of these materials.
- Amorphatization followed by a rearrangement of atoms at high irradiation temperatures (900 °C) can result in recrystallization. Recrystallization generally causes loss of strength in metallic alloys but “heals” cracks in ceramics which enhances strength.
- SiC fibers have shown irradiation hardening behavior when exposed to a mixed-neutron-energy spectrum, while low-fluence 14-MeV exposure has not produced any measurable changes in mechanical properties.
- The fundamental characteristic of CMCs is the interaction of matrix cracks with the reinforcement network. Furthermore, radiation damage effects of ceramics have shown low-fluence saturation levels that are dependent on ceramic type and temperature. Therefore, radiation damage in CMC materials is not expected to drastically affect its mechanical properties. It is believed that, following radiation damage, a certain degree of fracture toughness improvement can be expected in CMCs.

These observations indicate that it is reasonable to postulate that CMCs might outperform metallic alloys when it comes to fundamental radiation-damage effects. However, bulk-ceramic-material test results do not fully describe the response of mechanical properties of CMC materials to neutron irradiation. Therefore, it is obvious that neutron irradiation experiments on SiC composites (and other CMCs) are necessary in order to understand the response of this material to neutron irradiation.

Gas leak tightness is an important issue for fusion-reactor structural materials. Chemical vapor deposited (CVD) SiC has a very low hydrogen-diffusion coefficient even at high temperature ($\sim 10^{-10}$ m²/s at 1000 °C [67]). Such a low hydrogen-diffusion coefficient makes CVD SiC practically impermeable to helium. In particular, single-phase sintered SiC, which has a hydrogen-diffusion coefficient several orders of magnitude higher than CVD SiC, is found to be impermeable to liquids and gases at pressures in excess of 30 MPa and temperatures up to 1650 °C [68]. However, SiC composites contain a significant amount of interconnecting porosity ($\sim 10\%$). Therefore, after forming an SiC

composite component, a desired thickness of bulk SiC material has to be chemically vapor deposited onto the surface. This process renders the component leak tight against high pressure gases [21]. Furthermore, the presence of oxygen in the helium coolant stream can form a self-healing viscous SiO₂ surface layer that continuously coats newly developed surface microcracks. Therefore, control of coolant gas chemistry can be used to maintain the integrity of the oxide layer to ensure leak tightness of the CVD SiC layers.

1.5.2.2. Tritium-breeding material

The performance characteristics of the four potential solid-breeder candidates (Li₂O, Li₄SiO₄, Li₂ZrO₃, and LiAlO₂) under normal (pulsed and steady-state) and off-normal operating conditions were considered for the ARIES-I reactor. The primary performance parameters for normal operation are those for tritium breeding, lithium burnup, thermal transport, tritium transport, thermal and in-reactor volume change, chemical stability with cladding materials, lithium mass transport, and activation. Secondary parameters for normal operation include mechanical properties and grain growth. Additional properties considered for off-normal and accident conditions include decay heat rate, latent heat of melting, volume changes from high-temperature phase melting, and chemical compatibility with moisture and beryllium. This comparison was carried out for ITER and extended to ARIES-I.

In most categories, Li₂O performs very well relative to other breeder ceramics, particularly in the area of lithium atom density, thermal conductivity, tritium transport (expressed as the minimum temperature for a one-day average residency time for the tritium in the ceramic), and activation. Its volume change due to thermal expansion and helium-induced swelling may be a problem and has to be included in the design considerations. Lithium oxide also has a higher potential for problems than other breeders with regard to chemical compatibility with structural material, Be, and moisture. Lithium mass transport may also be a problem at high temperatures. While these issues may not be critical for ITER, they may seriously limit the upper temperature of Li₂O that will be required for ARIES-I.

Lithium orthosilicate properties appear to lie between those of Li₂O and the other two ceramics. It is better than Li₂O in terms of in-reactor volume change, compatibility, and lithium mass transport. It has very low activation. Since ARIES-I is investigating the feasibility of a very low-activation blanket, Li₄SiO₄ was considered as the first candidate. The major reason that Li₄SiO₄ was not selected as the primary candidate for ITER was due to concern about a possible tritium-release problem at higher burnup as Li₄SiO₄ is

converted to Li_2SiO_3 , which has poor tritium-release characteristics. For the ARIES-I blanket, the problem can be more severe because of the higher burnup and the higher breeder-material temperature.

Lithium zirconate has excellent tritium-release characteristics. It is very stable to the effects of temperature and irradiation but its activation and afterheat are the highest among the four breeders. Lithium zirconate has a low thermal conductivity, however this problem can be corrected by mixing the breeding material with Be. Lithium aluminate is stable at high temperatures. It was not selected, however, because of its waste disposal problem due to the production of ^{26}Al from $^{27}\text{Al}(n,2n)$ reactions. Isotopic enrichment will not alleviate this problem.

On the basis of the above comparison, isotopically tailored Li_2ZrO_3 is selected as the breeder material for ARIES-I. It should be noted that even after extensive isotopic tailoring, the off-site dose after a severe accident in the ARIES-I reactor is still dominated by Zr. This provides a strong incentive to develop alternate, low-activation solid-breeder materials. The second choice is Li_4SiO_4 . This material exhibits very low activation and afterheat without the need for isotopic enrichment. It would permit thermal design conditions comparable to those of Li_2ZrO_3 . Considerable uncertainty exists, however, regarding the chemical stability and tritium inventory of Li_4SiO_4 under high lithium burnup. This uncertainty should be resolved by the breeder-material development program. If the results of these experiments prove to be positive for Li_4SiO_4 , it could be substituted for Li_2ZrO_3 in the ARIES-I design with virtually no design changes. The third choice is Li_2O , which would have zero afterheat and induced radioactivity but would require a lower operating temperature than Li_2ZrO_3 or Li_4SiO_4 . The last choice is LiAlO_2 because of its unavoidably high levels of induced activity and afterheat.

1.5.2.3. Divertor materials

The ARIES-I reactor uses high-recycling divertors to reduce the plasma ion temperature at the divertor plate to below the sputtering threshold for high- Z materials, and achieves a very low erosion rate of the divertor target [69]. Molybdenum, tungsten, and several tungsten-tantalum-rhenium alloys were considered for the ARIES-I divertor target material. All have similar favorable thermomechanical characteristics. For a thin, plasma-sprayed coating on a structural substrate, alloying elements were not thought to be needed. The neutron activation properties of molybdenum, tantalum, and rhenium lead to long-lived products that would cause waste disposal concerns. Tungsten is the least activating of the high- Z materials [70] and is chosen for ARIES-I. To minimize

the accident dose potential and waste disposal problems of tungsten, isotopic tailoring is specified (Sec. 1.6).

Vanadium cooling tubes were initially considered for the divertor structure. Concern about differential thermal expansion between the tungsten and the vanadium, and about tritium diffusion into the divertor coolant led to investigation of SiC composites. Tritium ions from the plasma will implant into the tungsten target. To minimize diffusion of this implanted tritium through the tungsten into the helium coolant, a low permeability substrate (*e.g.*, SiC) should be used. The thermal expansion coefficient of SiC and tungsten are very similar, which reduces concerns about the thin surface layer spalling off the substrate. The high-temperature capability of SiC allows the ARIES-I divertor to handle the high heat fluxes ($\sim 5 \text{ MW/m}^2$) with coolant inlet/outlet temperature conditions the same as those used for the blanket. This in turn allows efficient recovery of the divertor power.

While the choice of a plasma-sprayed tungsten divertor target on an SiC composite substrate offers attractive potential for ARIES-I, engineering development of this combination of materials is needed.

1.5.3. Blanket and Shield Fabrication

The manufacture of fiber-reinforced ceramic composites starts with taking uniform arrays of fibers or yarns, putting them in a weave, cloth, or braid to form a fiber *preform* that is then infiltrated with ceramic matrix precursors. These precursors could be solids, powders in slurries, or liquids (such as polymers) that are then converted to ceramics. The other more widely used method of synthesizing ceramic matrix material is chemical vapor infiltration (CVI). Chemical vapor infiltration is performed inside a resistance-heated CVI reactor. By decomposing methyltrichlorosilane (CH_3SiCl_3) gas on the surface of the SiC fibers at temperatures around 1000°C , HCl gas escapes leaving behind SiC matrix. Previously, infiltration times on the order of weeks were necessary to produce millimeter-thick SiC-composite materials. However, processes developed by General Atomics and by the Oak Ridge National Laboratory reduce infiltration times from weeks to about 24 hours [64]. These new CVI techniques form the SiC matrix by a comparatively low-stress low-temperature process, avoiding many of the problems associated with conventional processes for ceramics manufacturing.

Mechanical working (*e.g.*, grinding, drilling, or milling) of ceramics initiates surface flaws, resulting in a reduction of strength and toughness of a component. A major advantage of the ceramic-composite manufacturing techniques mentioned above is that the

result is a near net-shape component that requires only minimal finishing touches. Another advantage of composites over bulk ceramics is the ability to create large irregular solid or hollow shapes. Attachment holes and flanges can be integrated during preform weaving without severing fibers, which reduces or eliminates subsequent brazing or bonding between component sections. Complex components for missiles, aircraft structures, integral hub and blade marine propellers, and liquid-propulsion thrust chambers, including the necessary attachments, are now routinely manufactured for government or private industry clients [71].

In practice, the shape of the component is limited to the weaving capability of the numerically controlled weaving machine. Currently, 3-D seamless patterns can be formed by continuous intertwining of fibers, resulting in damage-tolerant preforms that are resistant to interlaminar crack growth and delamination. Computer-aided filament-winding machines are capable of controlling individual fiber placement within one thousandth of an inch [71]. This automated, high-speed, filament-winding technique is embodied in a four-axis microprocessor-controlled machine that produces parts that are up to two meters in diameter and seven meters in length. At present, the shape and size of components is more limited by CVI furnace size than by weaving machine capabilities. However, over the past few years, furnace sizes have been increased from a few tens of cm in diameter to about 1.5 m in diameter. In these reactors, corrugated SiC-composite heat-exchanger panels with dimensions of 1 m \times 1 m \times 1 cm are now routinely manufactured [72].

Improved matrix-formation techniques, including alternatives to the CVI process, are under development. The primary goal is to enhance matrix densities. Currently, SiC composites with matrix densities as high as 90% theoretical density are routinely manufactured. Recent developments by the private sector have resulted in manufacturing nearly 100%-dense SiC composites by using SILCOMP as matrix material [73]. SILCOMP is the trade name for SiC that has been reaction-bonded by using fine graphite particles dispersed in pure silicon metal. When silicon is heated to its melting temperature (1412°C), it readily reacts with graphite to form SiC. The end product of this process is SiC that contains about 8% to 12% free silicon.

The first-wall and blanket interior of the ARIES-I reactor lends itself quite uniquely to current SiC-composite technologies. Recent developments by private industry have resulted in manufacturing an SiC-composite heat-exchanger panel that resembles the ARIES-I first-wall and blanket configuration [74]. The heat exchanger panel requires a tube sheet with channels having a 6-mm inner diameter and an 8-mm outer diameter. The weaving machine is programmed to weave an entire sheet of tubes by serpentine SiC fibers from tube to tube. It should be noted that such a tube sheet is structurally quite

different from conventionally known metallic tube banks. This is because welding metallic tubes together changes the microstructure of the tube wall in the vicinity of the weld and weakens the individual tubes. The ARIES-I blanket-module construction scenario has been produced through discussions with General Atomics [75] and the Amercom [21] Company. The assembly procedure is given schematically in Fig. 1.5-2.

1.5.4. Neutronics

The goals of the ARIES-I reactor design study include maximizing the safety attributes and minimizing the environmental impact of the reactor. Using a neutron-multiplier material increases the nuclear performance of the blanket, a desirable improvement for any fusion reactor. Neutron-multiplier material is also needed to achieve an adequate tritium breeding ratio (TBR) in almost all solid-breeder blanket configuration (a combination of SiC structure and Li₂O breeder is an exception). The only low-activation neutron-multiplier material is beryllium. Lead is the other possible non-fissionable neutron multiplier. However, the radiological hazard potential for lead in a fusion reactor is at least four orders of magnitude higher than for SiC, and is four orders of magnitude higher than for Be.

The best approach for effective utilization of the beryllium neutron multiplier is to locate the Be immediately behind the first wall and to maximize the Be fraction in this zone. To enhance the nuclear energy multiplication in the ARIES-I blanket, we also allow the excess neutrons to be absorbed in silicon ($Q = 8.5$ MeV), the constituent element in the SiC structural material. On the other hand, for the solid-breeder designs, the power density in the breeder zone should not be so high that the maximum operating temperature in the breeder exceeds the design limit. For these reasons, the ARIES-I reference design places a Be neutron-multiplying zone immediately behind the first wall and the tritium solid breeder is uniformly mixed with Be to reduce the operating power density. However, high ⁶Li enrichment in the solid breeder compound will be needed because of high ⁶Li burnup in the blanket.

Table 1.5-IV shows the zones and the material compositions of the ARIES-I blanket and shield and Table 1.5-V displays the neutronics performance of the ARIES-I blanket and shield. The ⁶Li enrichment in the Li₂ZrO₃ solid breeder is 80% at the blanket beginning of life. At the end of life (after 20-MW_y/m² neutron fluence), the ⁶Li enrichment is reduced to 20%. The TBR for ARIES-I from a 1-D full-coverage analysis is 1.21 at the beginning of life and is reduced by 5.6% to 1.15 at the end of life. The average TBR over the blanket life is 1.18, which is more than enough to guarantee adequate

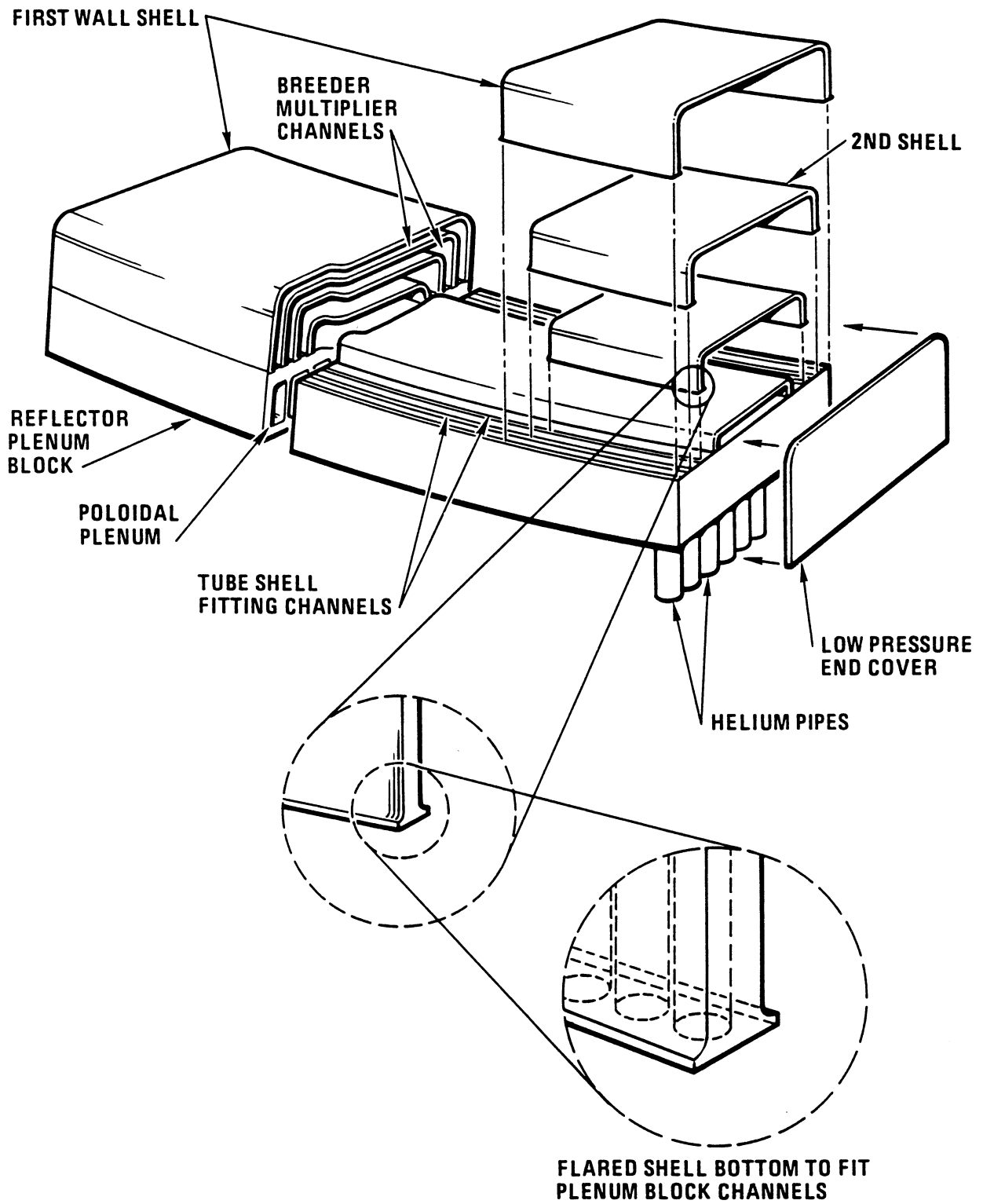


Figure 1.5-2. Assembly procedure for the ARIES-I nested-shell blanket module.

Table 1.5-IV.
The ARIES-I Reference Blanket

Zone	Thickness (cm)	Composition
First wall		
Sacrificial layer	0.2	100% SiC
Structural wall	1	67% SiC + 35% He
Breeding zone ^(a,b)	20	25% SiC + 70% breeder/multiplier + 5% He
Reflector 1 ^(b)	10	25% SiC + 70% Be + 5% He
Reflector 2 ^(b)		
Outboard	37	75% SiC + 20% void + 5% He
Inboard	37	75% SiC + 20% void + 5% He
Plenum	30	75% SiC + 25% He
Vacuum vessel ^(c)	1	Al alloy
Shield 1		
Outboard	40	66.5% SiC + 28.5% B ₄ C + 5% He
Inboard	40	56.0% SiC + 24.0% B ₄ C + 20% He
Shield 2		
Outboard	40	66.5% SiC + 28.5% B ₄ C + 5% He
Inboard	30	66.5% SiC + 28.5% B ₄ C + 5% He

^(a)Breeder/multiplier mixture is 20% breeder and 80% Be;
the reference breeder is Li₂ZrO₃.

^(b)Breeder and Be have 90% of theoretical density and a packing factor of 80%
(density factor of 72%).

^(c)In the final blanket design, the vacuum vessel is located outside the shields.

Table 1.5-V.
Neutronics Performance of the ARIES-I Blanket and Shield

	Beginning of Life ^(a)	End of Life ^(a)
Tritium breeding (T/DT neutron)		
⁶ Li (n,α)T	1.1994	1.1337
⁷ Li (n,n' α)T	0.0036	0.036
Be (n,T)	0.0112	0.0114
Neutron multiplication (reactions/DT neutron)		
Be (n,2n)	0.7516	0.7643
Nuclear heating (MeV/DT neutron)		
First wall	0.8375	0.8449
Breeder zone	13.35	13.06
Be reflector	1.317	1.413
SiC reflector	2.284	2.651
Plenum	0.5495	0.6345
Total blanket heating	18.34	18.60
Blanket energy multiplication	1.30	1.32
Maximum nuclear-heating rate (MW/m ³) ^(b)		
SiC first wall	6.7	
Breeder/multiplier mixture average	11.0	
At superconducting magnet (inboard)		
Maximum nuclear heating (W/m ³) ^(b)	370	
Maximum fast neutron flux (n/m ² -s) ^(b)	2.3×10^{13}	

^(a)Beginning of life: 0 MWy/m², 80% ⁶Li.

End of life: 20 MWy/m², 20% ⁶Li.

^(b)Normalized to 1 MW/m² of neutron wall loading.

tritium production in a realistic 3-D geometry that includes allowance for the divertors. The blanket energy multiplication is initially 1.30, and then increases slightly to 1.32 at the blanket end of life. The maximum volumetric nuclear heating of 11 MW/m^3 occurs at the breeder zone immediately behind the SiC first wall (normalized to 1 MW/m^2 of neutron wall loading). However, the volumetric nuclear heating at the SiC first wall is only 6.7 MW/m^3 . At the inboard region of the superconducting magnets, the maximum nuclear heating rate is $\sim 370 \text{ W/m}^3$ and the fast neutron (energy above 0.1 MeV) flux is $2.3 \times 10^{13} \text{ n/m}^2\text{-s}$ (also normalized to 1 MW/m^2 of wall loading). The superconducting magnet is more than capable of operating continuously for 40 full power years since the radiation damage limit is believed to be $1.0 \times 10^{23} \text{ n/m}^2$ fast neutron fluence and the neutron wall loading at the inboard region is 2.4 MW/m^2 .

1.5.5. Thermal and Structural Analysis

In order to optimize the thermal efficiency of the blanket system, thermal-hydraulic analysis was closely coupled with materials selection and with the structural, mechanical, and neutronics designs. The reference ARIES-I blanket is shown in Figs. 1.1-2 and 1.5-2. The blanket is configured in the form of nested SiC-composite shells in which small coolant channels (0.5- to 0.8-cm diameter) are embedded. The helium coolant enters the blanket from the inlet plenum which is located between the reflector and the shield. Coolant then flows radially inward towards the first wall. It cools the first wall while flowing in the toroidal direction before it turns and flows radially outward away from the first wall into the coolant outlet plenum. This coolant routing configuration was selected to provide adequate cooling of the blanket materials and to minimize the blanket pressure drop.

In order to maintain the breeder and Be within their respective material temperature limits, it is necessary to minimize the maximum local power density. The solid breeder is mixed with the Be in order to reduce the effective power density and to increase the effective thermal conductivity of the mixture. A detailed estimate of the thermal conductivity of the sphere-pac mixture was performed and the results were used in the heat transfer calculations. For the sphere-pacs of the breeder/multiplier mixture and of the Be (in the reflector zone), the estimated effective thermal conductivities are, respectively, 4.6 and 7.3 W/K-m.

Including the first wall, there are 17 nested shells that have built-in coolant channels. Thermal hydraulic analyses were performed using the detailed configuration at the mid-plane location of the blanket (where the neutron and surface wall loadings are at

their maximum values of, respectively, 3.87 and 0.61 MW/m²) and at the top and bottom locations of the outboard blanket (where the neutron and surface wall loadings are, respectively, 2.48 and 0.39 MW/m²). The temperature distribution in the blanket was evaluated for six radial zones. The blanket coolant channels have slightly different diameters at different vertical locations to allow for the poloidal variation of the neutron and surface wall loadings while maintaining similar pressure drops along the same blanket shell.

Results of the thermal-hydraulic calculations of the ARIES-I outboard blanket at the mid-plane location are presented in Table 1.5-VI. The first-wall maximum temperature is 1000 °C, less than the SiC design limit of 1100 °C. The Li₂ZrO₃ breeder has maximum temperatures of 908 and 933 °C occurring where the maximum volumetric power is generated, respectively, at the front and at the back of the blanket zone. This shows that the breeder material can be designed to within the recommended operational window of 400 to 1400 °C [76] for Li₂ZrO₃. The Be reflector zone can be designed to less than 900 °C. At the SiC reflector zone, the maximum SiC sphere-pac temperature is 1075 °C. These results should also be representative of the inboard blanket modules, which operate at somewhat lower wall load.

As shown in Figs. 1.1-2 and 1.5-2, the helium coolant enters the blanket from the inlet plenum which is located in the shield behind the blanket and reflector. It then flows radially inward towards the first wall. It cools the first wall while flowing in the toroidal direction before it turns and flows radially outward away from the first wall into the coolant outlet plenum. The pressure drop in the outboard blanket (including frictional losses, turns, and contractions and expansions) is estimated at 43.31 kPa. The external pressure drop through the steam heat exchanger and circulator is about 37.5 kPa [77]. Therefore the total blanket-loop internal and external pressure drop is 80.81 kPa. By assuming a similar pressure drop in the inboard blanket modules, the total pumping power is 17.1 MW. At a circulator efficiency of 90%, the blanket-loop pumping power is about 19 MWe.

1.5.6. Divertor Engineering

The ARIES-I divertor has a double-null configuration. Each of the 16 fusion-power-core (FPC) modules contains two upper and two lower divertor targets. The targets are pie-shaped for easy removal and installation, if necessary, prior to FPC module replacement. The targets are fabricated from individual SiC-composite tubes. Each tube receives coolant from a supply manifold located in the private-flux region between the

Table 1.5-VI.
Thermal-Hydraulic Results
(outboard module, mid-plane location)^(a)

	Velocity (m/s)	h (W/K-m ²)	Surface Temp (°C)	Maximum Temp (°C)	Pressure Drop (kPa)
First wall					
Inboard	19	2,088 ^(b)	655	718	20.2
Mid-plane	24	2,153 ^(b)	796	858	
Outboard	29	2,208 ^(b)	938	1,000	
Breeder/Be, Zone 1					
Inboard	14	2,079	504	613	22.0
Mid-plane	17	2,145	654	764	
Outboard	20	2,208	798	908	
Breeder/Be, Zone 2					
Inboard	10	2,148	500	610	24.6
Mid-plane	12	2,219	650	795	
Outboard	14	2,280	795	938	
Breeder/Be, Zone 3					
Inboard	9	1,520	535	645	11.6
Mid-plane	11	1,571	685	745	
Outboard	14	1,613	828	938	
Beryllium reflector					
Inboard	5	997	458	570	4.62
Mid-plane	7	1,030	607	720	
Outboard	8	1,058	754	866	
SiC reflector					
Inboard	6	1,132	476	780	6.12
Mid-plane	8	1,170	625	929	
Outboard	9	1,202	770	1,075	

^(a) First-wall channel diameter is 6.5 mm; shell channel diameter is 4 mm.

^(b) 20% reduction assumed due to non-symmetric surface heat flux (Sec. 8.7.).

inboard and outboard strike-points, as shown in Fig. 1.5-3. The SiC tubes can be manufactured either by 2-D braiding or helically winding the fibers around a mandrel, followed by SiC matrix infiltration. The individual tubes are tapered and placed side-by-side to form a tube bank with radial coolant flow. The plasma-facing side of the target is coated with a 2-mm-thick layer of tungsten that is plasma-sprayed onto the SiC tube bank. Excessive thinning of the tungsten coating will occur after several full-power disruptions, therefore *in-situ* plasma-spraying of tungsten will be used for repairs to the target surface if needed. The back of the tube bank (not facing the plasma) is reinforced with additional SiC to strengthen the tube bank and to provide leak tightness.

Helium cooling of the divertor target was selected based on safety concerns, reduced tritium inventory and clean-up, and compatibility with the primary-coolant system. The peak heat flux on the target, as calculated by the BRAAMS-2 [11] and EPIC [12] codes is 4.5 MW/m^2 . To optimize the thermal-hydraulic design, the target is contoured to give two differently heated zones. The first zone, near the strike point and the coolant inlet, is a flat plate inclined at a 10° poloidal angle to the incident particle flux. Along the plate in

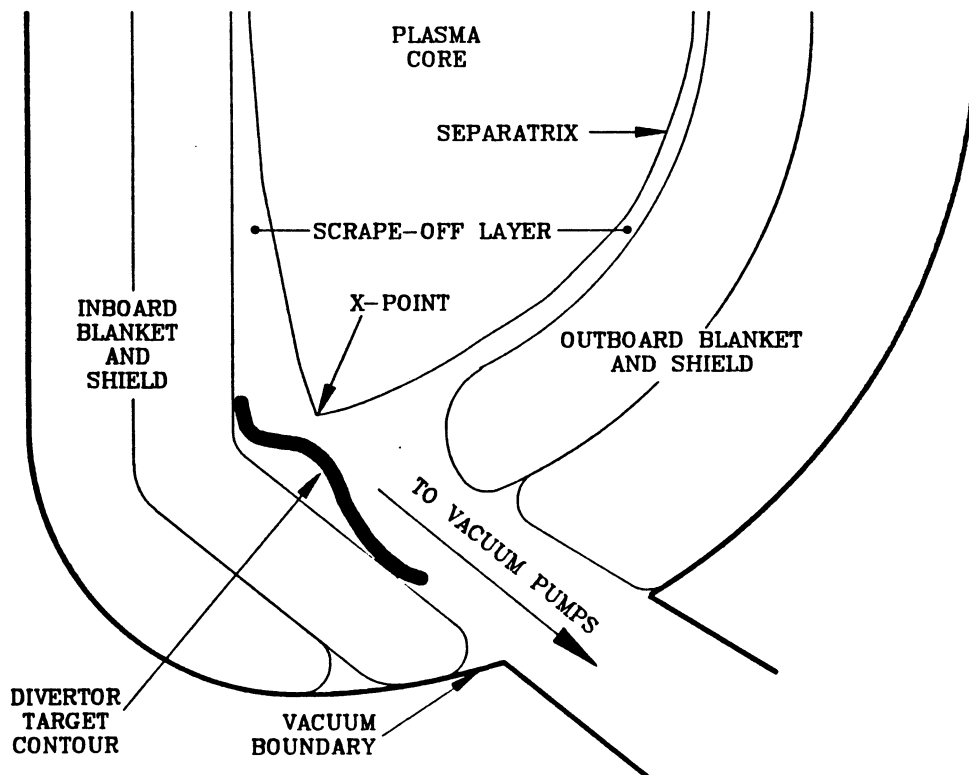


Figure 1.5-3. A schematic of the ARIES-I divertor layout, bottom target.

zone 1, the nominal heat flux drops exponentially from 4.5 to 0.7 MW/m². The heated length in this zone is 0.6 m and the plate penetrates 30 mm into the scrape-off layer (SOL). Zone 2 begins at the point where the heat flux is 0.7 MW/m² and is contoured to give a relatively uniform heat flux along the length of 0.4 m. This type of surface contouring gives the smallest target area while retaining an adequate safety margin to account for heat flux peaking due to target misalignment, toroidal peaking, *etc.* The inboard target is contoured to intercept more flux because the total power in the inboard SOL is about one-half of that in the outboard SOL. The target contour is illustrated in Fig. 1.5-3.

The thermal-hydraulic design of the divertor cooling system matches the inlet and outlet temperatures of the primary coolant system at the same pressure (350 and 650 °C at 10 MPa) so that the divertor thermal power is recovered by the power-conversion cycle. The coolant supply manifold is located in the private-flux region, near the ×-point, as shown in Fig. 1.5-3. Locating the coolant supply near the strike point of the target directs the cold inlet helium to the region of highest heat flux. Because of large uncertainty in edge-plasma parameters and because the above heat-flux estimate does not account for such factors as toroidal asymmetries or target misalignment, an engineering safety margin of ~2 was chosen as the divertor design goal (*i.e.*, localized heat fluxes twice as large as the estimated value that can be handled). To achieve this engineering safety factor, the target surface is contoured to have an inclination angle of 10° with respect to field lines in the poloidal plane for 0.60 m away from the strike point. In this region the heat flux is reduced (exponentially) to ~1 MW/m². The remaining 0.40 m of the target surface is contoured to have a constant heat flux of 1 MW/m². By contouring the target surface in the low flux region, the size of the target can be reduced and thereby provide more clearance behind the target for shielding.

Divertor coolant tubes have a hydraulic diameter of 2.5 mm and a wall thickness of 0.5 mm. Finite element analyses show that at the strike point (at peak heat flux of 4.5 MW/m²), the maximum tungsten temperature is 776 °C and the maximum combined thermal-plus-pressure stress is 121 MPa, both well below the design allowables. The pumping power required for the divertor circulators is about 35 MWe and represents 12% of the recovered thermal power from the divertor coolant circuit.

1.5.7. Tritium System

The design of the ARIES-I tritium system is focused on reducing the tritium inventory and simplifying the design. However, because of the material selection and system

configuration, some new problems have been uncovered during this study and they are documented here. Further work, both theoretical and experimental, will be required to address these problems. Because of its small size, the cost of the tritium system will be of secondary importance.

1.5.7.1. Plasma exhaust system

The largest tritium unit in a DT fusion reactor is the plasma-exhaust processing system. Even at the ARIES-I high burn fraction of 19%, however, the tritium throughput in the plasma exhaust is still over four times larger than the next largest tritium unit (*i.e.*, the blanket recovery system). Therefore, it is important to reduce the tritium inventory and the complexity of the plasma exhaust system. There are three components in this system that usually have large tritium inventories:

1. The cryogenic distillation (CD) unit, which is used to separate H, D, and T (can be large because of the large throughput and the high separation factor sometimes required).
2. A gettering bed for tritium separation, which is often used to separate hydrogen isotopes from the waste (also operates in a pulse mode); and
3. The cryogenic pumps, which operate in a pulse mode between the regenerating time (tritium inventory is proportional to the pulse time);

The complexity of the plasma exhaust system is primarily due to the multiple CD units and the equalizers required for the separation of H, D, and T.

A key concept developed in the ARIES-I study is that of using the CD process to separate only the H from D and T, while keeping the D:T ratio at 1. The fueling to the plasma is by DT pellet injection and because the D:T ratio in the exhaust is also 1, there is no need for separating D and T. The H is generated by the DD reaction in the plasma, which is very small. In order to minimize the throughput to the CD unit, the H concentration in the plasma is allowed to accumulate to $\sim 1\%$. Even at this level of H concentration, the plasma impurity concentration is still dominated by He, which is 10.7%. For such a system, only 10% of the plasma exhaust is required to pass through the CD unit to remove H. Since no additional separation of D and T is required, one CD column is sufficient, compared with three or four CD columns for a conventional fuel-processing system.

Because of the steady-state operation, a Pd diffuser is used to separate the hydrogen isotopes from the ^4He and other wastes (hydrogen will diffuse through the Pd diffuser, while the other gases will bypass it). The performance of a Pd diffuser in fuel cleanup has been demonstrated [78]. The waste processing is conventional (*i.e.*, using an oxidizer to convert all of the T in the waste to the HTO form, using a molecular sieve to separate HTO from other gases, and using a reduction unit to reduce the HTO to HT which will then recombine with the hydrogen stream from the Pd diffuser).

The cryogenic vacuum pump is another component that usually has a large tritium inventory. This is caused by the pump's pulsed mode of operation. To reduce the T inventory in the pumps, the ARIES-I design uses turbo-molecular pumps. Although a metallic turbo-molecular pump has to be shielded from the magnetic field, a ceramic pump, which doesn't require shielding, is being developed in Japan. At this time, the size of the pump is limited [79].

The major parameters of the ARIES-I fuel cycle are summarized in Table 1.5-VII. The tritium inventory in the CD unit is shown and compared to that for ITER in Table 1.5-VIII.

1.5.7.2. Blanket tritium inventory

For the ARIES-I design, the structural material is SiC composite, through which the tritium permeation rate is very low. Therefore, tritium release, if any, will be by leakage and not by permeation. Tritium leakage is caused mainly by cracks that develop in the coolant tubes. Because the coolant pressure (10 MPa) is much larger than the purge gas pressure (0.4 MPa), any leakage will be toward the purge. Therefore, it can be assumed that the tritium leakage to the primary coolant and to the steam generator will be extremely small.

The tritium inventory and plasma-driven permeation in the first wall and in the impurity control system are always of concern in a fusion reactor design. The tritium inventory in the SiC due to the pressure-driven permeation does not appear to be a serious problem because of the slow kinetics on the surface and the low diffusivity. However, the kinetic energy of the plasma particles will drive the tritium into the SiC where it will remain because the tritium diffusivity in SiC is very low and the solubility is very high, especially at low temperatures [67]. To minimize the tritium inventory in the SiC, the material temperature is kept above 750 °C. To reduce the tritium permeation to the divertor coolant, the divertor target is made with a tungsten coating on the SiC-composite coolant tubes.

Table 1.5-VII.
ARIES-I Fuel-Cycle Parameters

Fusion power (MW)	1,925
Tritium burn rate (g/d)	295
Tritium burn fraction	0.193
Tritium feed rate (g/d)	1,528
Tritium exhaust rate (g/d)	1,233
D exhaust rate (g/d)	822
⁴ He exhaust rate (g/d)	393
H generation rate (g/d)	1
H/(D + T)	1%
He/(D + T)	12%

Table 1.5-VIII.
Cryogenic-Distillation Capacity Comparison

		ARIES-I	ARIES-I
	ITER	(Conventional)	(Only separation of H)
Throughput (mole T/d)	2,500	411	41
Number of columns	4	4	1
Tritium inventory (g)	800	150	50

Tritium inventory is also a concern in the breeding blanket. Because of the high blanket operating temperature and the good tritium release characteristics of Li_2ZrO_3 (the reference breeding material), the tritium inventory in the breeding material is calculated to be only 0.3 g. However, there is the potential of high tritium inventory in the beryllium. The ARIES-I reactor has a very large Be mass fraction in the blanket, and the breeder and multiplier are intimately mixed in a sphere-pac configuration. The total tritium deposited in the Be is estimated to be 1.4 kg/FPY (full-power year), 1.1 kg/FPY of which is due to the $\text{Be}(n,T)$ reaction with the remainder produced in the breeder and deposited in the surrounding Be because of recoil.

The tritium release mechanism from the Be is highly uncertain. The difficulty is to separate the effect of the bulk diffusion inside the Be from the surface effect caused by the oxide. Transport and retention in Be has been highlighted as an ITER R&D issue. Experimental work (Hollenberg and Baldwin, PNL; and Longhurst, INEL) are underway. The new data by Baldwin [78] show very little tritium release (0.01% to 4%) from the irradiated Be in the temperature range of 300 to 510 °C. At 610 °C, however, there is a sudden burst of tritium released. For ARIES-I calculations, we are assuming that there is no tritium released below 610 °C and a complete release of tritium above 610 °C. With this assumption, it is possible to estimate the tritium inventory inside the Be. The volume fraction of Be with temperatures below 610 °C is calculated to be 25%. Since the total tritium deposited inside the Be is 1.4 kg/FPY, the total amount of tritium retained inside the Be is 0.64 kg/FPY. If the blanket is heated above 610 °C once a year while the plasma is down (or in partial power), the maximum tritium inventory in the Be is then 0.64 kg.

The tritium inventories of the ARIES-I major components have been calculated and are summarized in Table 1.5-IX. Minimizing the inventory is key and the important assumptions are listed on this table. The total tritium inventory in the reactor is 700 g, 90% of which is in the beryllium. The tritium release characteristics of Be are highly uncertain. Experimental work is in progress and more definite answers should be available in about one year.

1.5.8. Power Cycle

The thermal power produced in ARIES-I is removed by the primary coolant, helium, at 10 MPa pressure. The inlet and exit temperatures of the primary coolant are 350 and 650 °C, respectively. Because of the high coolant-exit temperature, advanced conventional and nonconventional thermal power cycles are possible. The following three categories

Table 1.5-IX.
Estimates of Tritium Inventory in the ARIES-I Design

Components	T Inventory	Comments
Fuel cycle		
Vacuum pumping	Small	Using ceramic turbo-molecular pump
Helium separation	Small	Using Pd diffuser
Cryogenic distillation	50 g	Using CD unit to remove H only
First wall	6 g	Sputtering removes C and T
Divertor wall	10 g	Using W coating on SiC
Blanket		
Breeder material	1 g	Selection of breeding material and operating temperature
Beryllium	640 g	1. Complete tritium release $>610^{\circ}\text{C}$ 2. Blanket heat to 610°C once a year

of power cycles were considered for the ARIES-I reactor: dissociating gas, inert gas Brayton, and Rankine steam. Among the advantages of the dissociating gas cycles are their compactness and higher efficiency when compared with inert-gas Brayton cycle and Rankine steam cycle [80, 81]. However, the dissociating gases such as nitrogen tetroxide (N_2O_4) and nitrosyl chloride (NOCl) are highly toxic and corrosive. Safety hazards and the need to develop advanced corrosion-resistant structural materials are the main disadvantages of the dissociating gas cycles. An inert-gas Brayton cycle is more compact than the Rankine steam cycle. However, the Rankine steam cycle has significantly higher efficiency for the same maximum cycle temperature. An advanced supercritical Rankine steam cycle is currently under development by the industry for use in near-term coal-fired plants; this cycle is selected for the ARIES-I reactor.

In the United States, there are 159 supercritical units in a total of 89 plants representing 15% of the total United States plants [82]. The supercritical cycles use double reheat. At present, standard practice at operating power plants is to use the steam condition of 24 MPa and 566/566/566 $^{\circ}\text{C}$ (3500 psia and 1050/1050/1050 $^{\circ}\text{F}$). Although

advanced supercritical steam cycles are also operational at present, they are still in the testing, data gathering, and appraisal phases. The Eddystone Station (unit-1) of the Philadelphia Electric Co. has the steam conditions 35 MPa and 649/566/566 °C and the Electric Power Development Company of Japan is studying cycles with the steam condition of 35 MPa and 649/593/593 °C [26]. A recent study sponsored by the Electric Power Research Institute [26] concludes that, for the near future, an economically optimum advanced steam cycle would have the steam condition of 31 MPa and 593/593/593 °C and an expected availability of 87% to 88%. Consistent with this, the steam conditions of the ARIES-I power cycle are 31 MPa and 600/600/600 °C.

Because the primary-coolant exit temperature is 650 °C, the superheater and the two reheaters are arranged in parallel in order to obtain the maximum steam temperature of 600 °C from each. The computer code, PRESTO [83], has been used to analyze the performance of this cycle. The parameters optimized are the feedwater inlet temperature, the number of regenerative feedwater heaters, and the steam condition at the extraction points. The main parameters and results are given in Table 1.5-X. A gross thermal efficiency of 49% is calculated.

1.5.9. Maintenance

The complexity of the maintenance operation and the required time for its completion are strongly influenced by the machine design and plant layout. Because of this interconnection, operational and maintenance aspects of the ARIES-I reactor have been incorporated into the design process from the beginning. The maintenance philosophy of the ARIES-I reactor is based on our examination of the maintenance procedures for commercial fission power plants, other conceptual fusion-reactor designs, and existing experimental fusion facilities. This evaluation resulted in several guidelines that can lead to drastic reduction in the maintenance time for a fusion facility. Most of these guidelines simply allow for ready access to components that have to be replaced.

We have also reviewed remote maintenance in some of the existing (and planned) fusion facilities and commercial fission reactors and also the use of robotics in production factories. Our review indicates that, rather than using manipulators with human operators, the maintenance operations for a fusion facility should be standardized and highly automated so that robots can be utilized. The maintenance approach to unscheduled events should be similar to that for scheduled events and work in the reactor vault should be limited to replacing components. Repairs to failed components, if desired, should be made afterward and outside of the reactor vault.

Table 1.5-X.
Major Parameters of the ARIES-I Power-Conversion System

Total thermal power (MW)	2,543
Total helium flow rate (kg/s)	1,631
Total steam flow rate (kg/s)	892
Number of turbine generator sets	2
Arrangement of the turbines	Tandem
Number of reheats	2
Number of regenerative feedwater heaters	9
Steam conditions	
Maximum throttle pressure (MPa)	31
Temperature after superheat (°C)	600
Temperature after 1st reheat (°C)	600
Temperature after 2nd reheat (°C)	600
Extraction pressures (MPa)	
Heater 1	9.0
Heater 2	3.8
Heater 3	2.4
Heater 4	1.7
Heater 5	1.14
Heater 6	0.47
Heater 7	0.26
Heater 8	0.14
Heater 9	0.048
Condenser back pressure (MPa)	0.0067
Feedwater inlet temperature (°C)	301
Gross thermal efficiency	0.49

The ARIES-I maintenance philosophy is, therefore, based on high degrees of standardization and automation. The ARIES-I FPC comprises 16 large-scale, identical modules. The modules are self-contained and structurally independent of any neighboring component. Each of the modules consists of one toroidal-field (TF) coil, two inboard and two outboard first-wall, blanket, and shield sub-modules, two and upper and lower divertor targets with support structure, and a section of the vacuum vessel. The limit to the number of components within a module is principally determined by the total mass of the module to be transported. Since the TF coils are removed during module replacement, a removable cryostat seal is used (Fig. 1.4-3) which does not require the cutting and joining of welds to remove cryogenic structures, further reducing the time required for maintenance.

Each module is replaced as a single unit during both scheduled and unscheduled events (Fig. 1.5-4). Furthermore, all modules are pretested prior to installation in the reactor vault so that undetected defects become evident and high reliability can be achieved. As a result, new modules are always available for immediate installation in the reactor vault. Minimum repair is performed in the reactor vault. Instead, the module containing the failed component is removed and replaced with a new module. After the reactor is back on line, the modules that have been removed can be serviced for later use and/or prepared for recycling and waste disposal.

Several different maintenance schedules have been evaluated. Consideration has been given to whether annual, two-module replacement or replacement of all 16 modules every 8 years is preferable. Since the modules are self-contained, the interfaces with neighboring modules and support structure should be few. It is anticipated that two modules can be replaced within the allocated 28-day annual scheduled maintenance period. The schedule allows for one week each to remove and replace the two modules and two weeks for common maintenance activities, resulting in an overall plant availability of 76% (including 60 days for unscheduled maintenance). If module replacement and other associated activities require much more than the allocated 28 days per year, then a less frequent replacement schedule may be preferable to achieve the highest availability possible.

1.5.10. Fusion-Power-Core R&D Needs

In large measure, the economic, safety, and environmental performance of the ARIES-I reactor is due to its advanced, high-performance fusion power core (FPC). Achievement of this high performance will require numerous advances beyond the state-of-the-art of

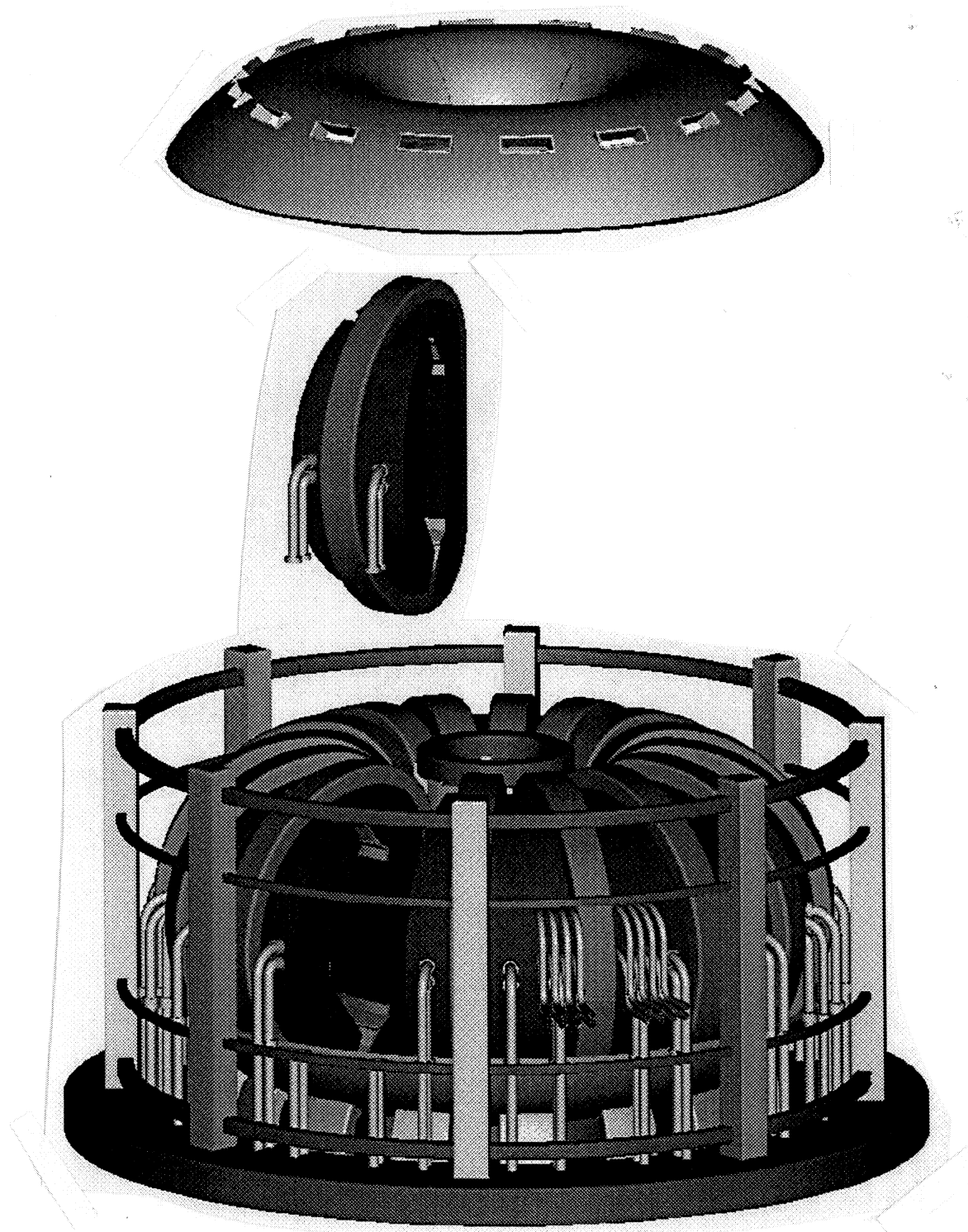


Figure 1.5-4. Schematic of the movement of components during removal and replacement of an ARIES-I FPC module.

today. The research and development needed to develop the technologies required for an ARIES-I-type FPC design are summarized below.

SiC-composite R&D. Silicon carbide has excellent high-temperature capabilities, thermal-shock resistance, chemical stability, and environmental resistance. These characteristics, coupled with very low induced activation and afterheat, make SiC a very promising material for future fusion applications. The ARIES-I reactor uses SiC-fiber-reinforced SiC-matrix composites (SiC composites) as the primary structural material. A large-scale R&D effort to develop this material is currently underway by aerospace and automobile industries in the U.S., Japan, and Europe. Ceramic composite materials, however, are still in their developmental infancy (10 years) and, consequently, the thermomechanical data base is limited and no irradiation data for SiC composites exist (some irradiation data on fibers and bulk material is available). Therefore, many engineering issues will require intense R&D efforts before SiC composites reach levels of reliability similar to that of metallic alloys. The research and development efforts can be divided into four categories: (1) understanding fundamental material performance, (2) developing manufacturing techniques that result in standardized and economical production processes, (3) development of radiation-damage-tolerant composite materials, and (4) light-ion interactions.

Because of the large-scale industrial effort, the fusion composite-materials R&D program will be able to focus on fusion-specific issues. For fusion applications, the critical issue that needs to be addressed is radiation response of ceramic matrix composites (CMCs) to neutron and ionizing radiation so that appropriate materials can be developed. This is an issue that is not being pursued by the CMC industry. Areas for R&D of radiation effects on CMCs for use in fusion applications are: (1) understanding fundamental processes (which are quite different from those of metallic alloys), (2) effects of irradiation on a composite microstructure, and (3) effects of ionizing radiation on the thermomechanical properties of CMCs. In addition, for in-vessel applications, interaction of light ions with CMCs should be studied.

The manufacturing issues for an SiC-composite FPC include: (1) manufacturing large-scale components, (2) gas leak tightness, (3) brazing and joining, and (4) joining to other materials. The SiC composite industry has developed dedicated solutions to all of the above issues. However, most efforts to date have only demonstrated solutions for small component sizes with emphasis on one or two of the problems at a time. It is generally recognized that there is a need to develop and demonstrate the ability to incorporate these solutions into one all-encompassing manufacturing technique.

Breeder material R&D. Isotopically tailored Li_2ZrO_3 is selected as the breeder material for ARIES-I. It should be noted that even after extensive isotopic tailoring, the off-site dose after a severe accident in the ARIES-I reactor is still dominated by Zr. This provides a strong incentive to develop alternate, low-activation solid-breeder materials such as Li_4SiO_4 that exhibit very low activation and afterheat without the need for isotopic enrichment. Lithium orthosilicate would permit thermal design conditions comparable to those of Li_2ZrO_3 . Considerable uncertainty exists, however, regarding the chemical stability and tritium inventory of Li_4SiO_4 under high lithium burnup. This uncertainty should be resolved by the breeder-material development program. If the results of these experiments prove to be positive for Li_4SiO_4 , it could be substituted for Li_2ZrO_3 in the ARIES-I design with virtually no design changes. An alternative breeder choice for ARIES-I is Li_2O , which would have zero afterheat and induced radioactivity. At high temperatures, chemical compatibility of Li_2O with the structural material, Be, and moisture and lithium mass transport are critical issues. As such, Li_2O may require a lower operating temperature than Li_2ZrO_3 or Li_4SiO_4 . If Li_2ZrO_3 remains the only choice as the ceramic breeder, isotopic tailoring of zirconium in Li_2ZrO_3 at an acceptable cost is a key issue.

Tritium systems R&D. The ARIES-I design effort has focused on reducing the tritium inventory in the system. The largest tritium unit in a DT fusion reactor is the plasma exhaust system. Since fueling is done by pellets (no neutral beams), there is no need to separate D and T in the plasma exhaust, and the T inventory in the cryogenic distillation system is reduced by a factor three to four. By using a Pd diffuser instead of gettering beds, the T inventory in the helium separation system is very small. Also, the inventory in the vacuum pumps is drastically reduced by using ceramic turbo-molecular pumps instead of cryogenic pumps. These ceramic pumps, which do not require magnetic shielding, are being developed in Japan, but the pump size is small at present.

The ARIES-I blanket tritium inventory is low but highly uncertain. The tritium inventory of the SiC first wall due to pressure-driven permeation is small because of low T diffusivity in SiC. The inventory due to plasma-particle implantation in SiC is highly uncertain and requires confirmation data, preferably from experiments in a tokamak. About 90% of the ARIES-I tritium inventory is in the Be neutron multiplier. The tritium release mechanism from Be is not well-known. The difficulty is to separate the effect of the bulk diffusion inside the Be from the surface effect caused by BeO. Further experimental work in this area is necessary.

Power cycle R&D. The ARIES-I reactor utilizes an advanced supercritical Rankine steam cycle, which is currently under development by the industry for near-term coal-fired plants.

Blanket design R&D. The thermostructural design of the ARIES-I fusion power core is based on the limited available data base for various materials. Measurements of the heat transfer characteristics of sphere-pac beds of beryllium and solid-breeder/beryllium mixtures and measurements of properties of irradiated SiC composite, breeder, and beryllium neutron-multiplier materials are required to validate the design. The ARIES-I blanket is the first design utilizing SiC composites and, therefore, is not necessarily an optimum design configuration. More detailed neutronics, thermostructural, and configurational studies are needed in order to optimize the design. Further design studies should also focus on using an alternate low-activation breeder and reducing (or eliminating) the Be neutron multiplier.

Divertor engineering R&D. The impurity control system is probably the most difficult engineering subsystem in a fusion reactor. ARIES-I uses poloidal divertors operating in the high-recycling regime to achieve acceptable heat fluxes and low plasma temperatures at the divertor target. The divertor target is coated with tungsten to reduce erosion to manageable levels. Experimental verification of high-recycling divertors with high- Z -coated divertor plates is needed to validate this design approach. Considerable uncertainty exists in estimates of the edge-plasma parameters by edge-physics codes and further experiments are required to validate these codes. Because of the strong physics/engineering interaction, divertor engineering R&D should focus on approaches for reducing the heat flux arriving at the divertor plate (*e.g.* radiative core plasmas, slot divertors, gas and/or impurity injection in the scrape-off-layer, *etc.*), as well as on engineering designs for the divertor plate itself. Since most of the plasma power is deposited on the divertor target plate during a disruption, detailed engineering analyses of the impact of disruptions is also a key issue.

1.6. ENVIRONMENTAL AND SAFETY FEATURES

Throughout the ARIES-I study, the design effort has been directed to maximize the environmental and safety advantages of fusion through the careful selection of materials and care in design. The ARIES-I design achieves Level 2 of safety assurance (large-scale

passive safety) as defined in Ref. [27] (*i.e.*, reactor requires no active systems to protect the general public. The ARIES-I design may achieve Level 1 (inherent safety) if the reference breeder material (lithium zirconate) can be replaced by lithium orthosilicate or lithium oxide (although the tungsten coating of the divertor plates is still a safety concern). All ARIES-I components also qualify for Class-C waste disposal in shallow land burial as described by Federal Regulation 10CFR61 [29].

1.6.1. Material Selection

The primary structural material (silicon-carbide composite) is a low-activation material with high melting temperature. Because of the low peak temperatures calculated for a loss-of-coolant accident (LOCA), the release fractions of induced activity are low. Helium is the choice of coolant for the first wall, blanket, and divertor, which thereby removes concerns about coolant activation and chemical interactions between the coolant and blanket materials. In particular, the use of helium, rather than water, in the divertor eliminates concerns about tungsten-steam reactions and the transport of the tungsten activation products from the reactor.

The reference tritium-breeder material is Li_2ZrO_3 because of the demonstrated high-temperature-stability data base. However, other breeders, specifically Li_4SiO_4 and Li_2O , have much lower afterheat and activation and are preferable from safety and environmental viewpoints. The use of zirconium in the breeder will necessitate isotopic tailoring to remove ^{90}Zr which produces ^{89}Zr , and ^{94}Zr which produces ^{93}Zr and ^{94}Nb . The ^{89}Zr isotope poses accident concerns while ^{93}Zr and ^{94}Nb lead to waste management problems. Laser isotope separation is the only feasible technique for accomplishing this tailoring since both light and heavy isotopes are to be removed. The breeder contains 36.6 tonnes of zirconium that would be isotopically tailored. The waste disposal rating for Li_2ZrO_3 using natural Zr is about 7 because of ^{94}Nb activity. The Li_2ZrO_3 breeder with isotopically tailored Zr, however, will qualify as 10CFR61 Class-C waste because of the reduction of ^{94}Nb activity by a factor of 10 lower than that for natural Zr.

Beryllium is used as the neutron multiplier in the ARIES-I blanket. The total beryllium inventory in the ARIES-I reactor is 192 tonnes compared with the present U.S. annual demand of 250 to 275 tonnes. Recycling of beryllium will be necessary in order to optimize the use of beryllium resources; a major increase in mining and fabrication capacity may be needed for a large fusion economy. Because of concerns for occupational exposure to Be dust which can result in berylliosis (a lung disease), the overall safety of

the ARIES-I design may require screening workers for sensitivity to Be and some degree of automated, hands-off fabrication.

The divertor plates contain a 2-mm-thick coating of tungsten on the plasma-facing surfaces. The total amount of tungsten is about 6 tonnes. However, ^{186}W isotope is activated to ^{187}W and the ^{184}W to $^{186\text{m}}\text{Re}$. The waste disposal rating for natural-tungsten-coated divertor collector plates is about 1.5 after averaging with the SiC-composite coolant tubes. The tailored tungsten element, which enriches ^{183}W abundance to 90% and reduces the rest of the isotopes in proportion to their respective natural abundance, is estimated to reduce the waste disposal rating below 0.5. Furthermore, by using this tailored material, the prompt dose at 1 km is reduced to about 11 rem in case of a major accident resulting in the release of all of the mechanistically vulnerable material in the divertor plates.

1.6.2. Loss-of-Coolant Accident Analysis

A 2-D finite-element model of the first wall, blanket, and shield was analyzed using the computer code, TOPAZ [84], to determine the maximum structure temperature in case of a loss-of-coolant accident (LOCA). The assumptions made are: (1) plasma is quenched at the onset of a LOCA; (2) the heat removal capacity of the primary coolant is negligible after depressurization; (3) all of the structure is at an initial, uniform temperature of 700°C ; and (4) the vacuum boundary remains intact and there is no conduction path across it. The results show a peak temperature of 780°C occurring at about 5 minutes into the event. This low peak temperature is due to the low level of afterheat in the structure (SiC) and high heat capacity of the blanket (due to Be). The afterheat level in the blanket is about 0.4 MW/m^3 at shutdown and drops by about an order of magnitude after 5 minutes.

A similar analysis was done for the divertor where, because of the W coating, the afterheat level is higher (5 MW/m^3 at shutdown and is approximately constant after one hour). It is assumed that the first wall has reached 780°C and remains constant, and that the divertor plate, which faces the plasma, radiates to the first wall. This analysis gives a peak divertor-plate temperature of 1020°C , well below the melting point of tungsten.

1.6.3. Radioactivity Analysis

The main sources of radioactivity are zirconium in the blanket and tungsten in the divertor plate. In particular, the zirconium isotopes ^{90}Zr and ^{94}Zr , and the tungsten

isotopes ^{182}W , ^{184}W , and ^{186}W are responsible for most of the activity. The activity produced by the SiC-composite structural material, the Be multiplier, and the $\text{B}_4\text{C}/\text{SiC}$ shield is small.

In order to calculate dose rates, it is necessary to estimate the fractions of the radioactive materials that could be released during an accident. For Zr in the Li_2ZrO_3 breeder, the release fraction is estimated at 2%. The blanket comprises 64 independent modules of which 3 at most can be expected to fail in a credible accident. To be conservative, the ARIES-I safety analysis assumes that 2% of the total Zr inventory of all 64 modules is released, which is equivalent to releasing the entire Zr inventory in 3 modules. The release fraction used for the tungsten divertor is based on experiments performed at INEL [85] in which air at 800, 1000, and 1200 °C flowed past samples of W-Re-Ta alloy for 1, 5, and 10 hours. Since the divertor is a single unit, the total tungsten inventory will contribute to the release fraction in a credible accident. The estimated release fractions are 0.0327% for W, 29.2% for Re, and 0.197% for Ta and other elements.

Using the release fractions given above and assuming 100% release of the maximum tritium inventory (Table 1.5-IX), the site-boundary (at 1 km) dose and waste disposal ratings for zirconium and tungsten are calculated by using the code FUSECRAC. The side boundary dose is calculated assuming highly adverse weather and release conditions (Pasquill F stability, 1 m/s wind speed, inversion layer at 250 m, release at ground level with no thermal plume rise, and a deposition velocity of 0.01 m/s).

A summary of the safety analysis is provided in Table 1.6-I which is based on isotopically tailored Zr and W. The isotopic concentrations of the tailored Zr and W (in %) are: $^{90}\text{Zr}=0.06$, $^{91}\text{Zr}=0.01$, $^{92}\text{Zr}=99.91$, $^{94}\text{Zr}=0.02$, $^{96}\text{Zr}=0.0$; $^{180}\text{W}=0.02$, $^{182}\text{W}=3.07$, $^{183}\text{W}=90.0$, $^{184}\text{W}=3.76$, $^{186}\text{W}=3.51$. Table 1.6-II gives the waste disposal ratings (in %) for ARIES-I components and shows that all components qualify as Class-C shallow-land-burial waste. It should be noted that with natural Zr and W, the site-boundary dose would be much higher and the waste disposal rating of Zr would be higher than 1.

1.6.4. Safety R&D Needs

The ARIES-I design achieves Level 2 of safety assurance (large-scale passive safety) by (1) using low-activation structural, primary coolant, and multiplier materials; (2) isotopic tailoring of zirconium in the breeder compound and tungsten used as coating on the divertor plates; and (3) reducing the release fraction by design improvement, which limits the structure temperature during a LOCA. The safety performance can be greatly

Table 1.6-I.
Summary of ARIES-I Off-Site Doses

Source	Dose (rem)	Comments
Zr	91.	Using 99.91% ^{92}Zr , 2% release
W	11.2	Using 90% ^{183}W , 10-h LOCA at 1000 °C
Tritium ^(a)	6.4	FUSECRAC analysis, $qf = 1$
Impurities ^(b)	21.	In SiC, B ₄ C, and Li ₂ ZrO ₃
Total	130.	

^(a)Based on a maximum tritium inventory in Be of 640 g (Sec. 1.5.7).

^(b)Based on impurity concentrations from ESECOM [28].

Table 1.6-II.
Waste Disposal Ratings (WDR) of ARIES-I Material

Component	WDR
Li ₂ ZrO ₃ breeder	0.05
Tungsten divertor target	0.10
Tritium	0
SiC first wall	0.12
SiC/B ₄ C shield	<0.10

enhanced by using lithium orthosilicate (Li_4SiO_4) or lithium oxide (Li_2O) instead of the reference Li_2ZrO_3 breeder. In that case, ARIES-I may achieve Level 1 of safety assurance (inherent safety). Considerable uncertainty exists, however, regarding the chemical stability and tritium inventory of Li_4SiO_4 under high lithium burnup. This uncertainty should be resolved by the breeder-material development program. The tungsten coating of the divertor plate is a safety concern and research to eliminate the high- Z coating of the divertor plates should be pursued.

The safety analysis of ARIES-I is based on limited available data. Further measurements of release fractions under accident conditions are needed to validate the design. The ARIES-I tritium inventory is also uncertain and R&D in this area (Sec. 1.5.10) is needed. More systematic studies of accident scenarios are desirable. The ARIES-I safety analysis assumes that the plasma can be shutdown in, at most, 10 s after initiation of an accident. Research in passive plasma shutdown methods is also a key issue.

REFERENCES

- [1] R. W. Conn and F. Najmabadi, "Visions of the Future, A Program in Tokamak Reactor Studies," University of California Los Angeles report UCLA-PPG-1201 (1987).
- [2] F. Najmabadi, R. W. Conn, and the ARIES Team, "The ARIES Tokamak Fusion Reactor Study," *Proc. IEEE 13th Symp. on Fusion Eng.*, Knoxville, TN (Oct. 1989), IEEE No. 89CH2820-9, IEEE, Piscataway, NJ (1990) p. 1021.
- [3] F. Troyon, R. Gruber, H. Sauernmann, S. Semenzato, and S. Succi, "MHD-Limits to Plasma Confinement," *Plasma Phys. Controlled Fusion* **26** (1984) 209.
- [4] N. J. Fisch, "Theory of Current Drive in Plasmas," *Rev. Mod. Phys.* **59** (1987) 175.
- [5] S. P. Hirshman, "Finite-Aspect-Ratio Effects on the Bootstrap Current in Tokamaks," *Phys. Fluids* **31** (1988) 3150.
- [6] L. Grisham, "Aspect Ratio Scaling Studies in TFTR," presented at Transport Task Force Workshop, Hilton Head, SC (Feb. 1990).
- [7] C. E. Singer *et al.*, "BALDUR: A One-Dimensional Plasma Transport Code," Princeton Plasma Physics Laboratory report PPPL-2073 (1986).
- [8] D. A. Ehst *et al.*, "Fast Wave Heating/Current Drive Scenarios for ITER," ITER Internal report ITER-IL-Ph-6-9-U19 (1989).
- [9] R. McWilliams and R. C. Platt, "Fast-Wave Current Drive in the Irvine Torus," *Phys. Rev. Lett.* **56** (1986) 835.
- [10] T. L. Owens, "A Folded Waveguide Coupler for Plasma Heating in the Ion Cyclotron Range of Frequencies," *IEEE Trans. Plasma Sci.* **PS-14** (1986) 934.
- [11] B. Braams, "A Multi-Fluid Code for Simulation of the Edge Plasma in Tokamaks," NET report NET-68, EUR-FU/XII-80/87/68 (1987).
- [12] E. Vold, "Transport in the Tokamak Plasma Edge," Ph.D. thesis, University of California Los Angeles (1989).
- [13] S. Foner, C. L. H. Thieme, S. Pourrahimi, and B. B. Schwartz, "Practical Processing of A-15 Multifilamentary Superconducting Wire from Powders: Nb_3Al and Nb_3Sn ," *Adv. Cryo. Eng.* **32** (1986) 1031.

- [14] S. Pourrahimi, C. L. H. Thieme, and S. Foner, "21 Tesla Powder Metallurgy Processed Nb₃Sn (Ti) Using Nb-1.2 wt.% Ti Powders," *IEEE Trans. Magn.* **MAG-23** (1987) 661.
- [15] J. Martin, R. G. Ballinger, M. M. Morra, M. O. Hoenig, and M. M. Steeves, "Tensile, Fatigue, and Fracture Toughness Properties of a New Low Coefficient of Expansion Cryogenic Structural Alloy, Incoloy 9XA," *Adv. Cryo. Eng.* **34** (1988) 149.
- [16] M. M. Morra, I. S. Hwang, R. G. Ballinger, M. M. Steeves, and M. O. Hoenig, "Effect of Cold Work and Heat Treatment on the 4-K Tensile, Fatigue and Fracture Toughness Properties," in *Proc. Magnet Technol.* **11** (1989).
- [17] R.G. Ballinger, Massachusetts Institute of Technology, private communication (1989).
- [18] "ITER Conceptual Design Report," ITER Documentation Internal Series No. 7, International Atomic Energy Agency, Vienna (1989).
- [19] J. Miller *et al.*, "Report of the Work by the Magnet Design Unit," Lawrence Livermore National Laboratory report LLNL-ITER-89-020 (1989).
- [20] C. V. Renaud, E. Gregory, and J. Wong, "Production of High Conductivity/High Strength *In-Situ* CuNb Multifilamentary Composite Wire and Strip," *Adv. in Cryo. Eng.* **32** (1985) 443.
- [21] R. Bustamante, Amercom Inc., Chatsworth, CA, private communication (Feb. 1989).
- [22] Kato and Kagawa, Nippon Carbon Corp., Japan, private communication (July 1990).
- [23] G. Vogel, Dow Chemical Co., Midland, MI, private communication (July 1990).
- [24] A. Fresco, Lanxide/Du Pont Inc., Willmington, DE, private communication (July 1990).
- [25] W. Tarasen, BP Chemical Corporation (HITCO), Gardena, CA, private communication (Feb. 1990).
- [26] "Development of Advanced Fossil-Fuel Power Plants," Electric Power Research Institute report EPRI CS-4029 (1985).

- [27] S. J. Piet, "Approaches to Achieving Inherently Safe Fusion Power Plants," *Fusion Technol.* **10** (1986) 7.
- [28] J. P. Holdren, D. H. Berwald, R. J. Budnitz, J. G. Crocker, J. G. Delene, R. D. Endicott, M. S. Kazimi, R. A. Krakowski, B. G. Logan, and K. R. Schultz, "Report of the Senior Committee on Environmental, Safety, and Economic Aspects of Magnetic Fusion Energy," Lawrence Livermore National Laboratory report UCRL-53766 (1989); also, J. P. Holdren, D. H. Berwald, R. J. Budnitz, J. G. Crocker, J. G. Delene, R. D. Endicott, M. S. Kazimi, R. A. Krakowski, B. G. Logan, and K. R. Schultz, "Exploring the Competitive Potential of Magnetic Fusion Energy: The Interaction of Economics with Safety and Environmental Characteristics," *Fusion Technol.* **13** (1988) 7.
- [29] "Standards for Protection Against Radiation," U.S. Nuclear Regulatory Commission, Code of Federal Regulations, Title 10, Parts 0 to 199 (1986).
- [30] J. G. Delene, K. A. Williams, and B. H. Shapiro, "Nuclear Energy Cost Data Base," U.S. Department of Energy report DOE/NE-0095 (1988).
- [31] J. G. Delene, H. I. Bowers, and B. H. Shapiro, "Economic Potential for Future Water Reactors," *Trans. Am. Nucl. Soc.* **57** (1988) 205.
- [32] J. Schwartz, J. R. Miller, and J. E. C. Williams, "TF Overall Current Density Scaling," Massachusetts Institute of Technology, ARIES Program Internal memo (Nov. 1988).
- [33] J. G. Delene, R. A. Krakowski, J. Sheffield, and R. A. Dory, "GENEROMAK Fusion Physics, Engineering, and Costing Model," Oak Ridge National Laboratory report ORNL/TM-10728 (1988).
- [34] M. F. Reusch and G. H. Neilson, "Toroidally Symmetric Polynomial Multipole Solution of the Vector Laplace Equation," *J. Comput. Phys.* **64** (1986) 1416.
- [35] C. E. Kessel, Jr. and M. A. Firestone, "Determination of Gross Plasma Equilibrium form Magnetic Multipoles," *Trans. Am. Nucl. Soc.* **52** (1986) 185.
- [36] S. C. Jardin, N. Pomphrey, and J. DeLucia, "Dynamic Modeling of Transport and Positional Control of Tokamaks," *J. Comput. Phys.* **66** (1986) 481.
- [37] D. J. Strickler *et al.*, "MHD Equilibrium Methods for ITER PF Coil Design and Systems Analysis," Oak Ridge National Laboratory report ORNL/FEDC-88/7 (1989);

- also D. J. Strickler, N. Pomphrey, and S. C. Jardin, "Equilibrium Shape Control in CIT PF Design," *Proc. IEEE 13th Symp. on Fusion Eng.*, Knoxville, TN (Oct. 1989), IEEE No. 89CH2820-9, IEEE, Piscataway, NJ (1990) p. 898.
- [38] T. Tsunemitsu *et al.*, "Operational Limits and Disruptions in Tokamaks—Status and Application to ITER," Japan Atomic Energy Research Institute report JAERI-M-89-056 (1989).
- [39] R. C. Grimm, J. M. Greene, and J. L. Johnson, "Computation of the Magnetohydrodynamic Spectrum in Axisymmetric Toroidal Confinement Systems," *Methods Comput. Phys.* **16** (1976) 253; also R. C. Grimm, R. L. Dewar, and J. Manickam, "Ideal MHD Stability Calculations in Axisymmetric Toroidal Confinement Systems," *J. Comput. Phys.* **49** (1983) 94.
- [40] M. W. Phillips, A. M. M. Todd, M. H. Hughes, *et al.*, "MHD Stability Properties of a High Current, High Beta Tokamak," *Nucl. Fusion* **28** (1988) 1499.
- [41] J. A. Leuer, "Passive Vertical Stability in the Next Generation Tokamaks," *Fusion Technol.* **15** (1989) 489.
- [42] D. J. Ward, S. C. Jardin, and C. Z. Cheng, "Stability of Axisymmetric Modes in Tokamak Plasmas with Active Feedback," *Bull. Am. Phys. Soc.* **34** (1989) 1974.
- [43] W. Houlberg, Oak Ridge National Laboratory, private communication (1989).
- [44] D. Stotler, Princeton Plasma Physics Laboratory, private communication (1989).
- [45] F. C. Jobses, S. Bernabei, T. K. Chu, *et al.*, "Start-Up and Ramp-Up of the PLT Tokamak by Lower Hybrid Waves," *Phys. Rev. Lett.* **55** (1985) 1295.
- [46] T. Imai, "Recent Results of LHCD Experiments on JT-60," presented at U.S.-Japan Workshop on Advanced Current Drive Concepts, Livermore, CA (1990).
- [47] S. Itoh, N. Hiraki, Y. Nakamura, *et al.*, "Study on Steady-State Tokamak Operation by LHCD in TRIAM-1M," presented at U.S.-Japan Workshop on Advanced Current Drive Concepts, Livermore, CA (1990).
- [48] G. V. Pereverzev, "Non-Inductive Startup and Current Ramp-Up Scenario Optimization for a Tokamak Reactor," *Proc. 12th Int. Conf. on Plasma Phys. and Controlled Nucl. Fusion Research*, Nice, France (Oct. 1988), International Atomic Energy Agency, Vienna (1989) p. 739.

- [49] D. H. Preist and M. B. Shrader, "The Klystrode—An Unusual Transmitting Tube with Potential for UHF-TV," *Proc. IEEE* **70** (1982) 1318.
- [50] G. R. Haste, D. J. Hoffman, "High-Power Testing of the Folded Waveguide," *Proc. 8th Top. Conf. Radio-Frequency Power in Plasmas*, Irvine, CA (1989), *AIP Conf. Proc.* **190** (1989) 266.
- [51] M. F. A. Harrison, P. J. Harbour, and E. S. Hotston, "Plasma Characteristics and Gas Transport in the Single-Null Poloidal Divertor of the International Tokamak Reactor," *Nucl. Technol./Fusion* **3** (1983) 432.
- [52] E. Vold, A. K. Prinja, F. Najmabadi, and R. W. Conn, "The Neutral Diffusion Approximation in a Consistent Tokamak Edge Plasma-Neutral Computation," *J. Nucl. Mater.* **176&177** (1990) 570.
- [53] W. L. Stirling, W. R. Becraft, J. H. Whealton, and H. H. Haselton, "A Neutral Particle Beam System for ITER with RF Acceleration," *Proc. IEEE 13th Symp. on Fusion Eng.*, Knoxville, TN (Oct. 1989), IEEE No. 89CH2820-9, IEEE, Piscataway, NJ (1990) p. 1448.
- [54] W. S. Cooper, "Summary of the Status of Negative-Ion Based Neutral Beams," *Nucl. Technol./Fusion* **4** (1983) 632.
- [55] "IAEA Large Coil Task; Chapter 3: Characteristics of the Coils," D. S. Beard, W. Klose, S. Shimamoto, G. Vecsey, Eds., *Fusion Eng. Des.* **7** (1988) 23.
- [56] S. Shimamoto, H. Nakajima, K. Yoshida, and E. Tada, "Requirements for Structural Alloys for Superconducting Magnet Cases," *Adv. Cryo. Eng.* **32** (1988) 23.
- [57] H. Boenig and F. Cibulka, "A Static VAR Compensator Using a Superconducting Coil," *IEEE Trans. Power Apparatus and Systems* **10** (1982) 259.
- [58] D. L. Smith, G. D. Morgan, M. A. Abdou, *et al.*, "Blanket Comparison and Selection Study—Final Report," Argonne National Laboratory report ANL/FPP-84-1 (1984).
- [59] F. Najmabadi, N. M. Ghoniem, R. W. Conn, *et al.*, "The TITAN Reversed-Field-Pinch Fusion Reactor Study, Scoping Phase Report," University of California Los Angeles report UCLA-PPG-1100 (1987); also F. Najmabadi, R. W. Conn, R. A. Krakowski, K. R. Schultz, D. Steiner, and the TITAN Research Group,

- "The TITAN Reversed-Field-Pinch Reactor Study—The Final Report," University of California Los Angeles, General Atomics, Los Alamos National Laboratory, and Rensselaer Polytechnic Institute, University of California Los Angeles report UCLA-PPG-1200 (1990); also, F. Najmabadi, R. W. Conn, R. A. Krakowski, K. R. Schultz, D. Steiner, and the TITAN Research Group, "Engineering and Physics of High-Power-Density, Compact, Reversed-Field-Pinch Fusion Reactors: The TITAN Study," *Proc. 15th Symp. Fusion Technol. (SOFT)*, Utrecht, the Netherlands (Sept. 1988), *Fusion Technology* 88, A. M. Van Ingen, A. Nijsen-Vis, H. T. Klippel, Eds., North-Holland, Amsterdam (1989) p. 1779.
- [60] G. R. Hopkins and R. J. Price, "Fusion Reactor Design with Ceramics," *Nucl. Eng. Des./Fusion* 2 (1985) 111.
- [61] J. A. DiCarlo, Deputy Chief, Ceramics Branch, Material Division, National Aeronautics and Space Administration, Lewis Research Center, OH, private communication (April 1989).
- [62] O. Koyama, Materials Science Department, University of Tokyo, Japan, private communication (Dec. 1989).
- [63] R. Kamo, "Ceramics for Advanced Heat Engines," *High Technology Ceramics*, P. Vincenzini, Ed., Elsevier, Amsterdam (1987) p. 2473.
- [64] D. Stinton, A. J. Caputo, and R. A. Lowden, "Synthesis of Fiber-Reinforced SiC Composites by Chemical Vapor Infiltration," *Am. Ceram. Bull.* 65 (1986) 347.
- [65] P. J. Lamicq, G. A. Bernhardt, M. M. Dauchier, and J. G. Mace, "SiC/SiC Composite Ceramics," *Am. Ceram. Bull.* 65 (1986) 336.
- [66] J. J. Kibler, "Composite Laminate Analysis System (CLASS)," Materials Sciences Corp., ASM International, Metals Park, OH (1987).
- [67] R. A. Causey, J. D. Fowler, C. Ravanbakht, T. S. Elleman, and K. Verghese, "Hydrogen Diffusion and Solubility in Silicon Carbide," *J. Am. Ceram. Soc.* 61 (1978) 221.
- [68] M. C. Kerr, "Advanced Ceramic Heat Exchanger Utilizing HEXOLOY™ SA, Single Phase Silicon Carbide Tubes," *High Technology Ceramics*, P. Vincenzini, Ed., Elsevier, Amsterdam (1987) p. 2441.
- [69] K. R. Schultz, R. Gallix, C. Baxi, *et al.*, "Divertor and First Wall Armor Design for the TIBER-II Engineering Test Reactor," *Fusion Eng. Des.* 9 (1989) 15.

- [70] E. T. Cheng, "Radioactivity Aspects of Fusion Reactors," *Fusion Eng. Des.* **10** (1989) 231.
- [71] "Capability Brochure," Atlantic Research Corporation, a Subsidiary of the Sequa Corp., Virginia Propulsion Division, 5945 Wellington Rd., Gainesville, VA (1989).
- [72] A. N. Scoville, P. Reagan, and F. N. Huffman, "Evaluation of SiC Matrix Composites for High Temperature Applications," *Adv. Mater. and Manufacturing Processes* **3** (1988) 643.
- [73] Fred Mazandarany, General Electric Materials R&D, Schenectady, NY, private communication (1988).
- [74] "Capability Bulletin," Amercom Inc., Chatsworth, CA (1989).
- [75] J. Chin, Ceramics Division, General Atomics, San Diego, CA, private communication (Nov. 1989).
- [76] C. E. Johnson, K. R. Kummerer, and E. Roth, "Ceramic Breeder Materials," *Proc. 3th Int. Conf. Fusion Reactor Mater.*, Karlsruhe, Germany (Oct. 1987), *J. Nucl. Mater.* **155-157** (1988) 188.
- [77] M. Huggenberger, "Helium-Cooled, Solid Breeder Blanket Design for a Tokamak Fusion Reactor," General Atomics report GA-A16308 (1981).
- [78] D. L. Baldwin, O. D. Slagle, and D. S. Gelles, "Tritium Release from Irradiated Beryllium at Elevated Temperatures," *Proc. 4th Int. Conf. Fusion Reactor Mater.*, Kyoto, Japan (Dec. 1989), *J. Nucl. Mater.* **179-181** (1991) 329.
- [79] H. Yoshida, Japan Atomic Energy Research Institute, private communication during ITER workshop (1988).
- [80] V. B. Nesterenko, "Thermodynamic Schemes and Cycles of APS Using the Dissociating Gases," *Dissociating Gases as Heat-Transfer Media and Working Fluids in Power Installations*, A. K. Krasin, Ed., American Publishing Co., New Delhi (1975) p. 8.
- [81] H. Huang and R. Govind, "Studies of Power Plants Using Dissociating Gases as Working Fluids," *Chem. Eng. Comm.* **72** (1988) 95.
- [82] "Assessment of Supercritical Power Plant Performance," Electric Power Research Institute report EPRI CS-4968 (1986).

- [83] L. C. Fuller and T. K. Stoval, "User Manual for PRESTO: A Computer Code for the Performance of Regenerative Superheated Steam-Turbine Cycles," Oak Ridge National Laboratory report ORNL-5547 (1979).
- [84] A. B. Shapiro, "TOPAZ—A Finite Element Heat Conduction Code for 2-D Solids," Lawrence Livermore National Laboratory report UCID-20045 (1984).
- [85] G. R. Smolick, R. M. Neilson, Jr., and S. J. Piet, "Volatility from Copper and Tungsten Alloys for Fusion Reactor Applications," *Proc. IEEE 13th Symp. on Fusion Eng.*, Knoxville, TN (Oct. 1989), IEEE No. 89CH2820-9, IEEE, Piscataway, NJ (1990) p. 670.